MAGNET DESIGN TECHNICAL REPORT—ITER DEFINITION PHASE*

Edited by: Carl Henning
Lawrence Livermore National Laboratory,
University of California
Livermore, CA 94550

April 28, 1989

UCID--21681
DE89 012809

*This work was performed under the auspices of the U.S. Department of Energy by Lawrence Livermore National Laboratory under Contract W-7405-Eng-48.

Contents

Chapter 1

Introduction—Carl Henning

During the course or the Definition Phase of ITER there was a considerable effort by both the team members at Garching and in the home countries to arrive at an early definition of the magnet system. It is not practical to comprehensively catalogue all calculations and design efforts. However, this report attempts to summarize that work. Recognition for all of the contributors would be difficult. Instead, certain members of the team have tried to characterize and summarize the progress of the work.

1.1 Design Philosophy and Requirements

The TF and PF magnet systems for ITER will represent significant advances in the state-of-the-art in superconducting magnet technology. They are the core of the basic machine. As such, they will be designed to be semi-permanent, i.e. they are not expected to need repair or replacement during the life-time of the reactor, yet they must be replaceable it the need arises. High reliability of these magnet systems must be achieved by designs based on relevant experience, comprehensive analyses, and component verification in a well-coordinated development program.

An ITER Specialists Meeting was convened May 9–13, 1988, to gather data and prepare for the ITER magnet design. Data from existing superconducting tokamak magnet systems were reviewed to guide future design efforts. The Large Coil Task (LCT), T-15, and Tore-Supra are recent examples of superconducting tokamak magnet designs. Each used a different method of coil construction, and all worked. However, because field levels in ITER will be extended from 9 to 12 T or higher, forced-flow, niobium-tin conductors are preferred. The achievable current density in niobium-tin superconductors was reviewed. The data can be adequately represented by the following design formulas for niobium-tin performance with zero intrinsic strain:

$$J_{cm}(B,T) = J_{c0m}\left[1 - \frac{T}{T_{cm}(B)}\right],$$

$$T_{cm}(B) = T_{c0m}\left(1 - \frac{B}{B_{c20m}}\right),$$

Table 1.1: Properties at 4.2 K of cryogenic steels.

Material	Yield stress (MPa)	Ultimate stress (MPa)	Fracture toughness (MPa$\sqrt{m}$)	Design stress (MPa)
C SUS-JWI	1250	1650	200	825
C SUS-JKAI	1200	1650	210	800
02×20H16A 6	1326	1834	180	700
03×13H9 19AM2	1530	2000	—	750

$$J_{c0m}(B) = \frac{[111(1 - B/B_{c20m})]^2}{B^{1/2}},$$
$$T_{c0m} = 18\ \mathrm{K},$$
$$B_{c20m} = 27.8\ \mathrm{T},$$

where J is the current density in A/mm^2 over the non-copper fraction of the conductor, B is magnetic field, and T is temperature. The subscript c refers to the critical value; the subscript 0 on T_c refers to zero field; the subscript 0 on J_c and B_{c2} refers to zero temperature; and the subscript m refers to the maximum value of that parameter (i.e., at zero intrinsic strain). The curves in Fig. 1.1, from a survey show critical current for wires with various compositions and manufacturing processes.

Several conductor systems applicable to ITER have been studied and developed. Although the configurations of these conductors are varied to accommodate structural and stability considerations, there is general agreement on the levels of current density that can be achieved with reasonable development. In the superconducting (non-copper) fraction of the conductor, about 800 A/mm^2 at 12 T and 4.2 K is considered reasonable. Also, structural materials could be designed to two-thirds of yield stress, or half of the ultimate stress with a resulting value up to 800 MPa. Good advances have been made in such material properties in recent years, particularly in Japan, so that reliable cryogenic fabrications are possible. Table 1.1 lists some of the more advanced alloys from Japan and the USSR that are useful for the primary magnet structure. Table 1.2 lists alloys for a niobium-tin conductor conduit that must receive the reaction temperature heat treatment.

There has been considerable disagreement about radiation tolerance of insulators that will receive doses from 5×10^8 to 10^{10} rads. Some information exists on glass epoxies from compression and flexural tests; less information exists for polyimides (most tests have been on mixtures of epoxies and polyimides—not pure polyimides). No information exists on shear stress effects at doses ranging from 10^9 to 10^{10} rads. The results generally show decreases in strengths of 30–60% versus unirradiated values with doses approaching 10^{10} rads. With an optimization of the epoxy resins and the glass fibers, some data indicate that epoxies could be used up to 10^{10} rads. In particular, the data in Fig. 1.2, from a 1985 CERN report [1], show that certain epoxy resins can withstand close to 10^{10} rads and retain shear strength. Cleaning the fiberglass mat by heating to 400°C helps remove binders and impurities that cause degradation during irradiation.

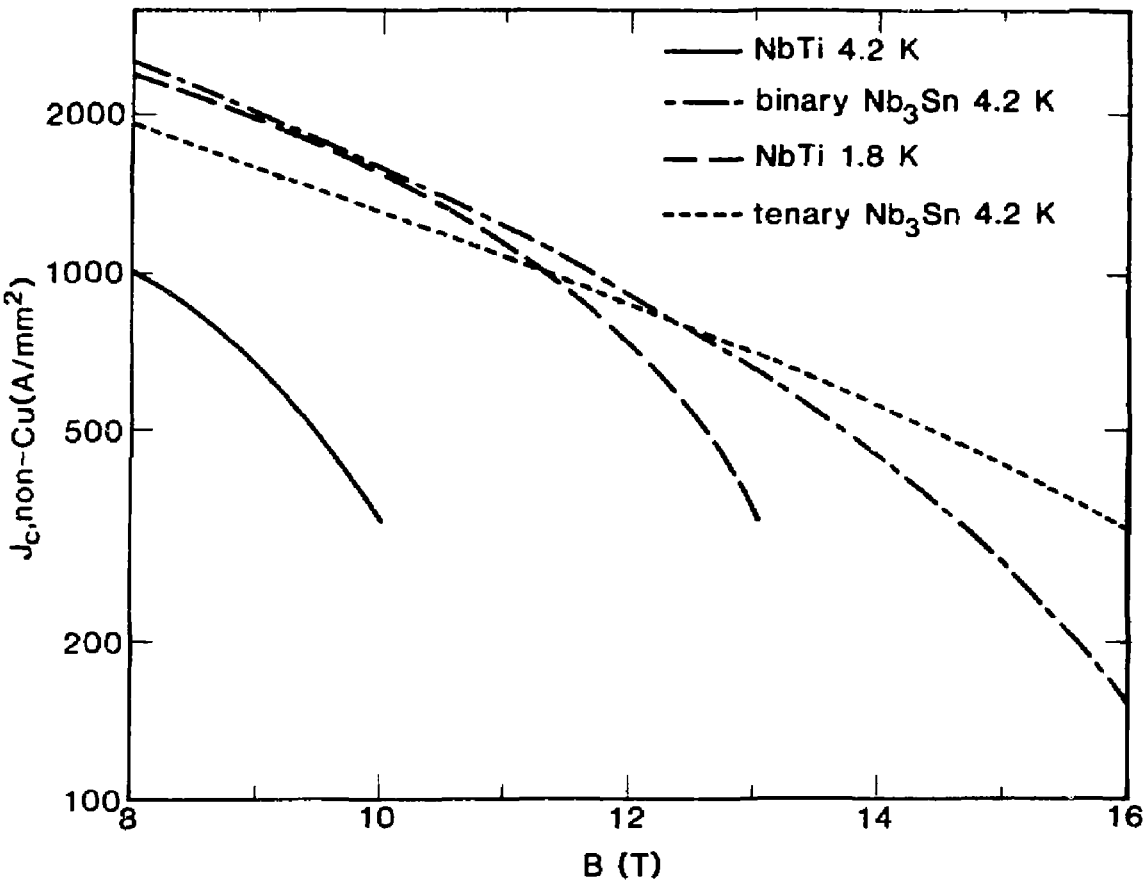

Figure 1.1: Critical current densities attainable in the non-copper fraction of state-of-the-art, technical, composite superconductors vs magnetic field at the conductor.

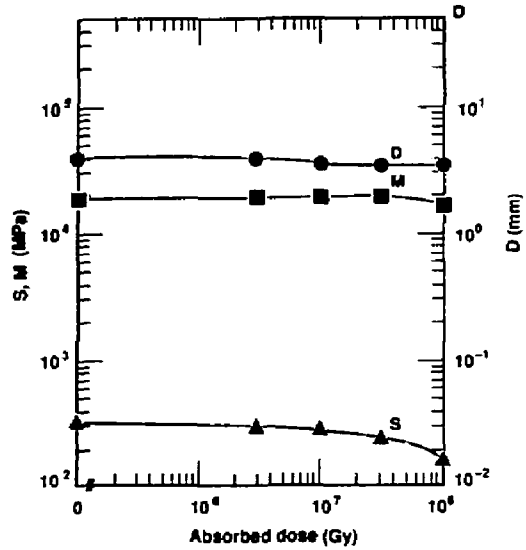

Material:	**Solventless epoxy resin No. 332. Base DGEBA MNA other components reinforced with fiber–silanized glass–cloth backing (type 3)**
Type:	**Oriltherm–D insulation**
Supplier:	**BBC Baden**
Remarks:	***Magnet coil insulation application***

Curve property	Initial value
S Flexural strength at maximum load	**324.0 MPa**
D Deflection at maximum load	**4.2 mm**
M Modulus of elasticity	***19,240.0 MPa***
Ri Radiation index (10^5 Gy/h)	**8.0**

Figure 1.2: Radiation damage to epoxy-glass.

Table 1.2: Properties of candidate materials for conductor conduit to be heat-treated at about 700°C.

Material	Modulus (GPa)	Yield stress (MPa)	Ultimate stress (MPa)
JBK-75	207	1250	1750
A286	207	similar	similar
Incoloy 908	180	similar	similar

Regarding superconductors, irradiation experiments by M. Guinan at LLNL, using 14-MeV neutrons have been conducted on commercially available materials at room temperature and at 4.5 K, with tests at 14 T (see Fig. 3) [2.3]. Neutron doses up to 1.4×10^{22} n/m^2 at 4.5 K and 2.5×10^{22} n/m^2 at room temperature were applied. The results show no degradation up to 2.5×10^{22} n/m^2. Critical current densities (non-copper) ranged from 250 to 500 A/mm^2. Because the actual neutron energy spectrum in the ITER magnets will be much softer than a 14-MeV source, the expected neutron dose in the magnet at which no degradation is expected is larger than 2.5×10^{22} n/m^2 (approaching 10^{23} n/m^2); the actual dose will depend on the design of the inner shield and magnet.

1.2 Design Criteria

Standard design codes like the ASME Pressure Vessel Code are not fully applicable to large magnet system design, although the general principles embodied in such codes might be. To allow the start of the ITER predesign process, tentative criteria have been collected by surveying and evaluating the relevant experiences in designing and fabricating previous magnet systems. Lacking a complete design code, the ITER team will rely heavily on detailed analyses and developmental testing of critical components.

1.2.1 Mechanical Design Criteria

All tensile principal stresses will have a fatigue/fracture-mechanics limit, as well as a stress-intensity limit, which acts to keep structural materials below the point where yielding occurs. The stress-intensity criterion is the Tresca maximum shear condition and will be limited in designs according to

$$S_m = min(2/3S_y, 1/2S_u),$$

where:
S_m is the maximum allowable stress intensity,
S_y is the "0.2 % offset" yield stress, and
S_u is the ultimate tensile strength.

Based on the properties of newly developed cryogenic structural steels in Japan and the USSR, the allowable stress intensity S_m at liquid-helium temperatures appears to be 800 MPa. An allowance for local yielding will be made, provided that elastic-plastic analyses

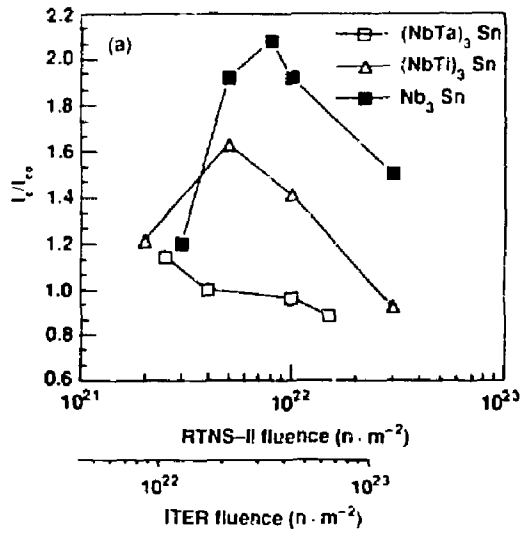

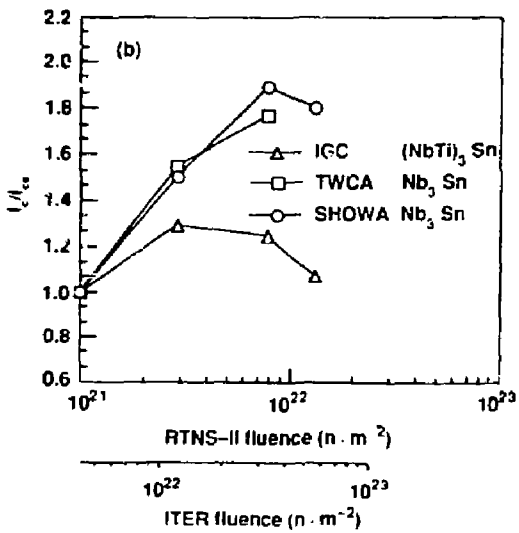

Figure 1.3: Damage to superconductors.

Table 1.3: Expected nuclear radiation environment of the ITER Baseline TF windings for normal operation.

	Shield Cooling	
Parameter	water	borated water
Maximum local heating rate (kW/m^3)	1.3	0.7
Maximum local insulator dose (Gy)	1.0×10^7	1.1×10^7
Maximum local neutron fluence (n/m^2)	7.8×10^{21}	7.5×10^{21}
Maximum local copper damage (dpa)	4.8×10^{-4}	4.7×10^{-4}

are performed to define the extent of the local plasticity and to determine that yield is not exceeded after one or two load cycles.

Interlaminar-shear in epoxy-glass insulations, and shear in the bond between insulation and conductor are critical stresses whose limits must be defined separately. Since static shear tests show ultimate strengths over 100 MPa in properly designed and manufactured layups, a limit of 30 MPa, or approximately one-third the ultimate, appears reasonable. In addition, a strain limit of 0.25% in the plane of the glass fabric reinforcement will be imposed to preclude microcracking in the composite. Normal to the insulation layers, compressive strengths over 900 MPa at 4.2 K have been demonstrated, and a limit of 1/2, 450 MPa, that is proposed.

1.2.2 Nuclear Design Criteria

In the ITER design, the neutron flux reaching the TF magnets will cause significant heating, and the total neutron fluence that will accumulate there may cause damage. Different aspects of the nuclear radiation environment of the TF windings are listed in Table 1.3. The total nuclear heat load on the TF system for normal operation is around 20 kW, but an extended condition is proposed in which the neutron shielding thickness is reduced by 100 mm, and the plasma current is increased to more than 22 MA. Under such conditions, the local nuclear heating will be raised by a factor of five, but with a reduced duty cycle and for a limited number of shots, so that the average refrigeration requirement will be approximately the same. However, conductor and cryogenic system designs must permit the removal of the higher local heat loads, which may exceed 5 kW/m^3.

1.3 Preliminary Designs and Analyses

Based on the system requirements and design criteria stated above, preliminary designs and analyses of the magnet systems for the machine have been carried out. In fact most of the analyses were done for a design of slightly larger size, but close enough in dimension that the magnet systems performance requirements are quite similar.

Although a variety of conductor designs were proposed for the various coils in the TF and PF magnet systems, there is also a great deal of commonality among the designs. For example, all designs are to be cooled by forced flow of supercritical helium, all will use a

steel jacket as distributed structure, and all conductors for the TF and CS windings will use Nb_3Sn. For the CS, only cable-in-conduit, wind-and-react designs are proposed. Force-cooled NbTi designs are being considered for the outer PF coils.

Design of the structural support systems for the magnets is the single most important issue in the overall ITER magnet systems design. Two general concepts have been and continue to be scrutinized for the support of the TF system in the inboard region: wedging and bucking against the CS. For the geometries studied that use the wedging concept, finite element analyses have shown quite high combined stresses being developed in the noses of the TF coils. The bucked-against-CS concept eases this problem somewhat, but has much more complicated load paths, especially for handling the overturning moments. On the whole, each concept offers similar machine capabilities and similar radial build in the inboard region. More detailed analyses are needed of both concepts. It has been decided to take the wedged concept as the reference for the baseline design and to continue to study the bucked-against-CS as an alternative.

The outboard TF geometry is not a pure tension shape, so that intercoil structure will react to in-plane loads. Preliminary analyses show the outer intercoil structure supporting toroidal tension up to 60 MN. Some concern has been expressed about the ability of designs simultaneously to handle such loads and to allow independent radial deflection of the TF outboard legs, if such deflection is needed to avoid stresses caused by non-uniform cooldown. Accordingly, future detail structural design efforts will include thermal stresses with the magnet geometry analyses.

The high-stored energies in the ITER magnet systems make protection in the event of quench a serious concern. A discharge-time constant of less than 10 s for the transfer of the stored energy to an external dump resistor has been proposed, subject to the limitation of voltages less than 20 kV being developed, either between terminals or between coil and ground. The need for rapid discharge of the coils is set by the requirement that the maximum allowable hot-spot temperature by an adiabatic calculation be 150 K.

Bibliography

[1] G. Liptak, R. Schuler, P. Maier, H. Schoenbacher, B. Haberthuer, H. Mueller, and W. Zeier, *Radiation Tests on Selected Electrical Insulating Materials for High-Power and High-Voltage Application,* CERN report 85-02, Geneva, Switzerland (March 1985).

[2] R. Fluekiger, W. Maurer, F. Weiss, P. Hahn, and M. Gilinan, *IEEE Trans. Magn.* **MAG-23**, 976 (1987).

[3] M. Guinan, R. Hahn, and T. Okada, *Studies of Superconductors and Stabilizers for Fusion Magnets,* Lawrence Livermore National Laboratory, Livermore, CA, UCID-21298 (1988).

Chapter 2

Conceptual Design—E. Tada

2.1 Magnet Configuration

These are 16 TF magnets located toroidally with the design peak field of 12 T so as to provide a magnetic field of 5.3 T at the plasma center in normal operations. In addition, 12 PF magnets are set outside of the TF magnets in updown symmetry for an inductive heating and position control of the plasma; these magnets are coaxially located in the vertical direction for maintenance reasons.

Figure 2.1 shows the external geometry and location of TF and PF magnets in ITER machine. The coil case cross-section in the outboard leg region of the TF magnet is tentatively specified to be 1.1 m × 1.1 m to give reasonable access area to the heating system and plasma facing components. The TF intercoil structure area to sustain magnetic forces is also limited as shown in Fig. 2.1 for the same reason. The central solenoid magnets are enveloped by the TF inboard legs in a 1.9-m radius and should be partially mechanically supported by the TF structure. These geometry, coil location and the structural area will be fixed on the basis of the detail stress analysis in the predesign phase.

2.2 Design Analysis

2.2.1 Design Criteria

The following are tentative design criteria evaluated from the magnet design and fabrication experience to start the predesign of ITER magnet and more detailed analysis will be needed.

2.2.1.1 Mechanical Design Criteria

1. For metallic components in a static loading,

$$\begin{aligned} Sm &= \min\{ 2/3Sm,\ 1/2Sy) = 800\ \text{MPa}\} \\ \text{where} &= Sm : \text{the allowable stress intensity} \\ &\quad\ Sy : \text{the 0.2\% yield strength} \\ &\quad\ Su : \text{the ultimate strength.} \end{aligned}$$

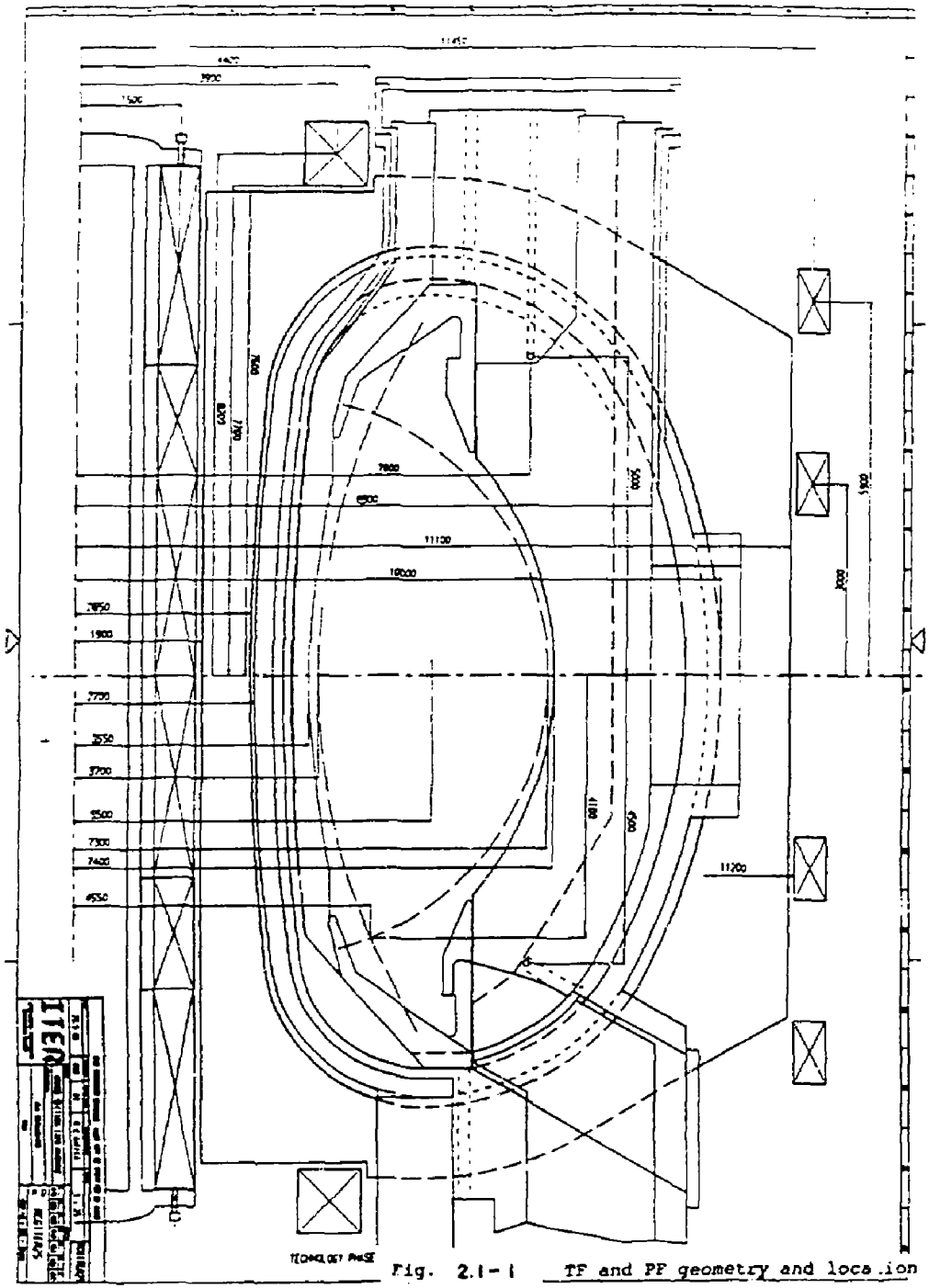

Figure 2.1: TF and PF geometry and location.

2. For a cyclic loading, a stress limit will be 2/3 Sm.

3. For Nb_3Sn-base superconductor, a stress limit should be 0.5%.

4. For the insulation materials, a bonding stress limit will be 1/3 of the ultimate strength.

5. For a insulation materials, a strain limit will be 0.25%.

6. For a insulation materials, a compressive stress limit will be 1/2 of the compressive ultimate strength.

2.2.1.2 Electrical design criteria

1. For Nb_3Sn-base superconductor, a critical current density is 800 A/mm^2 at 4.2 K, 12 T and zero strain.

2. For protection of the magnet system,

the discharge time constant	: less than	10	sec.
the insulation voltage	:	20	kV.
the maximum hot-spot temperature rise	:	150	K.

2.2.1.3 Radiation limit

Insulation dosage	:	5×10^8 to 5×10^9	rads
Nuclear heating rate	:	1.0 to 5.0	mW/cc
Neutron fluence	:	1×10^{19}	n/cm^2
Copper dpa	:	5×10^{-4}	dpa

2.2.2 Design analysis

Based on the system requirements and the design criteria, the following design analysis has been conducted and more detail analysis will be needed.

2.2.2.1 Magnet Field Analysis

The magnetic field profile was calculated; the results show that the design peak field of 12 T is required for the TF magnet to produce a magnetic field of 5.3 T at the plasma center. The total electromagnetic stored energy of the 16 TF magnets is about 40 GJ with a magnetic capability of about 9 MAT each. In addition, the field ripple at the plasma edge is expected to be less than the specified value of 1.5 percent.

Regarding the PF magnet design, it is expected that an inductive capability of 250 Volt-second may be available at the design magnetic field of 12 T for the central solenoid (PF1 to PF3) and 7 T for the equilibrium magnet (PF4 to PF6). The total stored energy of PF magnets is around 14 GJ.

2.2.2.2 Structural Analysis

Regarding TF support design, two possible concept (wedging of the magnet inner legs and the bucking onto the central solenoid) were considered based on the preliminary stress analysis. In case of wedging support, the centering force can be sustained by the vault of each TF inboard leg. The 2D and 3D FEM analysis gives a peak case stress of about 700 MPa, this is less than the allowable stress of 800 MPa. Alternate is the bucking support concept and the 3D stress analysis gives a case stress less than 400 MPa but more detail analysis considering shear transmission and interaction between TF and central solenoid magnets is required.

Regarding the intercoil structure, a preliminary analysis shows that the outer intercoil structure has to support a toroidal tension up to 60 MN. This load is rather high and more detailed structural design including thermal stress is required.

The stress of the central solenoid magnets was evaluated based on an operating scenario. The result shows a peak stress of around 690 MPa at the end of burn. Since the central solenoid magnets are operated under cyclic loading conditions, this value is critical from the fatigue point of view.

2.2.2.3 AC Loss Analysis

In case of nominal operation of the TF magnet, a maximum field change is about 6.7×10^{-2} T/sec. The total heat loss in the TF magnets excepting the structure is about 3 kW at 4 K with an assumed time constant of 3 msec. Sweeping the plasma separatrix by ± 15 cm in 0.3 Hz, an additional field change of about 0.35 T/sec is applied during the plasma burning. In this case, the total heat load is increased by around 30 kW.

Figure 2.2 shows that the AC loss analysis results for both the nominal and plasma swing operation based on an operating scenario. In the nominal operation, the average heat load per cycle is less than 2 kW at 4 K. For the plasma swing, the PF magnets are requested to produce an additional field cahnge of 0.25 to 1.2 T/sec during the plasma burning. The total heat load during the burning is increased by around 35 kW; this analysis does not include loss in the magnet structure.

Accordingly, the plasma swing condition such as frequency should be revised to reduce the heat loss due to the magnet field change.

2.2.2.4 Thermal Analysis

The total cooling weight of the magnets is estimated to be 10,000 ton including the supporting structure. A preliminary cool-down analysis shows that a total flow rate of around 4 kg/sec is required for cooling the magnets within 300 hours but the cooldown time should be defined based on the pressure drop analysis and the conductor and case design.

The static heat load of the magnets are preliminary estimated in normal operation as listed in Table 2.1. The total static heat load including nuclear heating is about 42 kW. In this calculation, the operating current of all magnets is estimated to be 30 kA so that the required heat load of current leads is 3,000 liter/hour, corresponding to 10 kW at 4 K.

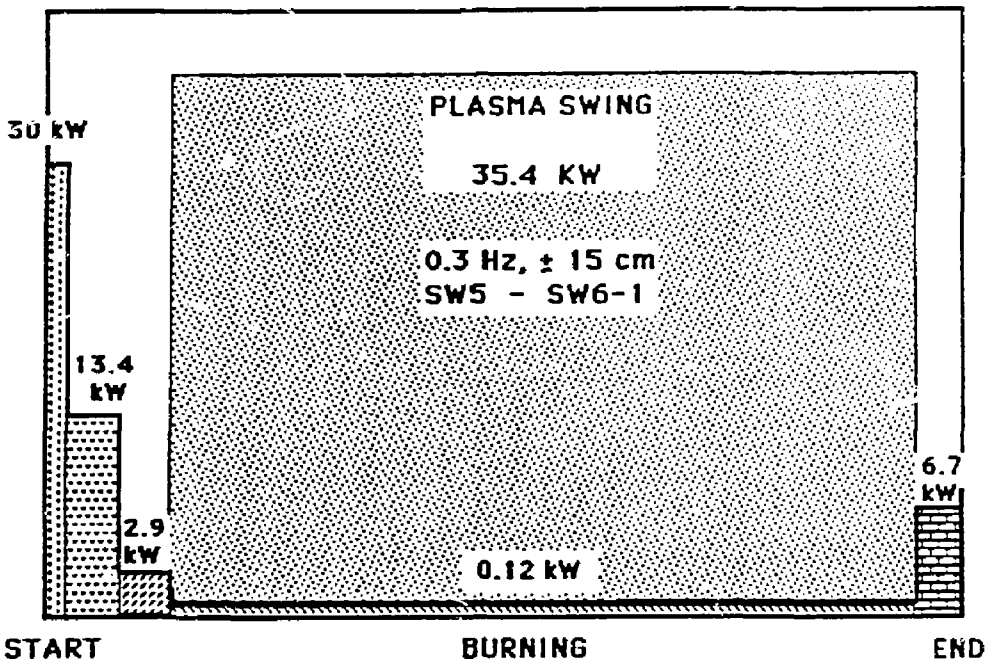

PF COIL AC LOSS

START	- BREAKDOWN	1 SEC
	- IGNITION APR.	31 SEC
	- BURN START	56 SEC
	BURN END	525 SEC
	- END	545 SEC

AVERAGE HEAT LOAD *1.3 kW for normal operation*

32 kW for plasma swing

Figure 2.2: AC loss analysis results of PF magnet.

Table 2.1: Heat load of magnet at nominal operation.

Items		Heat loads		
TF Magnets	:	Static heat	5	kW
		AC loss	3	kW
		Nuclear heat	20	kW
		Current lead	1500	liter/hour
PF Magnets	:	Static heat	2	kW
		AC loss	2	kW
		Current lead	1500	liter/hour
Total	:		42	kW

2.3 Magnet Design Concept and General Specification

A number of TF and PF magnets were designed to satisfy the system requirements and operating environment in compliance with the design criteria. Table 2.2 and 2.3 show the general specifications developed for the ITER magnet design based on these requirements. Table 2.4 shows the proposed magnet designs to meet the specifications using variety of conductors. More detailed analysis will be needed in the design phase to qualify the relative advantages. Typical conductor concepts are shown in Fig. 2.3 for the TF and central solenoid magnets.

2.4 Cryogenic and Power Supply Design Concepts

2.4.1 Cryogenic System

A preliminary design concept of the cryogenic system was developed as schematically shown in Fig. 2.4. The maximum refrigeration capacity of 100 kW at 4 K is specified; the cryogenic system will be divided into 3 or 4 units, each unit having a capacity of 25 to 30 kW. This capacity permits cooling magnets within 300 hours and corresponds to a refrigerator electrical power of 50 MW at room temperature.

A cryogenic circulation pump is proposed to circulate supercritical helium effectively. In addition, a cold compressor, which has the capbility to adjust operating temperature of magnets in the range of 3.5 to 4.5 K, is proposed. A double thermal shield concept, composed of 80 K and 5 K shield, is proposed in order to decrease the heat load at 4 K region. The TF coil case cooling is essential for the high field region on which high radiation heat is applied.

2.4.2 Power Supply System

Power supply requirements for all the main reactor systems except magnets were estimated in a preliminary design based on the operation scenario. These requirements are listed in Table 2.5

Table 2.2: General specifications of TF coil.

Items		Reference Values	Allowable Range
He inlet temperature	(K)	4.5	3.6-4.5
He inlet pressure	(bar)	10	5 10
He outlet pressure	(bar)	> 5	> 5
Nuclear heating	(mW/cc)	1	< 5
Insulator Dose	(rads)	2×10^9	5×10^8
5×10^9			
Neutron fluence (>0.1 MeV)	(n/cm^2)	1×10^{19}	1×10^{19}
Copper Dpa	(dpa)	5×10^{-4}	5×10^{-4}
Plasma disruption		40 T/s for 20 msec	
Poloidal cycles		< 100000	< 100000
Charging cycles		< 100	< 100
Cooldown cycles		< 20	< 20
Design peak field	(T)	12	11-12
Overall current density	(A/mm^2)	13-14	13-14
Rated current (Iop)	(kA)	30-40	16-45
Critical current at operating condition	(kA)	> 1.6Iop	1.6 2Iop
Temperature margin	(K)	> 0.5	> 0.5
Pressure drop	(bar)	< 3	< 8
Dump voltage	(kV)	< 20	< 20
Dump time constant	(sec)	< 10	5-10
Hot-spot temperature	(K)	< 150	< 150

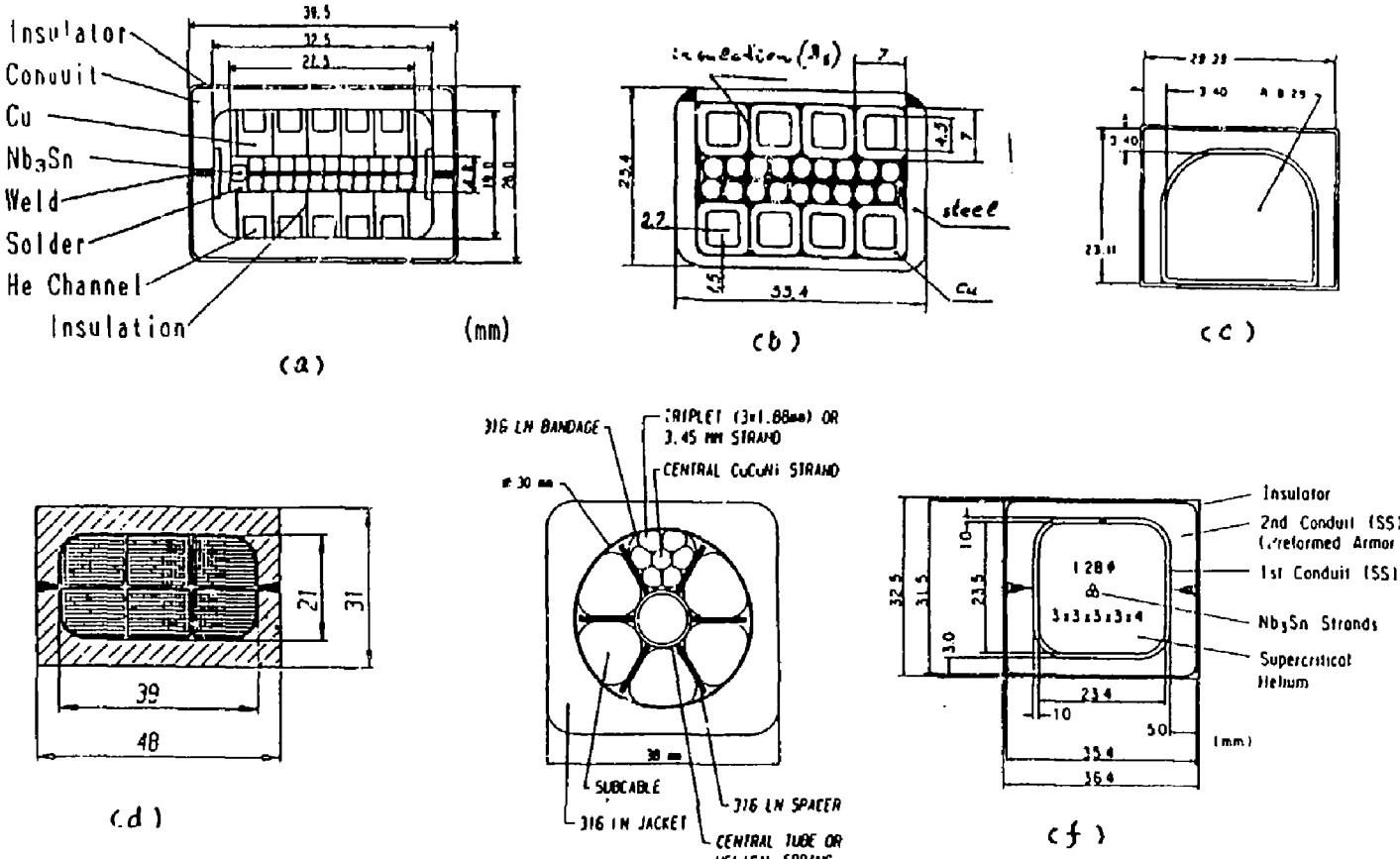

Figure 2.3: Super conductor concepts.

Fig. 2.3-1 Cross-sectional view of typical conductors,
(a)-(b) Monolithic TF conductors
(c)-(d) Cable-in-conduit TF conductors
(e)-(f) Cable-in-conduit PF conductors

Table 2.3: General specifications of TF coil.

Items		Reference Values	Allowable Range
He inlet temperature	(K)	4.5 Nb_3Sn	3.6-4.5
		4.5 NbTi	3.6-4.5
He inlet pressure	(bar)	10	5-10
He outlet pressure	(bar)	> 5	> 5
Design peak field	(T)	12 OH coil	12-13
		< 7 EF coil	< 7
Rated current (Iop)	(kA)	30-40	30-40
Critical current at operating condition	(kA)	> 1.6Iop	1.6-2Iop
Temperature margin	(K)	> 0.5	> 0.5
Pressure drop	(bar)	< 3	< 3
Dump voltage	(kV)	< 20	< 20
Hot-spot temperature	(K)	< 150	< 150

In case of the PF magnets, the positive and negative power supplies with a capacity of order of some GW will be required. Taking into consideration a reasonable limit for electrical power supply from the commercial line, a set of motor generators having a capacity comparable with the PF magnet requirements will be required. The rectifier system with a capacity of several GW will be necessary and may be based on GTO (Gate Turn Off thyrister) converters.

2.5 Structural Materials

The strutural materials of superconducting magnets for fusion are required to have higher strength and fracture toughness than those of ordinary commercial products such as 304 and 316 austenitic steel, mainly because of large electromagnetic forces. Based on the preliminary structural analysis, the following characteristics of 4 K are proposed as the required mechanical properties of the magnet structural material.

1) Yield strength : more than 1200 MPa

2) Fracture toughness : more than 200 MPa $\sqrt{m}$

There has been significant advance in such material properties in recent year, particularly in Japan, so that reliable fabrications of cryogenic structural materials are possible. Mechanical properties at 4.2 K of some steels and recommended design values for ITER are listed in Table 2.6.

2.6 TF Magnet Configuration and Magnetic Ripple

The variation of the toroidal ripple at the plasma edge depends on the distance between plasma edge and the center of TF magnet as well as the number of TF magnets. Figure 2.5 shows the toroidal field ripple with and without magnetic insert as a function of the number of TF magnets; the optimized stored energy of the PF magnet is also plotted.

Table 2.4: General specifications of TF coil.

	Toroidal Field Coil					Central Solenoid		EF Coil
Items	TF-1	TF-2	TF-3	TF-4	TF-5	OH-1	OH-2	EF-1
Design field (T)	11.6	11.7	11.2	12.0	12.0	13.0	12.0	7.0
Superconductor	A	B	B	C	D	D	D	E
Conductor type	CICC	MON	CICC	MON	CICC	CICC	CICC	CICC
Operating current (kA)	39.5	32.0	46.2	31.7	30.0	40.2	30.0	30.0
Critical current (kA)	61	64	97	63	60	98	60	65
Current density (A/mm^2)								
winding	27.1	31.2	45.0	390.0	33.5	26.0	25.0	28.4
cable	57.1	56.0	81.0	51.3	74.0	66.2	56.8	44.8
Winding type	pancake	pancake	pancake	pancake	pancake	layer	pancake	pancake
No. of pancake/coil	20	20	12	8	11		22	
No. of turn/pancake	12	15	18	18 x 2	14 x 2		12	
He path length (m)	458	600	336 *	366	280	240	128	550
Standard diameter (mm)	0.876	1.05	1.0	2.5	1.40	0.8	1.13	1.20
No. of strand	588	126	375	23	162		324	324
Cooling perimeter (cm)	75	14.4	100.5	15.8	59.4		95.9	101.8
Cross-section are (mm^2)								
Total	1365	875	1027	1027	895	1545	1201	1056
SC (non-Cu)	139	109	179	132	80	157	107	65
Cu	276	230	191	388	158	157	198	174
Helium	276	162	201	97.5	154	293	201	284
Stainless steel	526	210	393	345	413	860	583	
Insulation	148	94	64	64.5	76.0	78.0	90.0	
He flow/channel (g/s)	7.5		7.5	6.0	5.0		1.8	7
No. of flow path/coil	20	20	22	32	40		44	

A :Nb_3Sn or $(NbTa)_3Sn$ B :Nb_3Sn C :$(NbTi)_3$ and NbTi grading
D :$(NbTi)_3Sn$ E :NbTi
CICC :cable-in-conduit MON :monolithic

Table 2.5: Power supply requirements.

Equipment	Capacity (MW)
Plasma heating system	250
Cooling water system	100
Cryogenic system	60
Active control coil	40
Fuel and vacuum system	40
Utility	30
Total	520

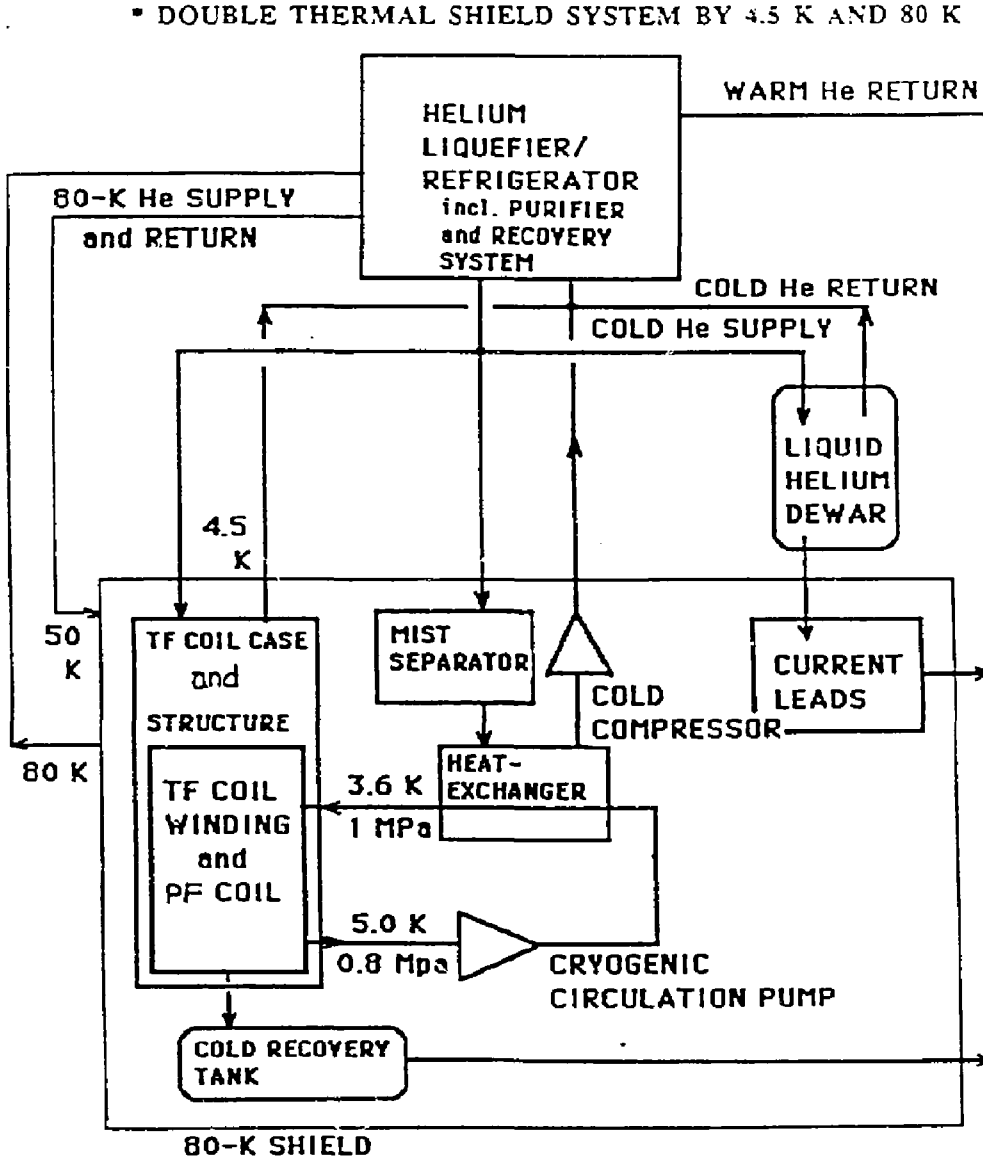

Figure 2.4: Typical cooling scheme.

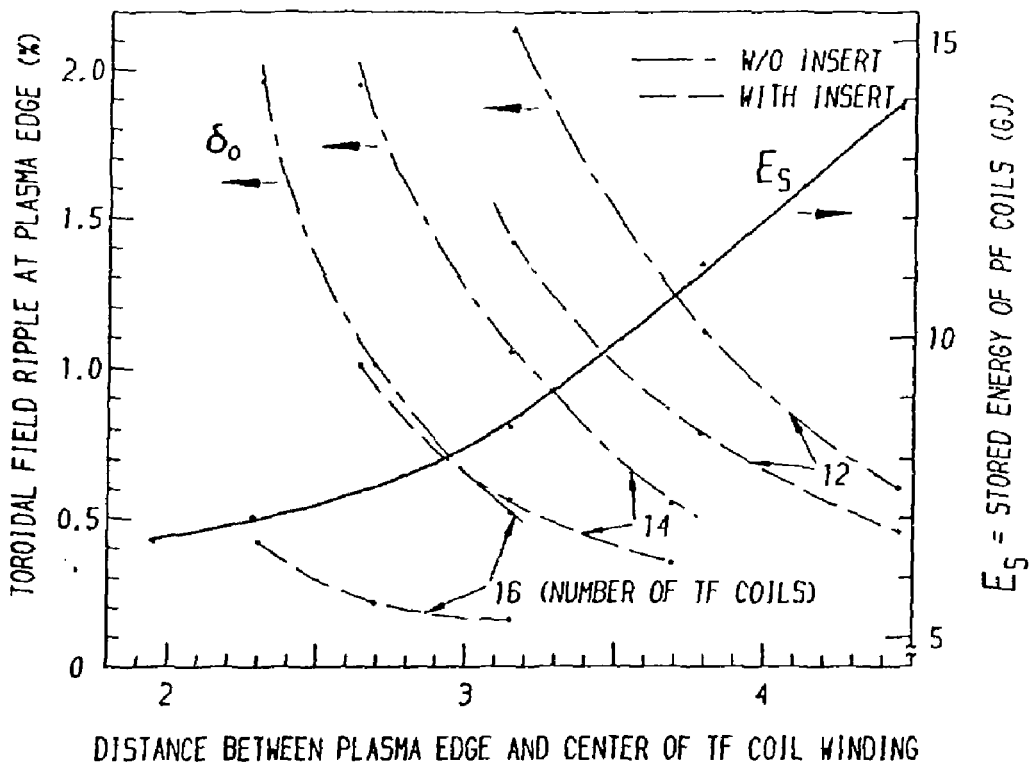

Figure 2.5: Toroidal field ripple with and without magnetic insert and optimized stored energy of PF system with plasma major radius of 5.65 m, minor radius of 2.05 m and elongation of 2.

Table 2.6: Structural materials proposed for ITER.

Material		Sy(MPa)	Su(MPa)	K_{1c}(MPa$\sqrt{m}$)
C SUS—JW1	(Japan)	1250	1650	200
C SUS—JKA1	(Japan)	1200	1650	210
03X20H16A 6	(SSR)	1326	1834	180
03X13H9 19AM2	(USSR)	1530	2000	—
Recommended Value		1200	1650	200

Sy : 0.2 % yield strength
Su : Ultimate strength
K_{1c} : Fracture toughness
* Allowable stress (Sm) = min{2/3Sy, 1/2Su} = 800 MPa

Generally, forromagnetic inserts under the TF magnets can reduce the ripple level and have the equivalent effect to increase the number of TF magnet by 2. The outer radius of the TF magnet determines the allowable position of the outer equilibrium magnets. The absolute radius of these magnets have strong influence on the toral energy of the PF magnet system. Therefore, it is desirable to have 16 or more TF magnets for optimizing the PF magnet system.

Chapter 3

Radiation Damage of ITER Magnet Systems—L. Summers, J. Miller

The inner leg of the ITER Toroidal Field (TF) coils will be subject to a high fluence of energetic neutrons and a high dose of ionizing radiation. Here we describe the selection of materials and review allowables used in the design of the ITER TF coil system for the 5.8 m case.

3.1 Radiation Environment

The superconducting magnets of the ITER machine will operate for extended periods of time at 4.2K. Normal operation will include periodic warm-ups to room temperature, however the number of temperature excursions will be limited due to the high machine availability demanded. The calculated nuclear environment of the ITER TF system is shown in Table 3.1 for two different shield cooling options. The values for dose, dpa, and fluence given in Table 3.1 are end of life values for the TF coil, and are calculated for the 5.8 m ITER option with 85 cm of shielding in the inboard region.

3.2 Organic Insulation

Radiation damage tolerance of the organic insulation may be the most limiting factor in the useful life of the TF coils. The insulation will be required to transmit high operation forces and to provide electrical stand off at potentials of up to 20 kV. In general it is felt that the failure criteria in such materials will not be a degradation of electrical properties, but will be a mechanical failure of the

Table 3.1: Radiation environment of the ITER TF system.

	Shield cooling	
Parameter	Water	Borated water
Maximum local heating rate (kW m^{-3})	1.3	0.7
Maximum local insulator dose (Gy)	1.0×10^7	1.1×10^7
Maximum local neutron fluence (n m^{-2})	7.8×10^{21}	7.5×10^{21}
Maximum local copper damage (dpa)	4.8×10^{-4}	4.7×10^{-4}

Table 3.2: TF coil insulation design allowables.

	Allowable	Design limit
Maximum compressive Strength	1/2 Ultimate Strength	450 MPa
Maximum allowable strain parallel to laminations		0.25%
Maximum interlaminar-shear/ bond-shear	1/3 Ultimate Shear strength	30 MPa

insulation that results in shorting [1]. Therefore the design allowables are based on the mechanical properties of the insulation, while electrical properties are only a secondary consideration.

The mechanical design criteria for insulations used in the analysis of the ITER TF coils are shown in Table 3.3. The design limits are for the end of life, i.e., the insulation must meet the allowables after exposure to the maximum radiation dose. The limits were determined using average mechanical properties values for fiber reinforced organic insulation obtained by a survey of the literature.

A number of studies have been undertaken to determine the effects of irradiation on the mechanical properties of organic insulation. The results of an Oak Ridge National Laboratory (ORNL) study are shown in Figs. 3.1 and 3.2 [2]. The G-10 CR (NEMA) material containing. E-glass is a solid type epoxy resin intended for cryogenic use. Spaulrad is a polyimide product of the Spaulding Fiber Company and is approximately 70% E-glass by weight. Norplex (also known as Kerimid) is a polyimide (pseudo-bis-maleimide) product of Norplex Division, UOP, Inc. Norplex contains 40–60% E glass by weight. Vespel is an unfilled polyimide and is a product of E.I. DuPont de Nemours and Company.

In the ORNL study the irradiation was conducted at 4.9K. The dose rate and neutron flux were 5.0×10^5 Gy hr^{-1} and 1.25×10^{15} n m^{-2} s^{-1} (E > 0.1 MeV) respectively. Following irradiation the samples were warmed to room temperature and cooled to 77K for mechanical testing. With the exception of Norplex all the materials were loaded parallel to the fiber laminations Norplex was loaded in compression in both the normal and parallel directions. Using the ITER design allowables and the dose calculation of 1.1×10^7 Gy, both Norplex and Spaulrad are acceptable for use. The initial compressive strength of Vespel is too low and the Epoxy resin system (G-10) shows a rapid decrease in compressive strength with absorbed dose.

A number of room temperature irradiation studies have been performed. The results of an extensive investigation at CERN are shown in Figs. 3.3–3.6 [3,4]. For the CERN data taken from Ref. [3] the irradiation temperature was 45–62°C. The γ-ray dose rates were between 1×10^4 and 2.5×10^5 By hr^{-1}. The neutron flux (E > 1 MeV) was 1.5–1.8 $\times 10^{10}$ n m^{-2} s^{-1}. For the data from Ref. [4] the irradiation temperature was 30–40°C. The γ-ray dose rate was 1–2 $\times 10^6$ Gy hr^{-1}. The neutron flux varied from 2–3 $\times 10^{12}$ n m^{-2} s^{-1}. Mechanical tests were conducted at room temperature. A description of the test samples is shown in Table 3.4.

Although the irradiation was not conducted at cryogenic temperatures, the CERN data are encouraging. Several of the materials show no major degradation of flexural strength to fluence levels greater than 10^7 Gy. Of particular interest are the VPI epoxies which could be useful for magnet impregnation after wind and react heat treatments.

Table 3.3: Descriptions of the insulation materials studied in the CERN investigation (Refs. 4 and 5).

Sample No.	Material description	Trade Name/manufacturer
119	Polyimide with glass fiber	Isola
152	Kinel 5.502 6 h 180°C + 2 h 200°C	Rhoñe-Poulenc
176	Orlitherm with glass tape (type 2) and silane finish	BBC, Baden
197	Kinel 5.504	Rhoñe-Poulenc
198	Kerimid 601 with glass fiber 181 E	Rhoñe-Poulenc
276	Orlitherm with silanized glass tape (type 3)	BBC, Baden
303	Orlitherm with silanized glass tape (type 3) and polyimide film	BBC, Baden
343	Solventless Epoxy resin with silanized glass cloth backing	Micadur Insulation BBC, Baden
344	Glassrope impregnated with Micadur resin	Micadur Insulation BBC, Baden
345	Glass reinforced epoxy resin	GFK 101 BBC, Baden
346	Solventless Epoxy resin with aromatic polyimide paper	Micadur Insulation BBC, Baden
347	Solventless epoxy resin with aromatic polyimide paper	Orlitherm-S BBC, Baden
349	Solventless epoxy resin with desized glass cloth	Orlitherm-S BBC, Baden
350	Solventless epoxy resin with desized glass cloth backing	Orlitherm-D BBC, Baden
358	Polyester (halogenated) with glass mat	Delmat 64.247 Isola
362	Epoxy (cycloaliphatic) with glass roving	Vetronit 7310 Isloa
363	Epoxy with glass roving	Fluoridit 22 Isola
365	Polyester with glass roving	Polyglass 31 Isola
366	Polyester with glass roving	Polyglass H-200 Isola

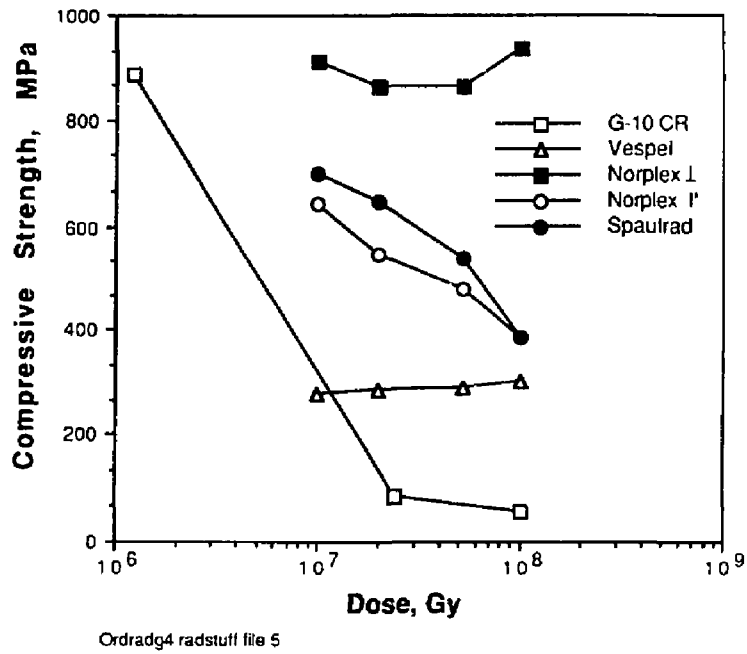

Figure 3.1: The compressive strength of organic insulation as a function of γ-ray dose. The G-10 CR material is an epoxy containing composite. The other materials are polyimides. The data for Norplex is shown for two test conditions; load applied normal to the fibers laminations ($\perp$) and the load applied parallel to the liminations ($\parallel$). Data from Ref. 2

Table 3.4: Irradiated thin sheet specimens tested in cyclic compression. Data from Ref. 5.

Material	Stress (MPa)	Cycles	Results
G-10	207	13,210	one failure
	276	6,275	two failure
	345	440	one failure
DGEBA	310	100,000	no failure
	345	165,701	no failure
TGPAP	241	195,413	no failure
	345	257,444	no failure
Kerimid	207	63,750	no failure
	310	83,377	no failure
	345	226,676	no failure

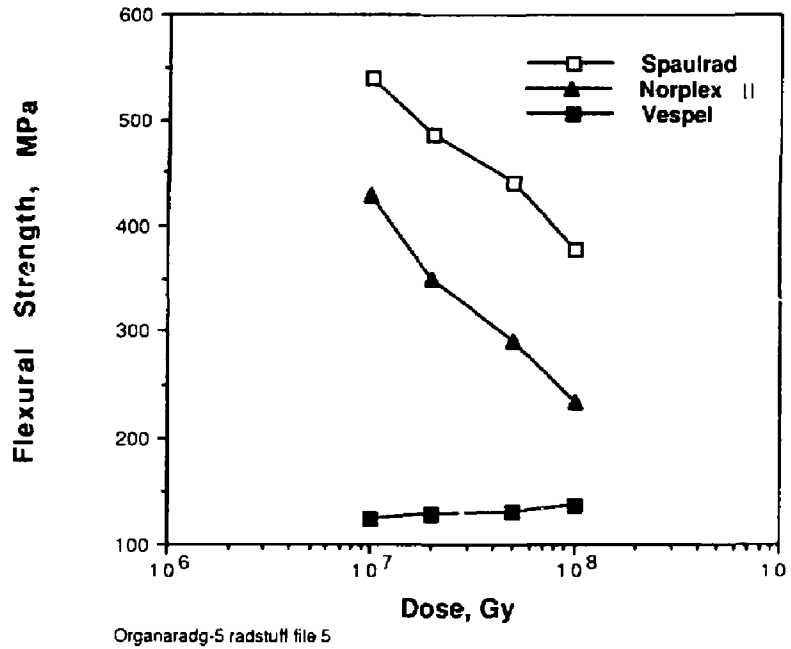

Figure 3.2: The flexural strength of organic insulation as a function of γ-ray dose. The data is taken from Ref. 2.

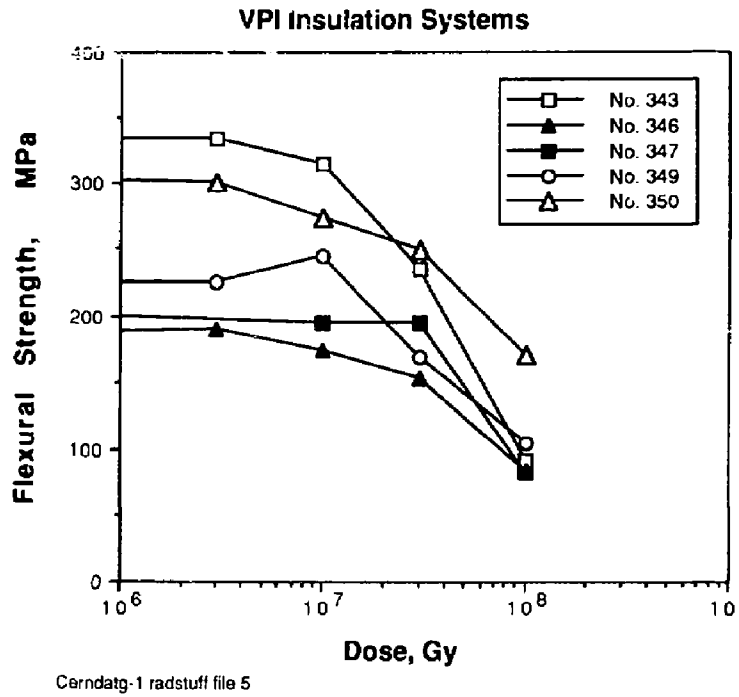

Figure 3.3: CERN data obtained on Vacuum-Pressure Impregnation (VPI) insulation systems. Irradiation conducted at room temperature. Data from Ref. 3.

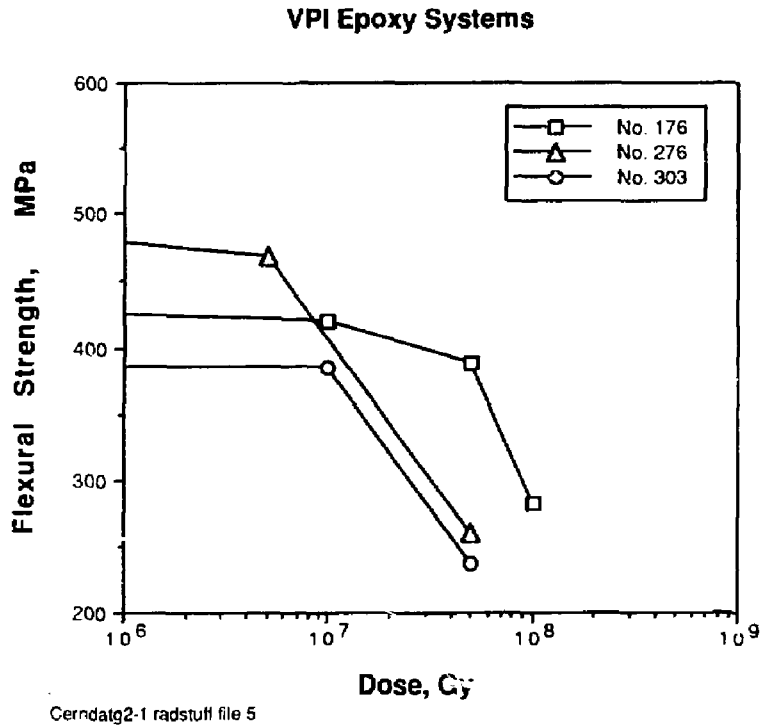

Figure 3.4: CERN data obtained on VPI resin systems. Irradiation conducted at room temperature. Data from Ref. 4.

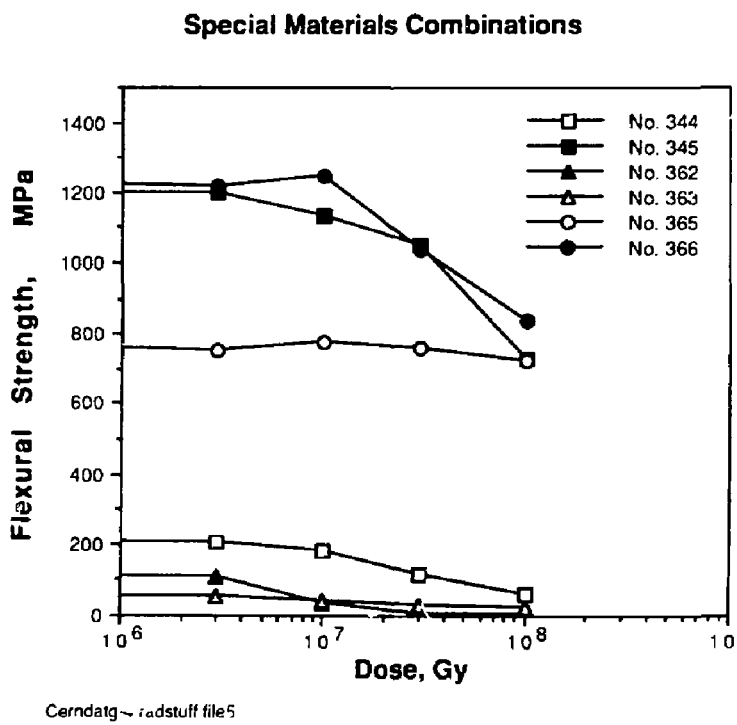

Figure 3.5: CERN data obtained on special resin systems. Irradiation conducted at room temperature. Data from Ref. 3.

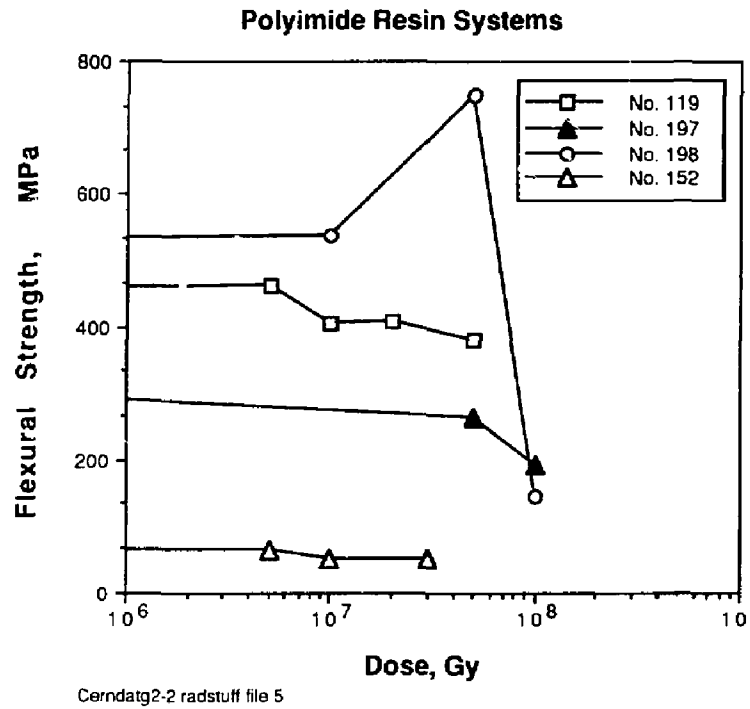

Figure 3.6: CERN data for polyimide resin systems. Irradiation conducted at room temperature. Data from Ref. 4.

A study by Schmunk, et al., looked at the effect of cyclic loading on thin sheets of insulation that had been irradiated at room temperature [5]. The results of this investigation are shown in Table 3.4. The specimens were irradiated to a dose of 3.2 x 10^9 Gy and a neutron fluence of 4 x 10^{23} n m^{-2} (E > 1 MeV). The Kerimid material is a polyimide, the remaining materials are variations of epoxies. The G-10 and G-11 CR contain E glass while the remaining specimens contain S and S-2 glass. It is interesting to note that the samples fabricated with S or S-2 glass performed exceptionally well due to the absence of B_2O_3 (resulting in a lower total dose absorbed).

The present data base indicates that polyimide materials and possibly epoxy resin systems will meet the requirements of the ITER base line design and operating scenario. However more detailed testing with irradiation at 4.2K will be required. This is particularly true of thin sheet specimens which are representative of the insulation configuration in the proposed ITER TF coils.

3.3 Superconductor

Radiation damage to the superconductor appears to be less limiting in the design of the TF coils than that to the organic insulators. The results of an LLNL/KfK investigation of Nb3Sn superconductors irradiated at 300 K are shown in Fig. 3.7 [6]. These wires were irradiated in the Rotating Target Neutron Source II (RTNS-II) located at LLNL. The RTNS facility produces a neutron spectrum that is very sharply peaked at an energy of 14 MeV. Therefore the data may be considered conservative in comparison to the "soft" neutron spectrum typical of a fusion reactor. Figure 3.7 shows a relative neutron flux scaling calculated for various reactor designs.

Additional studies at LLNL included tests of superconductors irradiated at 4.2 K. The results of this investigation are shown in Fig. 3.8 [7]. Again, these wires were tested in RTNS-II with a "hard" neutron spectrum. Results of these tests indicate the conventional Nb_3Sn superconductors will operate well beyond the 7.8 x 10^{21}n m^{-2} upper fluence limit expected in ITER.

3.4 Stabilizer

For magnet designs using force-cooled, cable-in-conduit conductors, studies have shown that full stability of the coils can be maintained if the stabilizer resistivity accounting for radiation damage and magnetoresistivity is about 1.2 nΩ·m or lower. We assume the increase of residual resistivity of copper due to irradiation can be described by

$$\Delta\rho_o = s\left[1 - exp\left(\frac{-iD}{s}\right)\right]$$

where s = 3.1 nΩ·m is the saturation level, D is the dpa, and i = 720 nΩ·m·dpa is the saturation rate [8,9].

Magnetoresistivity (in nΩ·m) is given by

$$\rho(B) = \rho)o\left[1 + 0.0339\left(\frac{B}{\rho_o}\right)^{1.07}\right]$$

where ρ_o includes the effects of radiation damage [10].

For state of the art superconductors we assume that initial zero field stabilizer resistivity values of 0.2 nΩ·m are achievable. Using this value and the calculated design maximum of 4.8 x 10^{-4} dpa,

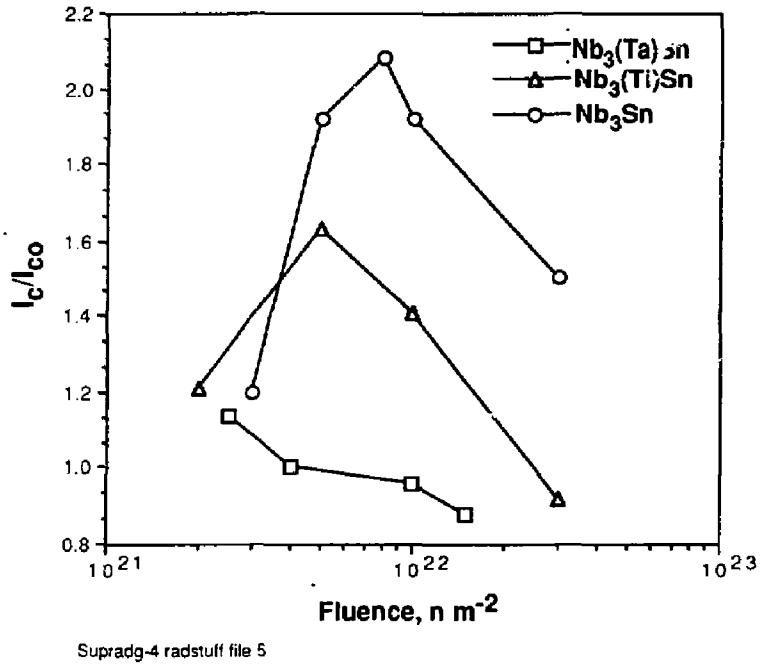

Figure 3.7: The effect of irradiation on the critical current of multifilamentary Nb_3Sn superconductors. The wires were irradiated at room temperature. Data from Ref. 6.

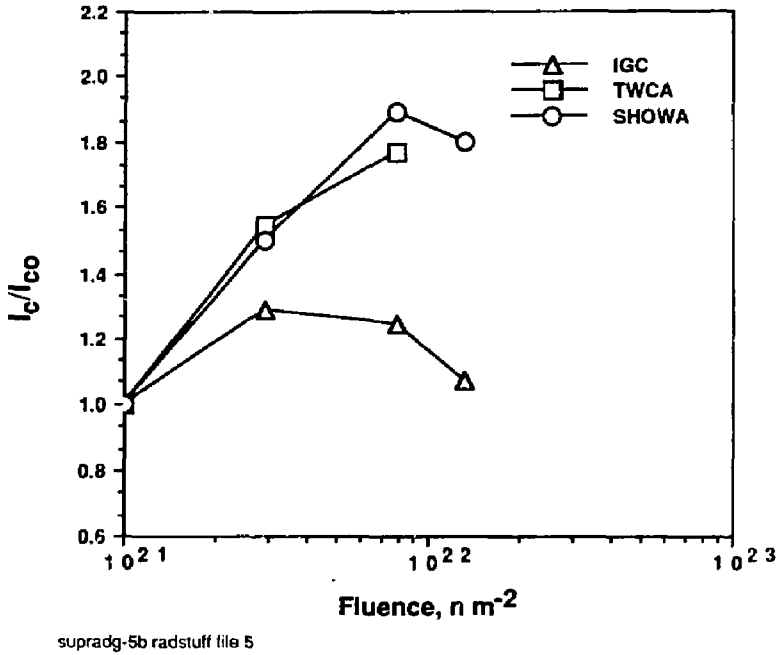

Figure 3.8: Critical current as a function of neutron fluence for multifilamentary Nb_3Sn superconductors irradiated at 4.2 K. The IGC material is a Ti alloyed wire. The TWCA and Showa wires are binary Nb_3Sn. Data from Ref. 7.

we find that at the end of life the Cu resistance at a 12 T field is approximately 1 nΩ·m sufficient to meet the requirements of full stability (1.2 nΩ·m).

An additional margin can be had by accounting for the effects of annealing of radiation damage at room temperature. It is generally accepted that annealing at room temperature will remove approximately 80% of the radiation induced resistivity in Cu. We assume that this effect will hold true for all subsequent anneals. Given that the ITER magnets will experience a minimum of 10 excursions to room temperature during their service life, a ratcheting of the radiation induced resistivity will occur. End of life resistivity, including magnetoresistivity, may be well below 1 nΩ·m.

3.5 Conclusions

The present state of development superconducting magnet materials is sufficient to meet the radiation damage limits of the of present 5.8 m baseline design. Superconductor and the stabilizer materials do not appear to be the limiting factor for the TF coils. Their radiation damage limits are well above the projected dose and fluence for the ITER 5.8 m machine. Radiation damage to the organic insulation may prevent the use of some materials, however, the present baseline machine has flux and dose limits that do not preclude the use of polyimide resins combined with S glass

reinforcement. Further low temperature irradiation data will be required to fully assess the use of epoxy based resins combined with S glass or high temperature fiber reinforcement. Such VPI resin systems would facilitate the use of wind and react technology eliminating the need for separation of magnet turns.

Bibliography

[1] W. Maurer, "Neutron and Gamma Irradiation Effects on Organic Insulating Materials for Fusion Magnets", Kernforschungszentrum Karlsruhe, Report No. KfK 3974, October 1985

[2] R.R. Coltman, Jr. and C.E Klabunde, J. Nuclear Mats., 103 and 104, 717, 1981.

[3] G. Liptk, et al., "Radiation Tests on Selected Electrical Insulating Materials for High-Power and High Voltage Application", CERN Report No. CERN 85-02, 1985.

[4] R. Poehlchen, Private communication, May 1988.

[5] R.E. Schmunk, L.G. Miller, and H. Becker, J. Nuclear Mats., V. 122 and 123, 1381, 1984.

[6] F. Weiss, et al., IEEE Trans. Mag., Vol. MAG-23, 976, 1986.

[7] M. Guinan, R. Hahn, and T. Okada, "Studies of Superconductors and Stabilizers for Fusion Magnets", Lawrence Livermore National Laboratory, UCID-21298, 1988.

[8] M. Sawan, J. Nuclear Mats, V. 122-123, 1376, 1984.

[9] C.D. Henning and J.R. Miller, "Magnet Technology for the Engineering Test Reactor," IEEE Trans. Mag., V. 24 (2), 1299, 1988.

[10] J.R. Miller, "TIBER Winding Pack Design", Lawrence Livermore National Laboratory, UCID-20510, 1986.

Chapter 4

Insulation System of the Magnets–R. Poehlchen

4.1 Introduction

The insulation of the magnet coils in Tokamaks is subjected to electrical stress, mechanical stress, thermal stress and irradiation by gamma-rays and neutrons. In the large machines which are at present either in operation or under construction or in the design phase (as for example JET, ASDEX Upgrade, NET, ITER) there is in general the need to go to the limit, at least in one respect, of the strength of the insulation. Usually the mechanical strength is the limiting factor in case of the Toroidal Magnet while the Poloidal Magnet will operate close to the limit of the electrical strength. An enhancement of the electric strength can be achieved rather easily by increasing the thickness of the insulation or by incorporating a layer of material with a high electric strength such as Polyimid for example. But the latter leads always to a considerable reduction of the mechanical strength. In order to achieve a maximum mechanical strength—in particular a maximum shear strength, interlaminar and for the bond to the conductor surface—a vacuum pressure impregnation (VPI) process has to be used. The insulation should consist of nothing but dry glass tapes (glass cloth, glass fabric) which has to be impregnated with a suitable epoxy resin system by a VPI process. For each individual application the resin system has to be selected on the basis of mechanical, thermal and electrical tests.

The insulation of the normal conducting Toroidal Coils of many tokamaks has been made this way, with excellent results. This manufacturing process is well established in industry. Therefore it is a big advantage when the same process can be used for superconducting coils as well, provided they are cooled by a forced flow of Helium through cooling channels in the individual conductors. It is planned to use this kind of cooling for all of the superconducting coils of ITER.

4.2 State of the Art, Illustrated by Examples

A good example for the kind of coil insulation described above is the set of Toroidal Coils for JET (Joint European Torus). Thirty-two D-shaped normal conducting coils form the Toroidal Magnet of JET. The total weight of each toroidal coil is about 12 ton. This is just the weight of the copper turns and the insulation there being no steel case around the individual coils. Using a carefully selected epoxy resin system the VPI process resulted in a monolithic winding. No deterioration of

the mechanical strength nor of the electric strength has been experienced during the five years of operation up to now.

Examples of large, superconducting coils with an epoxy insulation applied by a VPI process are the two European coils of the IAEA Large Coil Task (LCT) [1]. Some data about the EURATOM LCT coil which was manufactured by SIEMENS illustrate very well the present state of the art [2]:

	weight
Total weight of winding pack	18 ton
resin	600 Kg, approximate
glass fabric + filler	800 Kg, approximate
cross section of winding pack	(500 x 600) mm^2

The whole winding has been impregnated in one step. The actual impregnation, that is the filling of the mould with resin, took about 24 hours. The data given above reveals that a suitable resin system for large coils has to fulfill first of all the following requirements:

- low viscosity over a long impregnation time
- low reaction shrinkage.

The properties of such a insulation are well known at both—room temperature and at low temperature. See Figs. 4.1, 4.2, 4.3, taken from the Ref. [3] and [4]. The two types of specimen shown in these figures are seen by European coil manufacturers as the most suitable types. A rather comprehense description of insulation systems for Fusion Magnets is given in Ref. [6] with data about the mechanical strength and physical, thermal and electric properties at room temperature.

4.3 Recent Developments

Tests of small size test specimen have been carried out in European industry [10] in order to investigate if special glass fibres and ceramic fibres can be subjected to the reaction heat treatment ($\approx$ 700°C for 2 days) without causing a serious deterioration of the wetting property to the resin and the mechanical properties. The E-Modul, the UTS and the shear strength have been measured at LHe temperature—with good results. Therefore it appears to be feasible to apply the insulation (turn insulation and pancake insulation) to a coil, which is manufactured by using a "Wind and React" process, in the same way as it is done in case of a normal coil manufacturing process.

4.4 The Irradiation Resistance of an Organic Coil Insulation

The total irradiation dose seen by the coil insulation of ITER shall not exceed 5×10^9 rad.

This range is regarded as a realistic assumption for the design of the coils and the shield. A large number of data valid for room temperature are available about the degradation of the mechanical strength of organic insulation subjected to irradiation by neutrons and gamma rays [5,9]. Tables II, III, IV, V, VI are copies taken from these two reports. Only a few data are available on the same subject for liquid nitrogen temperature [3,7].

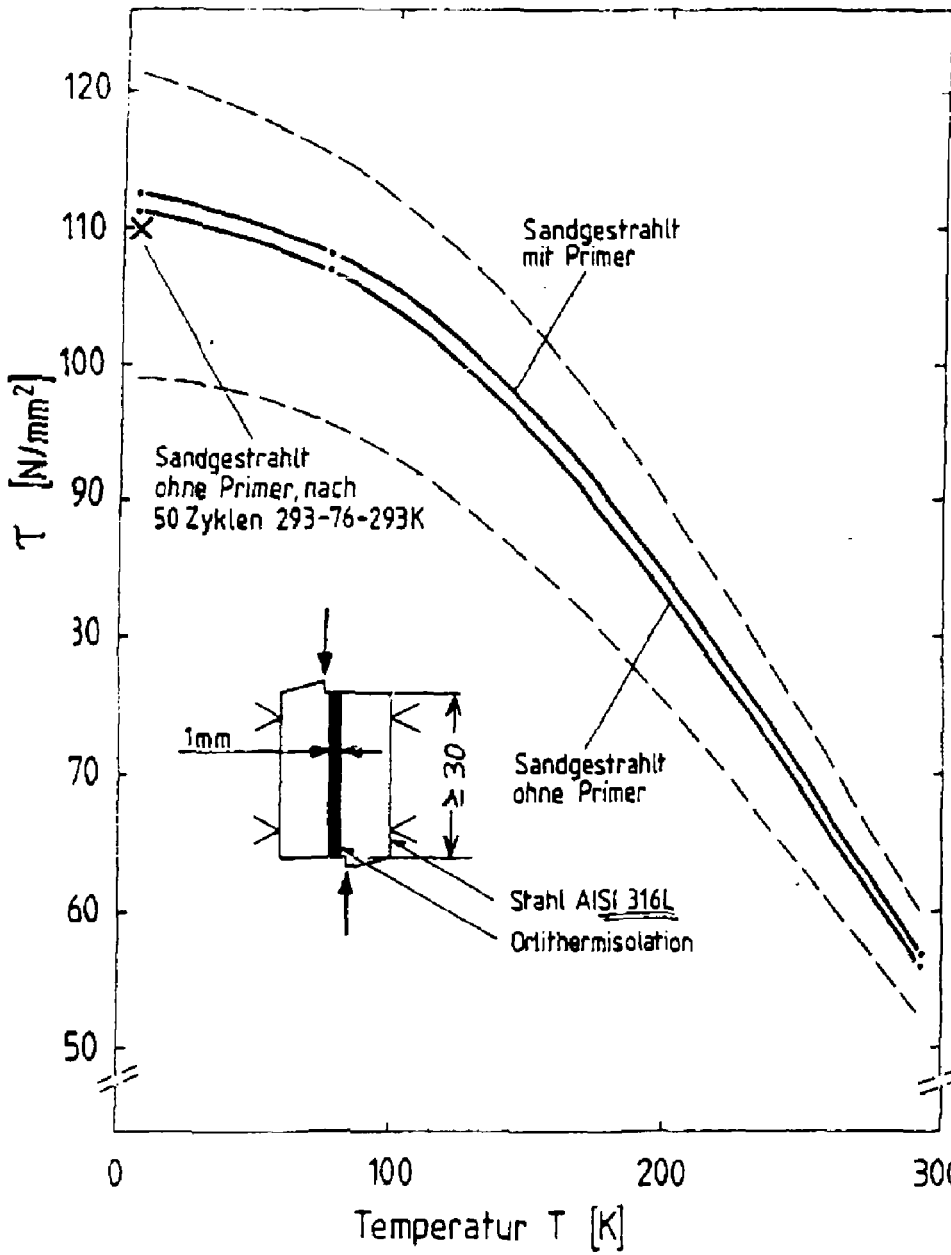

Figure 4.1: Shear testing, source BBC Zurick.

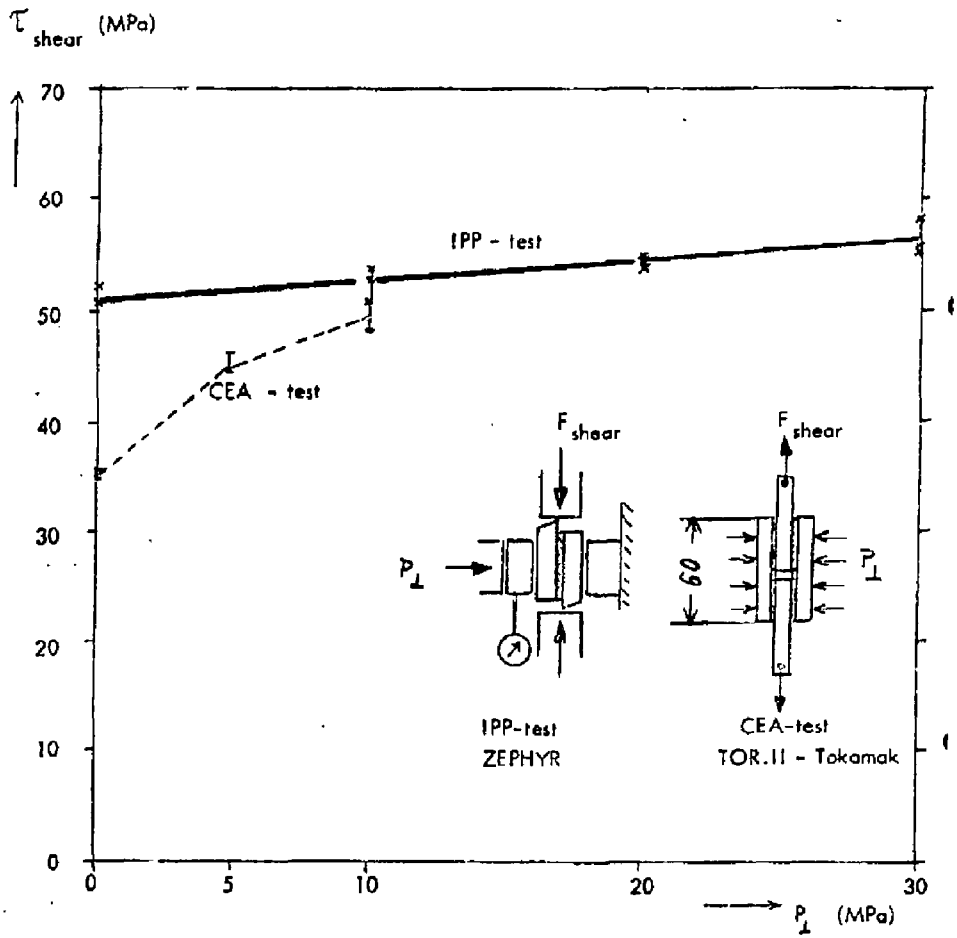

Figure 4.2: Shear breaking stress versus normal pressure. TF coil insulation between copper bars at RT, copper surface sandblasted and varnished.

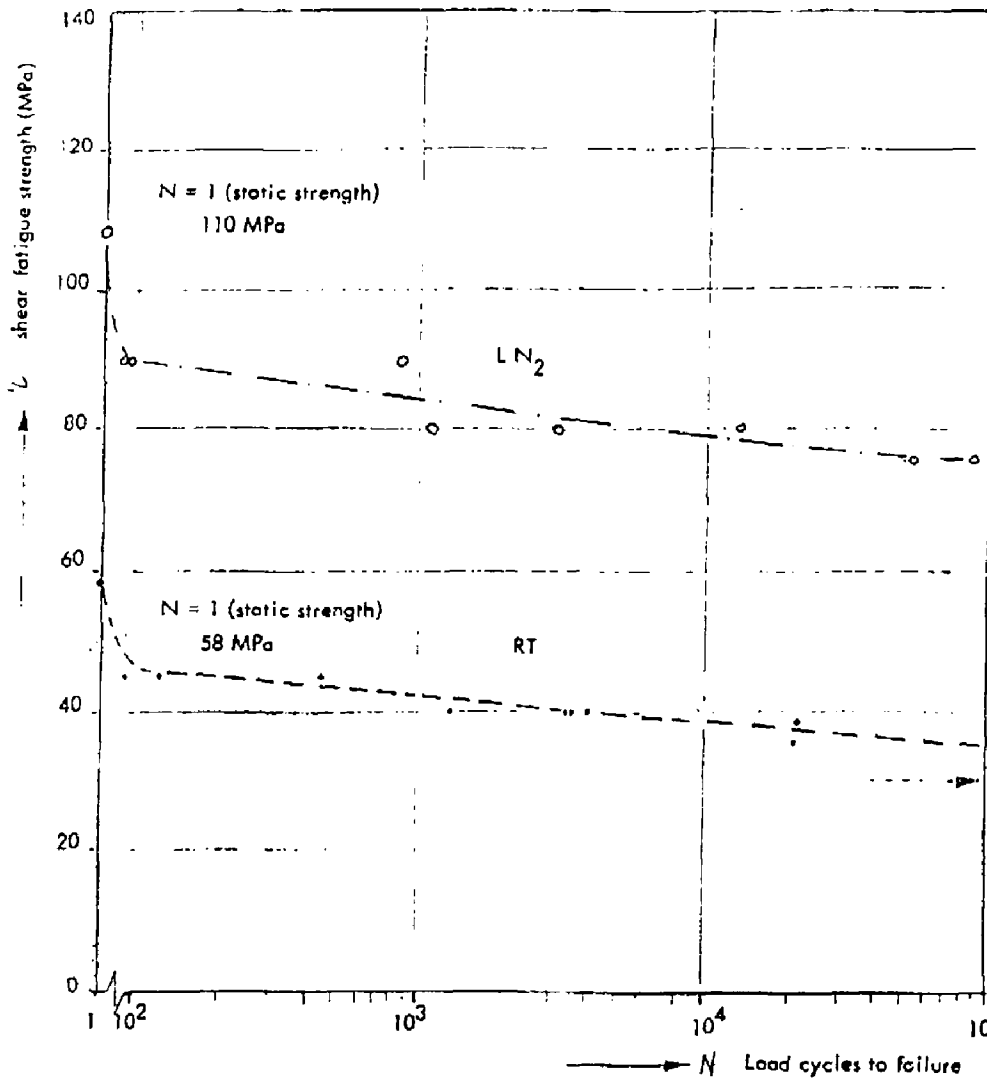

Figure 4.3: JET-shear sample, SS+/ insulation/SS+, insulation: 0.25 mm epoxy-glass, IPP-GFK Test IABG 11/80.

Table 4.1: Test samples have been irradiated to three different doses between 5×10^6 and 1×10^8 Gy at the ASTRA reactor in Seibersdorf (Austria).

No.	Material and Supplier	Dose (Gy)	Ultimate flex. strength S (N/mm^2)	Deflexion at break D (mm)	Modulus of elasticity M (N/mm^2)
176	Magnet coil resin Orlin-therm ©	0	450.3 ± 24.5	5.2 ± 0.3	$1.64 \pm 0.7 \times 10^4$
	reinforced with glass woven tape	1×10^7	419.9 ± 18.6	5.0 ± 0.1	$1.62 \pm 0.05 \times 10^4$
	type 2 with a special silane finish	5×10^7	387.5 ± 55 9	5.2 ± 0.5	$1.61 \pm 0.01 \times 10^4$
	12 h 165°C BBC Baden	1×10^8	281.5 ± 28.5	4.9 ± 0.3	$1.44 \pm 0.01 \times 10^4$
276	Magnet coil resin Orlin-therm ©	0	563.1 ± 25.5	4.8 ± 0 2	$2.22 \pm 0.14 \times 10^4$
	reinforced with a fibre-silanized	5×10^6	467.9 ± 58.9	4.5 ± 0.1	$2.15 \pm 0.29 \times 10^4$
	woven glass tape type 3	5×10^7	259.0 ± 28.5	3.2 ± 0.0	$1.76 \pm 0.15 \times 10^4$
	5h 135°C + 6h 160°C BBC Baden				
303	Magnet coil resin Orlin-therm ©	0	379.6 ± 14.7	4.7 ± 0.2	$1.76 \pm 0.23 \times 10^4$
	reinforced with a sandwich tape	1×10^7	385.4 ± 5.7	4.4 ± 0.2	$1.96 \pm 0.02 \times 10^4$
	built up of a fibre-silanized woven	5×10^7	236.2 ± 4.3	3.4 ± 0.9	$1.62 \pm 0.07 \times 10^4$
	16h 140°C BBC Baden	(5×10^9 rad)			

NOTE: This is a 7 MW pool reactor, and the irradiation position 11 is situated in the reactor core. The characteristics of the irradiation container and the radiation field are the following:

Dimensions of irradiation container:	4. diameter 46 mm; length 300 mm
Fast neutron flux (E > MeV):	2-3 $\times 10^{12}$n/cm^{2}sec;
Thermal neutron flux:	4 5 $\times 10^{12}$n/cm^{2}sec;
Gamma dose rate:	1-2 $\times 10^6$Gy/h
Irradiation medium:	water
Irradiation temperature:	30–40°C

The thermal neutron flux and the fast neutron spectrum are determined by means of activation detectors and the gamma dose rate is measured calorimetrically. More details about the irradiation conditions and dosimetry are given elsewhere [5].

No data are available on the strength of irradiated epoxy insulation of coils at liquid Helium temperature. It has to be stressed here that tests have to be carried out with test specimen which have been manufactured by a VPI process. Standard laminated sheets such as G10 and G11 are manufactured in a different way and will not give test results valid for this application

4.5 The Test Program

In order to establish a reliable data base for the ITER TF coils a test program has been initiated for measuring the shear strength of epoxy insulation after irradiation at liquid Helium temperature. This test programme is carried out by the NET Team using the low temperature irradiation facility of the TU Muenchen at Garching and the low temperature measurement laboratory at CEN/Grenoble. Figure 4 shows the test specimen. In a first step of the programme 40 specimens will be irradiated at liquid Helium temperature up to 5×10^8 rad which is the dose limit for NET. It can be foreseen to extend the programme to an increased dose limit of 10^9 rad for ITER. The shear strength will be tested at liquid Nitrogen temperature (30 specimens) and at liquid Helium temperature (10 specimens). For comparison 10 non-irradiated specimen will be tested at LN_2 temperature, and 10 at LHe temperature. Two types of resin will be tested with 4 types of reinforcing fibres (E glass, R glass, ceramic fibres, Trivoltherm (Kapton)).

Table 4.2: Insulation properties.

No.	Material and Supplier	Dose (Gy)	Ultimate flex. strength S (N/mm^2)	Deflexion at break D (mm)	Modulus of elasticity M (N/mm^2)
119	Polyimide + glass fibre	0	426.7 ± 71.6	3.3 ± 0.6	$2.31 \pm 0.11 \times 10^4$
		5×10^6	464.0 ± 83.4	3.6 ± 0.7	$2.33 \pm 0.06 \times 10^4$
		1×10^7	406.1 ± 102.0	3.1 ± 0.8	$2.23 \pm 0.20 \times 10^4$
		2×10^7	409.1 ± 84.4	3.2 ± 0.8	$2.22 \pm 0.22 \times 10^4$
	ISOLA	5×10^7	379.6 ± 50.0	3.4 ± 0.8	$2.09 \pm 0.11 \times 10^4$
152	KINEL 5.502	0	67.7 ± 7.8	2.1 ± 0.6	$5.82 \pm 0.07 \times 10^3$
	6h 180°C + 2h 200°C	5×10^6	63.7 ± 4.9	2.1 ± 0.2	$5.83 \pm 0.16 \times 10^3$
		1×10^7	53.0 ± 5.9	1.8 ± 0.3	$5.90 \pm 0.12 \times 10^3$
	Rhone-Poulenc	3×10^7	53.0 ± 6.9	2.1 ± 0.2	$5.27 \pm 0.48 \times 10^3$
197	KINEL 5.504	0	375.7 ± 18.6	2.1 ± 0.2	$2.03 \pm 0.03 \times 10^4$
		5×10^7	263.9 ± 1.0	2.9 ± 0.2	$1.73 \pm 0.06 \times 10^4$
	Rhone-Poulenc	1×10^8	193.3 ± 8.8	1.9 ± 0.1	$1.35 \pm 0.03 \times 10^4$
198	KERIMID 601	0	503.3 ± 42.5	5.0 ± 0.9	$3.05 \pm 0.28 \times 10^4$
	(glass fibre 181 E)	1×10^7	537.3 ± 16.7	5.3 ± 0.1	$2.97 \pm 0.13 \times 10^4$
		5×10^7	747.1 ± 159.5	5.3 ± 0.4	$3.34 \pm 0.31 \times 10^4$
	Rhone-Poulenc	1×10^8	143.6 ± 11.8	3.7 ± 0.2	$9.22 \pm 0.41 \times 10^3$
314	Polyimide + glass	0	108.9 ± 11.8	0.5 ± 0.1	$2.06 \pm 0.10 \times 10^4$
	Compound 17287	5×10^5	51.0 ± 0.8	0.6 ± 0.0	$8.74 \pm 0.13 \times 10^3$
	Shamban	1×10^5	55.9 ± 1.0	0.7 ± 0.0	$8.85 \pm 0.11 \times 10^3$
315	Polyamide-imide	0	144.9 ± 33.3	8.0 ± 4.0	$4.25 \pm 0.11 \times 10^3$
	Compound 17286	5×10^5	165.8 ± 9.2	8.7 ± 1.7	$4.36 \pm 0.15 \times 10^3$
	Shamban	1×10^6	145.2 ± 16.7	7.3 ± 2.0	$4.06 \pm 0.13 \times 10^3$
316	Polyimide	0	36.7 ± 4.2	2.8 ± 0.4	$6.61 \pm 0.47 \times 10^3$
	Compound 17242	5×10^5	49.6 ± 5.9	1.4 ± 0.2	$7.20 \pm 0.35 \times 10^3$
	Shamban	1×10^6	53.9 ± 0.4	1.4 ± 0.1	$7.75 \pm 0.13 \times 10^3$

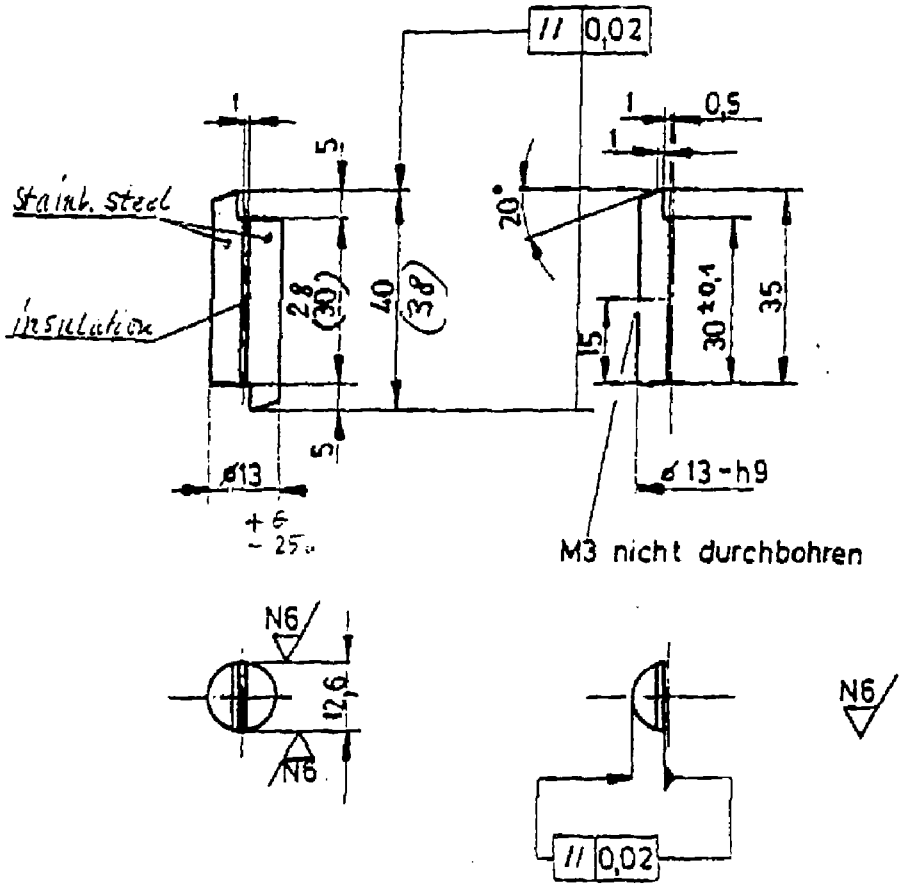

Figure 4.4: Test configuration.

Table 4.3: Characteristics of irradiation positions.

Irradiation position	Gamma dose rate (Gy/h)	Neutron flux ($cm^{-2}s^{-1}$)		Precision in dose (%)		Cooling	Sample temperature (°)
		Thermal	Fast (E > 1 MeV)	γ	n		
Plane 1 Central containers	2.5×10^3	4.3×10^{11}	1.8×10^{10}	±5	±7	Forced air	62
Plane 1 Lateral containers	1.75×10^5 to 1.95×10^5	1.6×10^{11}	1.5×10^{10}				
Position 35	1×10^4 to 1×10^5			±10 for central part		Air	45

Table 4.4: VPI insulation without mica content.

No.	Material type supplier remarks	Dose (Gy)	Flex. strength at max. load S (MPa)	Deflexion at max. load D (mm)	Modulus of elasticity M (GPa)	RI IEC 544-4 at 10^5 Gy/h
349	Solventless epoxy resin (CERN	0.0	231.0 ± 11.4	2.9 ± 0.3	17.55 ± 0.99	7.9
	(No. 97), reinforced with	3.0×10^6	225.6 ± 26.5	3.0 ± 0.3	16.88 ± 0.72	
	thermally desized glass-cloth	1.0×10^7	244.5 ± 17.2	3.3 ± 0.3	17.46 ± 0.66	
	Orlitherm-S insulation	3.0×10^7	168.0 ± 31.8	3.6 ± 0.6	15.81 ± 1.02	
	BBC, Baden	1.0×10^8	104.1 ± 10.3	2.6 ± 0.1	13.53 ± 0.88	
	Magnet coil insulation application					
350	Solventless epoxy resin No. 332	0.0	324.0 ± 18.8	4.2 ± 0.3	19.24 ± 0.65	> 8.0
	(Base: DGEBA + MNA + other					
	components), reinforced with	3.0×10^6	301.2 ± 19.2	4.0 ± 0.3	19.06 ± 0.63	
	fibre-silanized glass-cloth					
	backing (Type 3)	1.0×10^7	272.7 ± 8.8	3.6 ± 0.3	18.63 ± 0.94	
	Orlitherm-D insulation	3.0×10^7	248.8 ± 11.7	3.5 ± 0.2	19.16 ± 0.20	
	BBC, Baden	1.0×10^8	170.0 ± 8.0	3.5 ± 0.8	15.78 ± 0.51	
	Magnet coil insulation application					

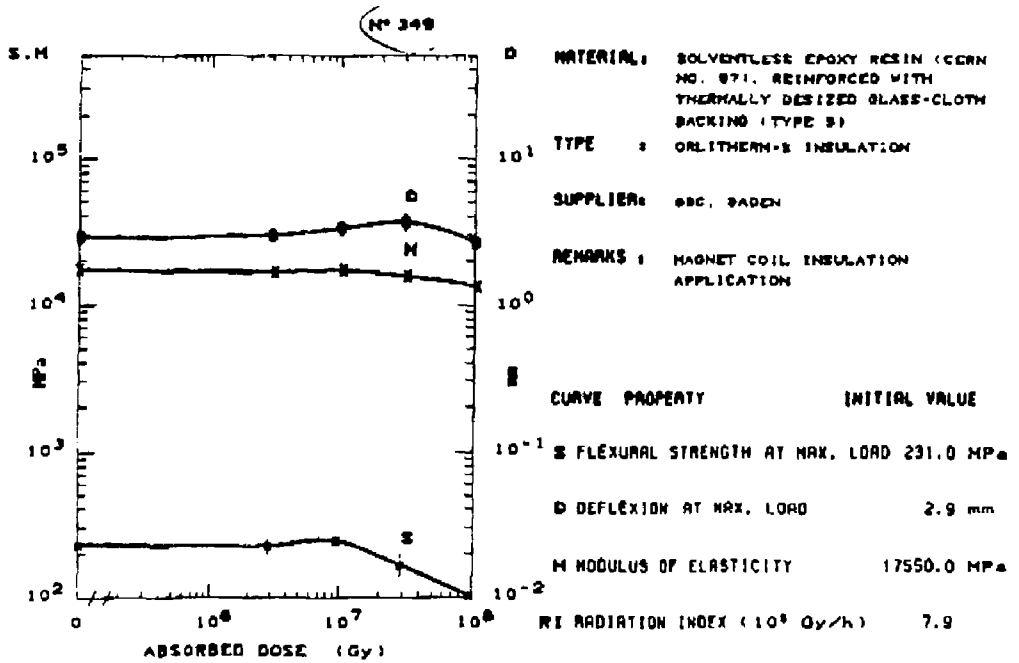

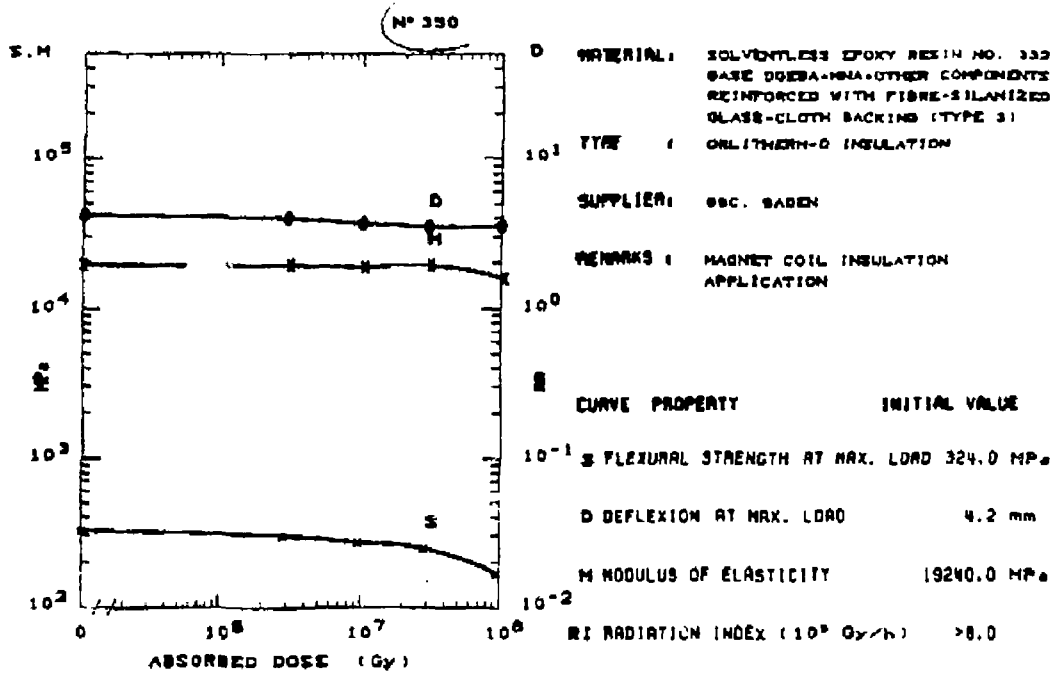

Table 4.5: Radiation damage.

Bibliography

[1] "The IEA Large Coil Task" Fusion Engineering and Design, Vol. 7 (1988) Nov. 1-2.

[2] Siemens report: "Epoxies for Low Temperature Application Inpregnation Technology" H. Haker, C. Albrecht, W. Ihlein, Siemens AG, Cryog. Eng. Conf. 1983.

[3] Internal ZEPHYR Report No. 35: "Insulation Materials for High Field Magnets of the ZEPHYR Experiment" IPP Garching, J.E. Gruber, 1981.

[4] Internal ABB report.

[5] CERN 85-02: "Radiation Tests on Selected Materials for High Power and High Voltage Application" Liptak, Schuler (BBC), Maier, Schoenbacher (CERN), Haberthuer, Mueller, Zeier (ISOLA Werke).

[6] Insulation Systems for Magnets used in Experiments for Nuclear Fusion and High-Energy Research, Publication No. CH-IM 312110 E.

[7] Journ. of Nucl. Materials 115 (1983): "Low Temp. Neutron and Gamma Irradiation of Glass Fibre Reinforced Epoxies", H.W. Weber (Atominstitute Wien), E. Kubasta, W. Steiner (Inst. Fuer Physik, Wien), H. Benz, K. Nylund (BBC).

[8] CERN 77-03, "Low Temperature Irrad. Effects on Materials and Component for S.C. Magnets for High Energy Physics Application, 1976.

[9] CERN 79-08, Part II, 1979 Compilation of Radiation Damage Test Data.

[10] ABB HISM 20313 Feasibility Study of the NET on Inner Poloidal Coils, May 1987.

Chapter 5

Critical Current Density and Strain Sensitivity—J.R. Miller

All the conductor designs presently proposed for ITER magnet systems are intended to be force-cooled by helium at supercritical pressures as a means of reliably extracting the sizable heat loads expected from both nuclear heating and ac losses. Consequently, the magnets cannot be operated isothermally, making knowledge of the temperature dependence of the critical properties of the candidate superconductors essential for their design. For NbTi, the cricial current density varies very nearly linearly with temperature, especially in the ranges of temperature and field where the ITER magnet designs are to be carried out, i.e.

$$J_c(B,T) = J_{c0}(B)\left[1 - \frac{T}{T_c(B)}\right].$$

The critical current density of Nb_3Sn can also be represented similarly with reasonable accuracy. However, a very complete experimental study done recently by Hamshire et al. [1] has established the functional form of J_c on B and T more precisely and has given it a firmer physical basis. For our purposes, their relation can be expressed in the following form:

$$J_c(B,T) = C_0\,[B_{c2}(T)]^{-1/2}\,(1-t^2)^2 b^{-1/2}(1-b)^2,$$

where

$$b = \frac{B}{B_{c2}(T)}$$

and

$$t = \frac{T}{T_{c0}}$$

Hampshire et al. did not give a specific form for $B_{c2}(T)$, but they did give data that is quite consistent with the form,

$$B_{c2}(T) = B_{c20}(1-t^2)\left(1 - \frac{t}{3}\right)$$

Hampshire et al. did not explore the strain dependence of J_c in their work, but it should be possible, with no loss of legitimacy, to meld their work with Ekin's [2] to include the strain

Table 5.1: Critical parameters for state-of-the-art Nb_3Sn conductors.

Superconductor	B_{c20m} (T)	T_{c0m} (K)	C_0 (A·T·mm^{-2})
Binary Nb_3Sn	24	16	26,400
Ternary Nb_3Sn	28	18	15,700

dependence. The basis of Ekin's Strain Scaling Law (SSL) is that the strain dependence of the critical current is determined by dependencies of the zero-temperature upper critical field B_{c20} and the zero-field critical temperature T_{c0}. For the conductors he examined, Ekin found that, to very good accuracy, these parameters depend on the intrinsic strain ϵ according to the following relations:

$$B_{c20}(\epsilon) = B_{c20m}\left(1 - a \mid \epsilon \mid^{1.7}\right)$$

and

$$T_{c0}(\epsilon) = T_{c0m}\left(1 - a \mid \epsilon \mid^{1.7}\right)^{\frac{1}{3}},$$

where a = 900 for $\epsilon < 0$ and a = 1250 for $\epsilon < 0$ gave the best fit to his data for multifilamentary Nb_3Sn wires. The subscript m on variables in the above equations indicates the maximum value, occurring at zero intrinsic strain.

The combination of Ekin's SSL with the B,T dependence of Hampshire et al. is then simply accomplished by the appropriate substitutions of $B_{c20}(\epsilon)$ and $T_c(\epsilon)$. Values for the parameters B_{c20m}, T_{c0m}, and C_0 that reflect the performance of state-of-the-art binary and ternary Nb_3Sn superconducturs are given in Table 5.1. As the final choice of conductors for ITER is narrowed these values will need to be tuned to match the eventual selection.

The field dependence of state-of-the-art NbTi alloy wires is given by relations of somewhat different form [3]. In the ranges of field and temperature where these wires might be useful for ITER designs, the following relations can be expected to hold:

$$T_c(B) = T_{c0}\left(1 - \frac{B}{B_{c20}}\right)^{0.59}$$

and

$$J_{c0} = J_{c00}\left(1 - \frac{B}{B_{c20}}\right),$$

where

$$T_{c0} = 9.3K, \;\; B_{c20} = 15\,T, \;\; \text{and} \;\; J_{c00} = 7300\ \text{A/mm}^2.$$

In all the above, the current densities refer to the fraction of the cross- section of the composite wire apart from any stabilizing copper. For the Nb_3Sn wires, this means the current density is over the Nb_3Sn layer, any unreacted Nb core, the residual bronze, and the barrier protecting the purity of the stabilizer.

Figure 5.1 gives a graphic representation of the field dependence of NbTi and binary and ternary Nb_3Sn as predicted by the above relations. For the Nb_3Sn conductors, -0.3% (compressive) strain has been assumed. The temperature for the Nb_3Sn data has been taken as 4.2 K. Note that in the neighborhood of 12 T, the 4.2 K performance levels of

both the Nb_3Sn conductors and the 1.8 K performance of NbTi are comparable. However, in magnet systems that must accept significant heat loads in the windings, whether from nuclear absorption or ac losses, operation at 4.2 K will be preferred because refrigeration will be less by about one-third. The reduced sensitivity to radiation damage of binary Nb_3Sn, as compared to that of the ternary, is a consideration that may make it the overall preferred choice for the TF windings.

There is evidence that Ekin's SSL for predicting the dependence of critical current of Nb_3Sn on uniaxial strain ϵ can be generalized by replacing that variable with the total distortional strain

$$< \epsilon >= \left[\frac{(\epsilon_1 - \epsilon_2)^2 + (\epsilon_1 - \epsilon_3)^2 + (\epsilon_2 - \epsilon_3)^2}{2(1+\nu)^2} \right]^{\frac{1}{2}}$$

and appropriately adjusting the fitting parameters [4]. Note that such a generalization would preclude the asymmetry in critical current degradation vs compressive and tensile strains shown by Ekin's SSL. However, even if such a generalization is warranted, it does not make the task of determining $< \epsilon >$ any less difficult. The determination of strains due to loads transverse to the longitudinal direction of a composite wire is a good example. This is made especially difficult by the complex series/parallel combinations of load paths through constituents of quite different mechanical properties.

We consider first the simpler case of determining the longitudinal strain in the composite wire and present some approximate methods. The strain in the superconducting filaments at operating conditions of the magnet depends not only on the complex electromagnetic loading but also on the composition of the total conductor system and the detailed history of fabrication of both the conductor and the magnet winding. If the magnet is to be manufactured by a wind-and-react technique, only cooldown and operating strains need to be taken into account. But these can be troublesome because of the large differential cool-down strains of some of the constituents of the conductor system. For the special case of wind-and-react fabrication with cable-in-conduit conductors (CICC), some simple relations may be useful for predicting the prestrain and total longitudinal intrinsic strain at operating conditions. Experiments on a group of CICC test specimens suggest the initial prestrain to be given by [5]

$$\epsilon_{init} = \frac{F(f_{He})E_{sh}\left[\left(\frac{\Delta l}{l}\right)_{sh} - \left(\left(\frac{\Delta l}{l}\right)_{fil}\right)\right] - (\sigma_{cu,y}A_{Cu} + \sigma_{bz,y}A_{bz})}{F(f_{He})E_{sh}A_{sh} + E_{fil}A_{fil}},$$

where

$$F(f_{He}) = 0.15 \exp\left[-\left(\frac{f_{He}}{0.4}\right)^2\right]$$

is an experimentally determined factor, depending on void fraction fHe, that accounts for strands of the cable not being rigidly linked to the jacket during cooldown (i.e. longitudinal, differential contraction of the sheath relative to the cable does not result directly in longitudinal compressive strain in the filaments inside the twisted strands of the cable since some of that contraction causes bending and torsion of the strands, which cause relatively less degradation of the critical current). The total longitudinal intrinsic strain in the filaments

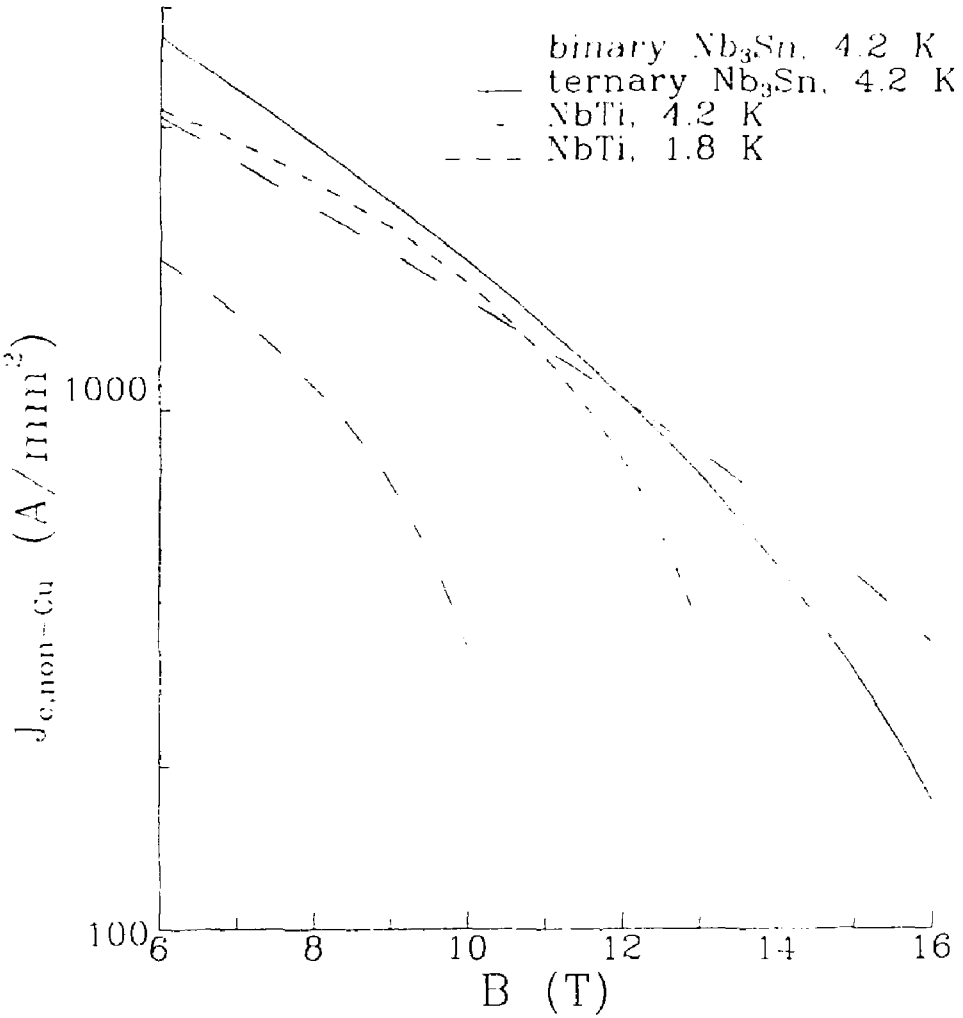

Figure 5.1: Field dependence of attainable non-copper critical current densities in ITER-relevant, technical superconductors.

then results from the superposition of any additional strain allowed by the structural support system in operating the magnet. For example, we might expect to write for the CICC system.

$$\epsilon = \epsilon_{init} + C\epsilon_{sh}$$

where ϵ_{sh} is the longitudinal strain allowed in the structural sheath of the CICC. The coefficient C accounts for the angle of twist of the cable and other features of its configuration. For a group of test specimens, $C = 0.86$ appeared to be an appropriate value [5,6]. The formulae above are still developmental in nature, but in principle, similar relations can be written for any conductor system or magnet fabrication technique. Producing predictive relations like these for ITER candidate conductor systems must be a primary objective of the magnet R&D effort.

In addition to cooldown and operating strains, magnet designs using react-and-wind fabrication techniques must also account for bend strains. Bend strains have opposite signs on either side of the neutral axis of the conductor with a maximum magnitude of

$$\epsilon_{b,max} = \left(\frac{1}{R} - \frac{1}{R_o}\right)\left(\frac{\delta}{2}\right),$$

where R_o is the original radius (i.e., that of the reaction spool), R is the bend radius of the winding, and d is the thickness of the active element of the conductor perpendicular to the axis of bending. In the high field region of a TF winding, R is practically infinite so that

$$\epsilon_{b,max} = \pm\frac{\delta}{2R_o}.$$

In principle, react-and-wind designs allow for the elimination of all the longitudinal strains except bending strains. But one must accurately predict the cooldown and operating strains and devise a means to precisely control the winding tension. Bending strains cannot be eliminated because they have opposite sign on either side of the neutral axis of the conductor.

The important effect of transverse strain on depressing the critical current of Nb_3Sn superconductors has been clearly shown [7,8,9]. The database is still slight at present, however, and the complexity of the load paths through the conductor in the transverse direction makes transverse stress σ_t a more convenient parameter for correlation of the data. Still, the proper estimation of σ_t from applied transverse load and conductor geometry is not totally obvious. Ekin [7] and Specking et al. [8] equated σ_t to the transverse load divided by the projected area of the conductor. Summers and Miller [9] suggested using the projected area of the core, the portion containing superconducting filaments and residual bronze, for a correlation that is more representative of the actual transverse stress at the filaments. They compared the data of Ekin and Specking et al. with their own, all taken at different fields, by using an adaptation of Ekin's SSL for correlation. The results are shown in Fig. 5.2. The scatter in the Summers and Miller data results from their use of multistrand CICCs, in which the transverse load path in the particular cable is complicated by location and orientation of individual wires relative to their neighbors.

The degradation of critical current due to transverse loads will have a major influence on the design of conductors for the TF magnets and possibly on the design of the overall TF

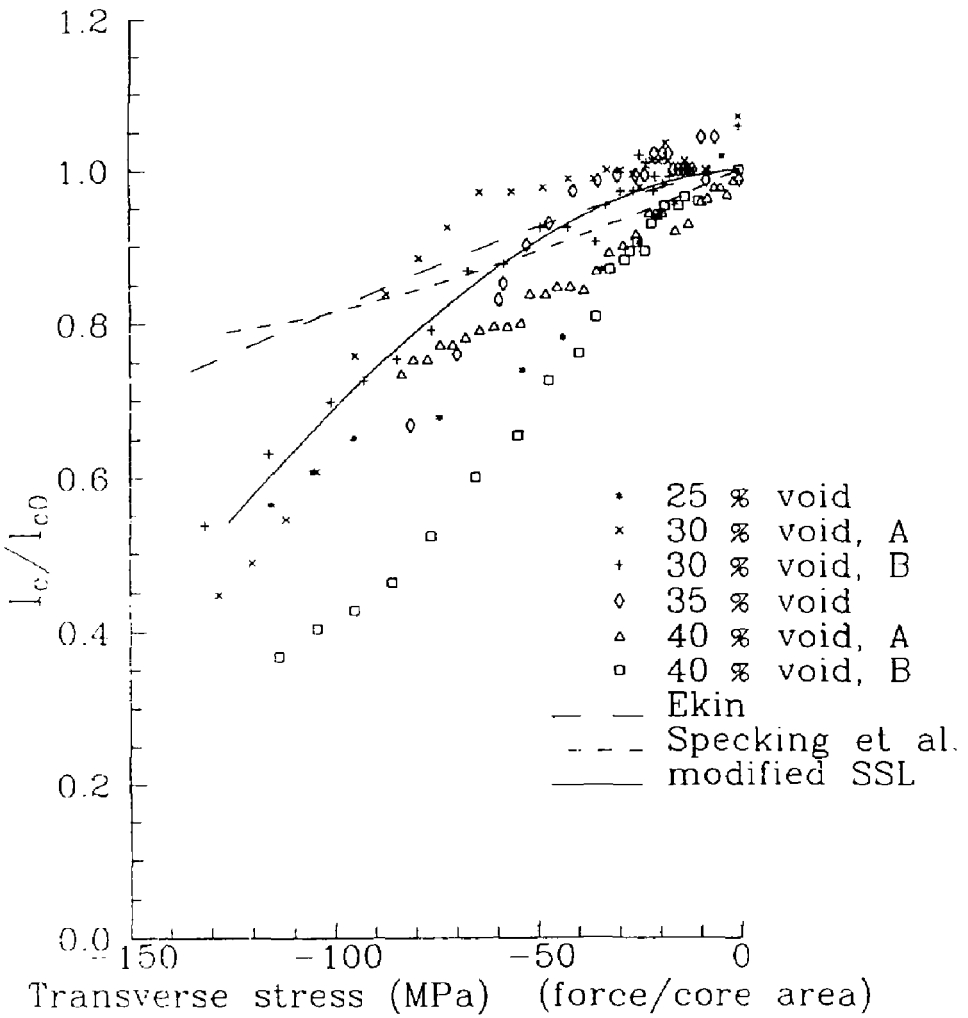

Figure 5.2: Normalized critical current vs transverse stress from recent experiments on both single wires and cables. The solid curve is a modification of the Strain Scaling Law, suggested for prediction of this effect.

magnet system as well. The windings of the TF magnets, because of the large out-of-plane loads caused by electromagnetic interaction with the PF system and the plasma, have high transverse loads imposed on them in certain regions. In addition, if the TF coils are wedged, as a means of helping to support the in-plane centering loads, the transverse loads on the conductors are even greater. Monolithic conductor designs, in which the superconductor and stabilizer elements of the conductor have high moduli, provide excellent structural support but are fundamentally more sensitive to degradation of their current capacity by these transverse loads. The cable-in-conduit conductor, as a consequence of its electrically active conductor element having an extremely low transverse modulus relative to the external sheath, should be relatively insensitive to externally applied transverse loads. There has been some trepidation that such conductors would be overly sensitive to internally generated transverse loads, because of enhancement of stresses at the wire crossings. However, preliminary tests indicate this may not be a serious problem [9].

Bibliography

[1] D.P. Hampshire, H. Jones, and E.W.J. Mitchell; *IEEE Trans on Magn. MAG-21* (1985) 289.

[2] J.W. Ekin, *Cryogenics* **20** (1980) 611.

[3] M.S. Lubell, *IEEE Trans on Magn. MAG-19* (1983) 754.

[4] R.M. Scanlan, R.W. Hoard, D.N. Cornish, and J.P. Zbasnik; *Mechanical Properties of High-Current Multifilamentary Nb_3Sn Conductors,* Filamentary A15 Superconductors; Suenaga and Clark, eds. (Plenum Press, NY, 1980) p. 221.

[5] J.R. Miller, M.R. Chaplin, L.T. Summers, M.M. Steeves, and M.O. Hoenig; *IEEE Trans on Magn. MAG-23* (1987) 1547.

[6] J.R. Miller, J.P. Zbasnik, L.T. Summers, and M.R. Chaplin; *Investigations of Cable-Sheath Interactions in Cable-in-Conduit Superconductors*, Lawrence Livermore National Laboratory Report No. UCRL-96000, June 8, 1987.

[7] J.W. Ekin, *J. Appl. Phys.* **62** (1987) 4829.

[8] W. Specking, W. Goldacker, and R. Flukiger, *Adv. Cryo. Eng.* **34** (1987) 569.

[9] L.T. Summers and J.R. Miller, *The Effect of Transverse Stress on the Critical Current of Nb_3Sn Cable-in-Conduit Superconductors*, presented at the 1988 Applied Superconductivity Conference, San Francisco, CA.

Chapter 6

Toroidal Field Coil Structural Analysis—N. Mitchell

6.1 Introduction

The structural analysis for the TF coils in the design definition phase falls into three categories:

1. Scoping analyses, using crude representations of the coil system but considering a range of major geometric variations and coil concepts
2. Detailed analyses, to look at one concept in some depth
3. Fault analyses, to look at the coil behaviour under fault conditions that may act in some areas as design drivers

The analyses are based on the set of working parameters for ITER with R = 5.8m, a = 2.0 that had a substantially larger plasma size than that finally recommended for the pre-design phase. The coil concepts follow the design philosophy derived at the start of the ITER joint work, and the aim of some of the scoping analysis was to investigate the structural philosophy. The main alternative option for the TF coils is the concept where the centre of the toroidal field reference solution where the legs are wedged together to form a vault with an independant central solenoid. The analyses have also enabled critical design features for the concept to be quantified to enable the impact of non-optimum design due to interfaces with other design areas (such as maintenance) to be assessed.

The overall electromagnetic loads on the coil are presented in Table 6.1. These loads are those used in the following analyses.

6.2 Scoping Analyses

The scoping analyses have concentrated on two models. The first of these uses a beam and shell representation of the coils to look at the effects of geometry and stiffness changes in the

Table 6.1: Electromagnetic Loads on Coil

Centring Force/coil	450 MN		
Vertical Force/1/2 coil	220 MN		
Overturning Moments	MNm		
Time	0	Start of burn	End of burn
Moment, R-axis	62	109	113
Moment, Z-axis	±31	±249	± 250
Peak value of out of plane force during burn	16 MN/m		

inner and outer intercoil structure [1], and to consider the possibility of bucking the coils on the solenoid. Examples of these models are shown in Fig. 6.1.

The second set of models considers a crossection of the coil inside the central vault [2,3] (Fig. 6.2) and looks at the effect of the shape of the winding pack on the peak compressive stresses in the vault.

After a series of preliminary calculations, two concepts were derived and analysed with the beam and shell model that appeared to be the most promising of the cases considered. The first utilises an independant TF coil structure where the inner legs of the TF coils are supported by wedging. The overturning forces are taken by an inner and outer intercoil structure and by friction between coils within the vault. The second utilizes a TF coil support integrated with the central solenoid. The inner legs are supported by a torsion/bucking cylinder and central solenoid. The overturning forces are taken by an inner and outer intercoil structure, and by the inner legs of the coils and the torsion cylinder. In each case the concept has been iterated to achieve stress levels in coils and insulation that appear broadly acceptable, although further minor adjustments may be necessary.

Using as a basis the reference wedged solution, sensitivity studies were performed on the following parameters:

- Effect of radial extent of inner intercoil structure
- Effect of coil stiffness over upper access gap
- Effect of coil stiffness near outer equator
- Effect of stiffness of outer intercoil structure

All of these have a significant influence on the overall stress levels. The extent of the inner intercoil structure is particularly important in influencing the shear stresses between adjacent coils within the central vault, as shown in Fig. 6.3. Minor changes in the radial extent of the structure have a significant influence on the torsion passed to the vault, or, it may be expected that changes in the out of plane load distribution can have a similar effect.

Due to the uncertainty of the out of plane force distribution, a restricted inner intercoil structure should be used to give high shear forces in the inner intercoil leg. Even with an extended structure, changes in the plasma parameters can produce a different equilibrium with a new out of plane force distribution, that could cancel the effect of the extension.

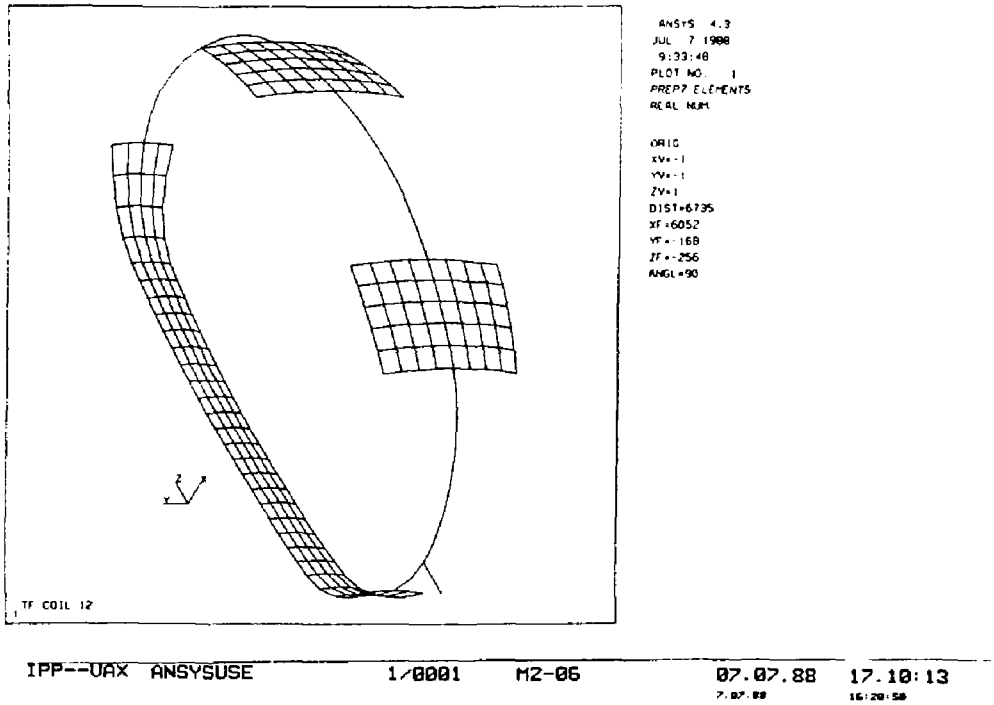

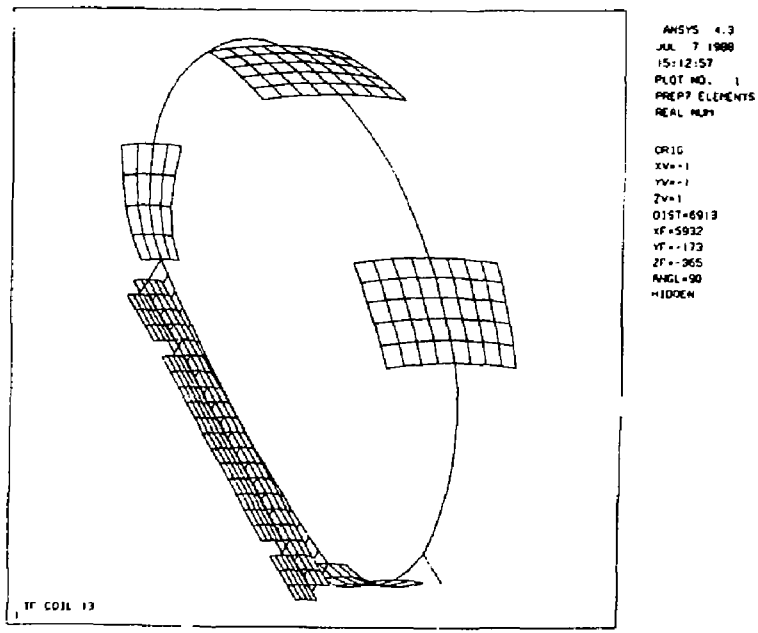

Figure 6.1: TF coil-beam and shell representation.

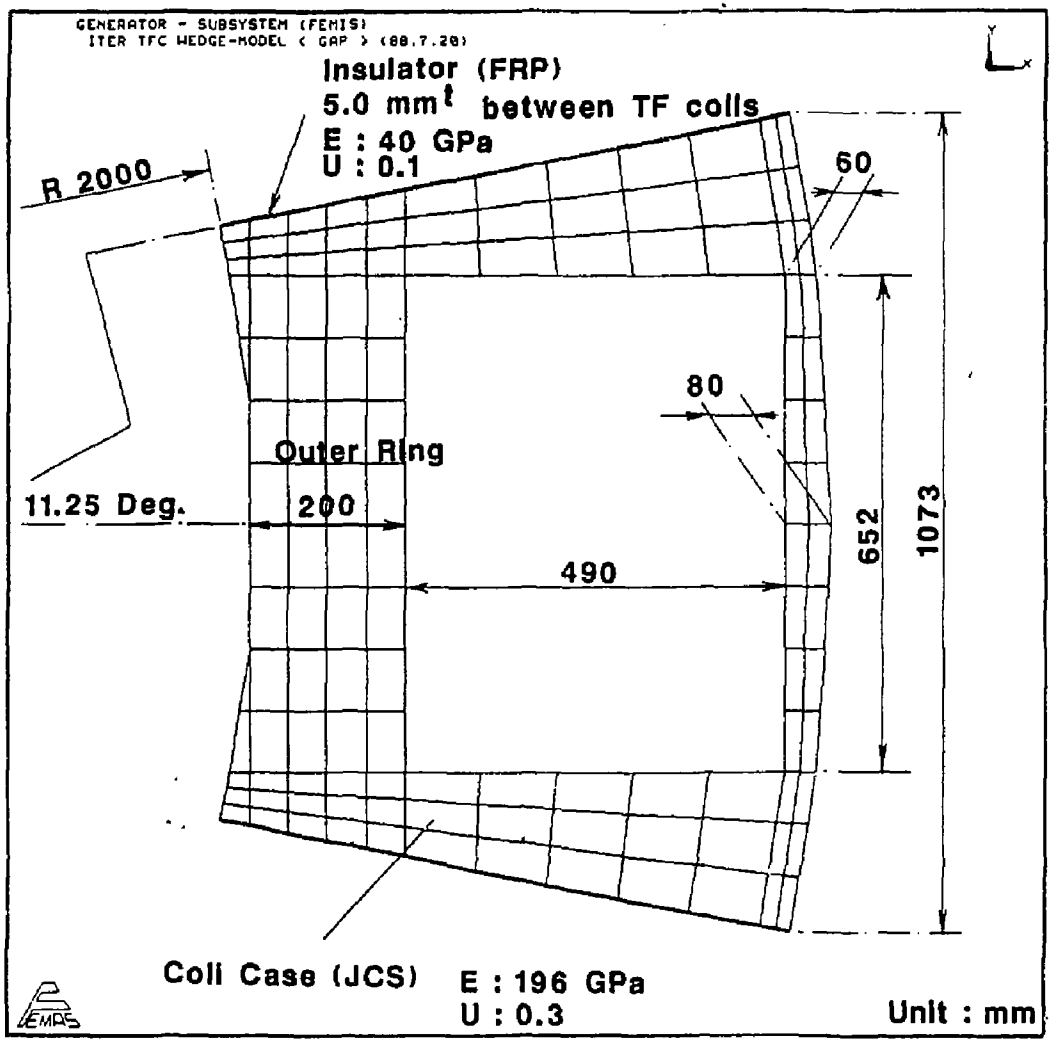

Figure 6.2: Cross section of ITER TF coil case: Model 2D-1.

Figure 6.3: Shear stresses between adjacent coils within the central vault.

It thus seems in line with the requirement for machine flexibility to adopt the more severe requirement.

The compressive loads in the central vault are dependant on the winding pack geometry. Figure 6.4 shows how the average hoop compression varies with the nose thickness, assuming that the winding carries none of the transverse load. There is a peaking factor on this average compression due to the shape of the wedge. This is analysed with a finite element model as shown in Fig. 6.2. The resulting Tresca stress is shown in Fig. 6.5 for the case and insulation. Figure 6.5 shows that the peaking factor for the case (peak/average) Tresca stress is 1.3. This peaking is due to variations in the compressive hoop stress.

6.3 Detailed Analysis

Various finite element models, shown in Figs. 6.6, 6.7, and 6.8 [1,5], have been used for a more detailed examination of the 'reference' coil geometry of Fig. 6.9 [1,3,4]. The models vary in the amount of support structure provided for the outer coil, but are generally in agreement with each other and with the earlier scoping calculations. Particular features and results from the models are as follows:

The model of Fig. 6.6 uses shell elements to represent the coil case and brick elements to represent the winding. It aims to find the shear stresses in the winding pack in local coordinates, since these are the shears acting across the insulation layers. Values of shear stresses up to 28 MPa are found, which are close to the allowable limit of 30 MPa. The model of Fig. 6.7 looks at the in-plane stresses in a two dimensional crossection and gives detailed stress distributions in the case (Fig. 6.10). The results from the model of Fig. 6.8 are still being postprocessed, but will provide detailed stress levels. An example of the stresses in the outer ring of the coil case due to in plane forces only is shown in Fig. 6.11.

6.4 Fault Analysis

Two TF coil models for faulted conditions have been developed. Fig. 6.12 shows the central vault crossection with one coil with zero current. Figure 6.13 show the whole coil assembly when shear transmission within the vault and inner intercoil structure is lost. Much more consideration of fault conditions is required but initial results are that neither of these conditions will cause castastrophic failure of the magnet system.

6.5 Analysis of Alternative Options

The main alternative option for the TF coils, that of bucking the coils onto the central solenoid instead of wedging them around an independent solenoid, has been analysed using beam and shell models such as those shown in Fig. 6.1. The attraction of the alternative is that it potentially allows the central solenoid to support the TF coils centering forces in compression which is then relieved as the solenoid is energised. This reduces the necessary space for TF and PF coil support. The problems of such a solution are that the force/stress

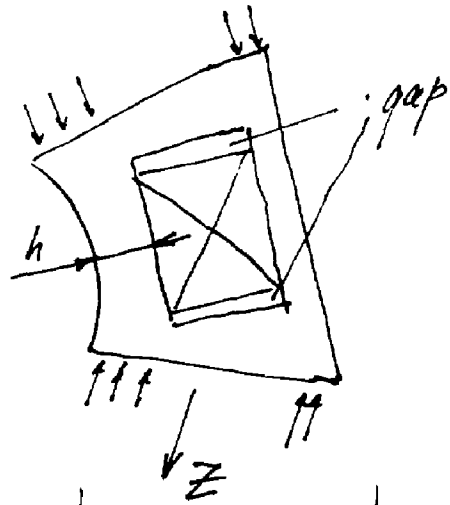

TFC Case : E_c = 200GPa

Winding pack: E_{wp} = 80GPa

Average stress in coil nose

table 1.

N	Variant	TFC Case σ_z (MPa)	TFC Case σ_{int} (MPa)	TFC Case $\delta_{in.leg}$ (mm)	TFC Case $\delta_{outer\ leg}$ (mm)	Winding pack σ_z (MPa)	Winding pack σ_{int} (MPa)	Outer vault σ_z (MPa)
1	h = 23cm	-520	700	-6,1	13,2	0	114	
2	h = 28cm	-450	600	-5,1	13,3	0	110	
3	h = 33cm	-390	530	-4,4	13,5	0	110	

Figure 6.4: Average stress in coil nose.

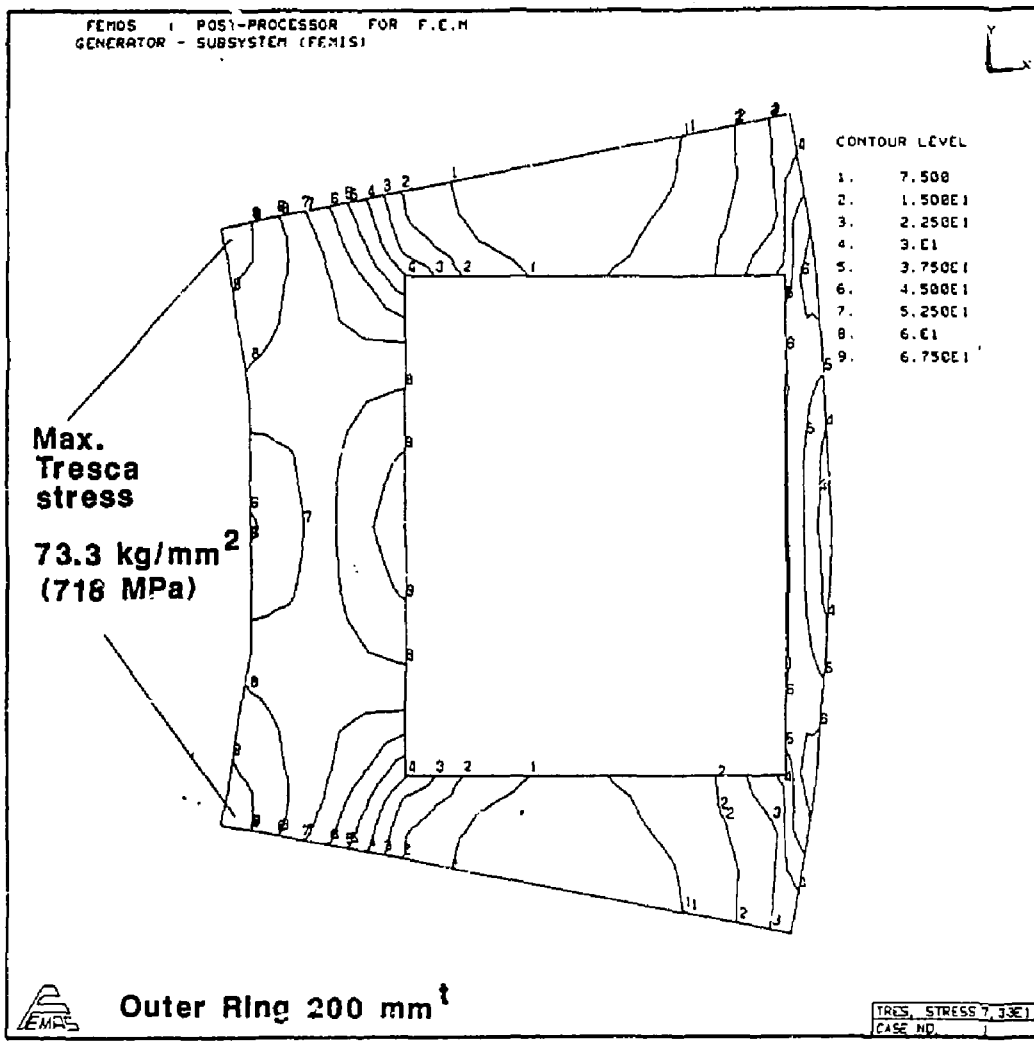

Figure 6.5: Contours of constant Tresca stress in TF coil case.

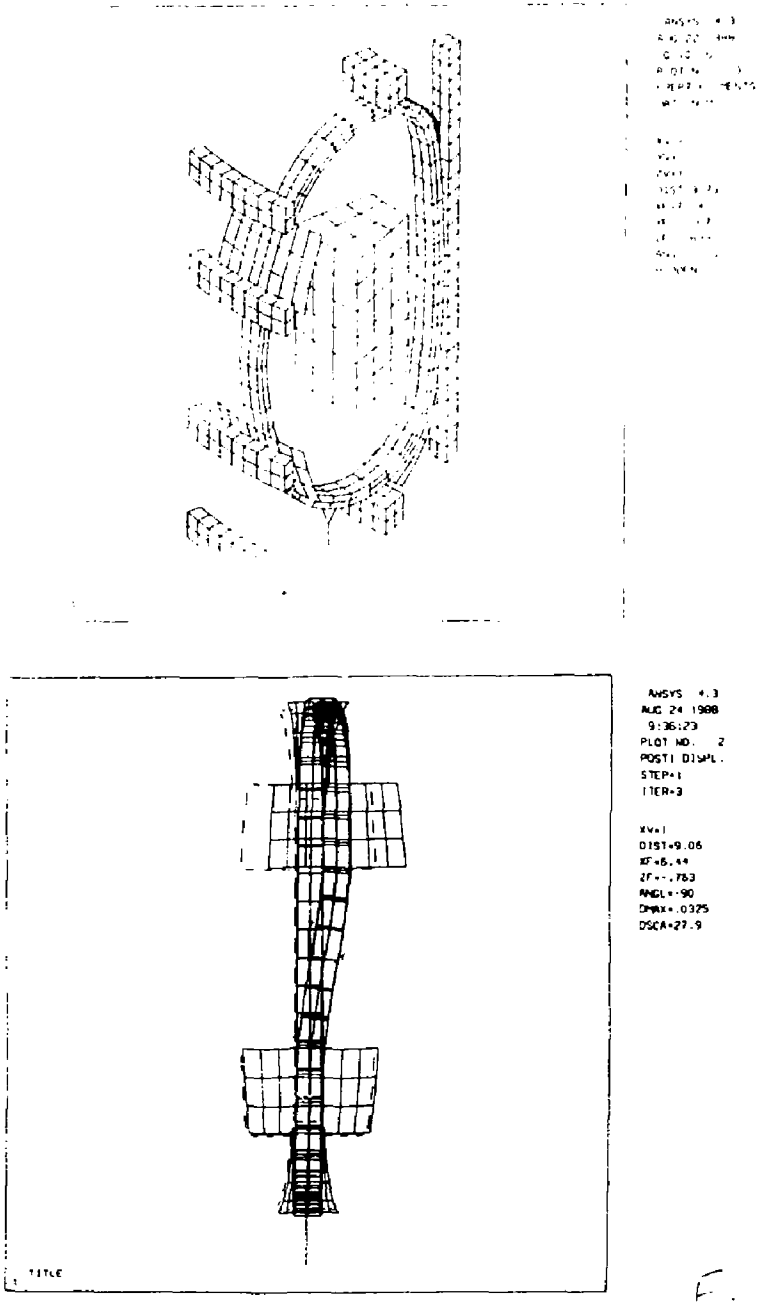

Figure 6.6: Shear stresses in the winding pack.

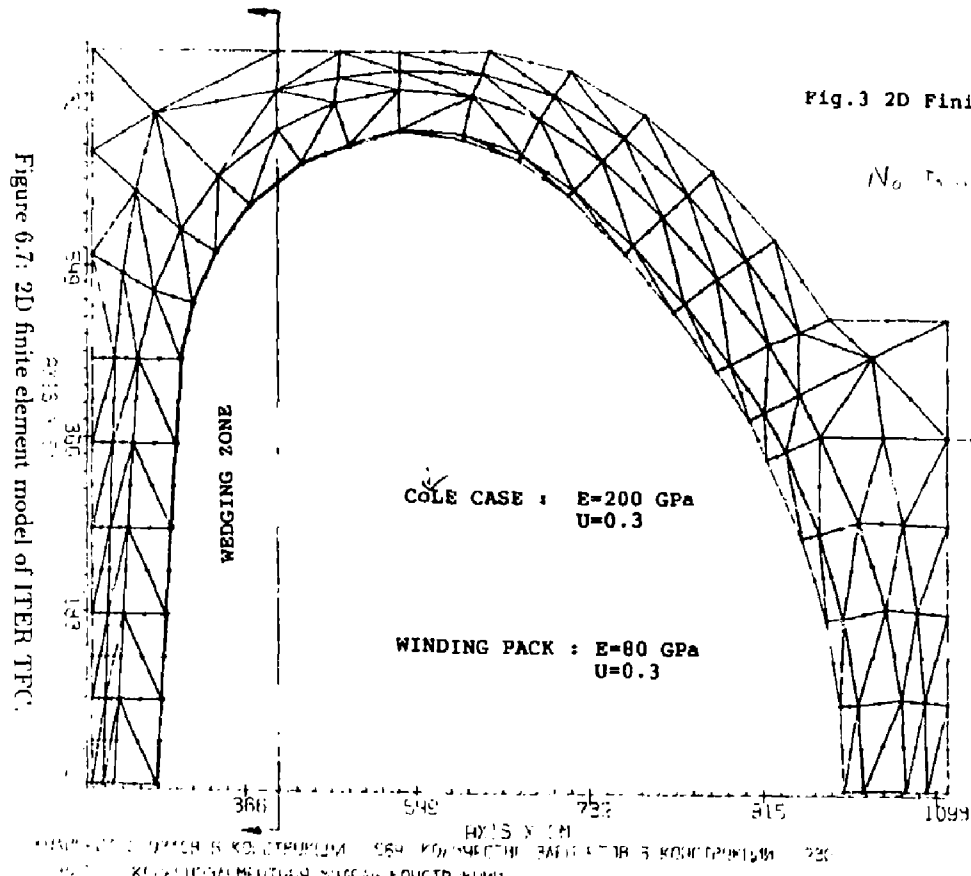

Figure 6.7: 2D finite element model of ITER TFC.

Fig.3 2D Finite Element Model of ITER TFC

Integral tensile force:
$F_y = 199\,MH$

Integral centering force:
$F_x = -225\,MH$

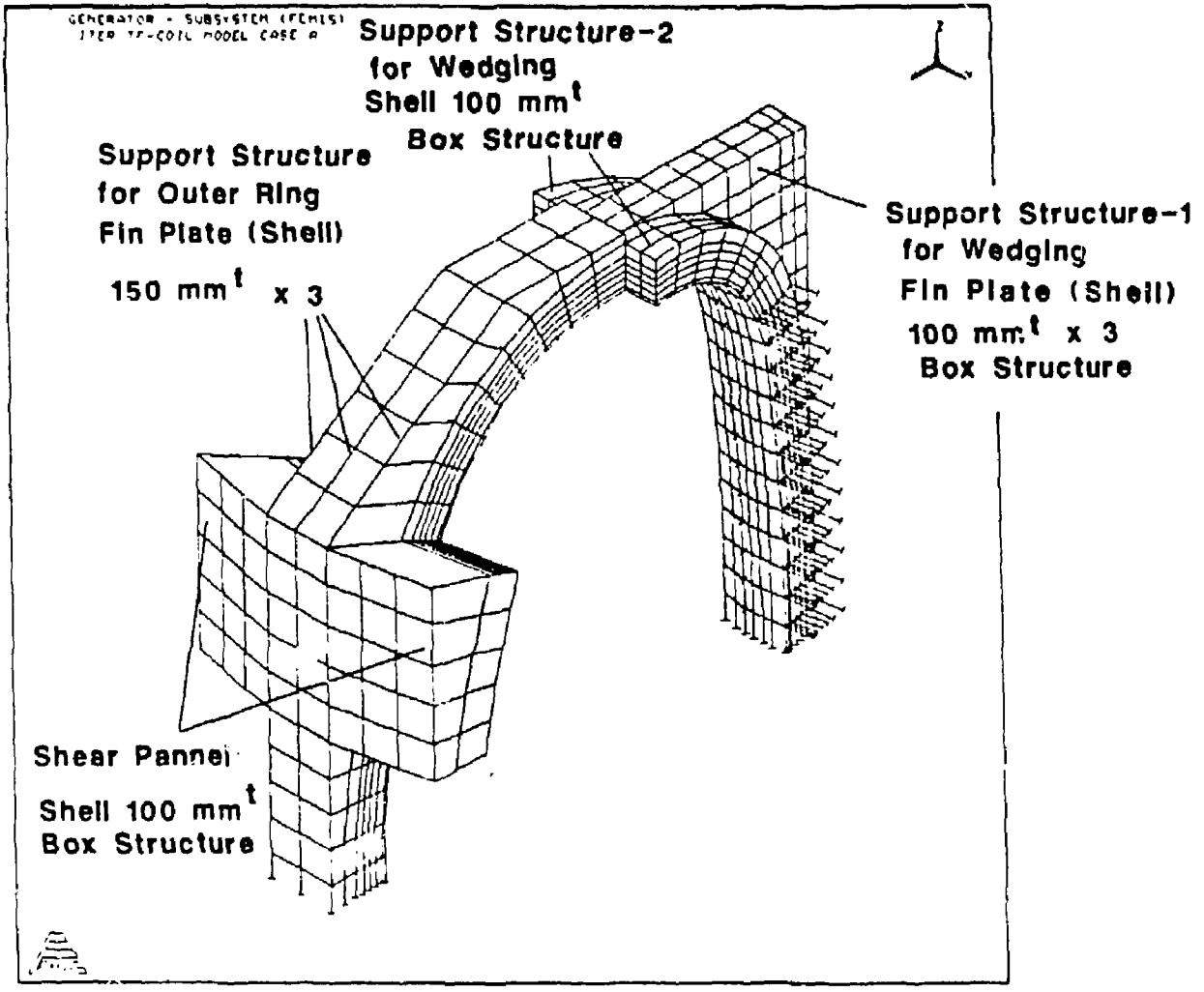

Figure 6.8: Stress analysis model of ITER TF coil: Model 3D-1.

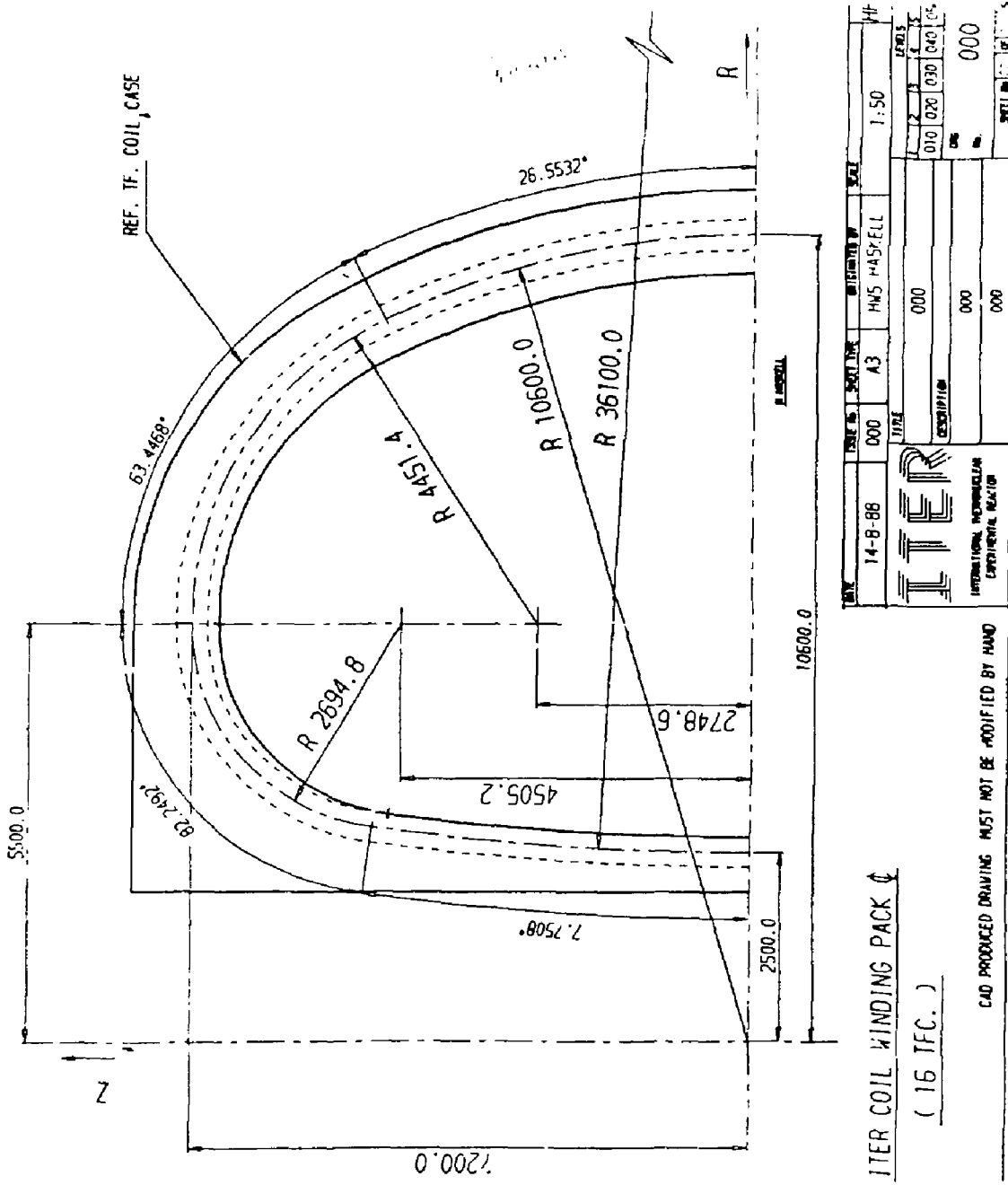

Figure 6.9: ITER coil winding pack.

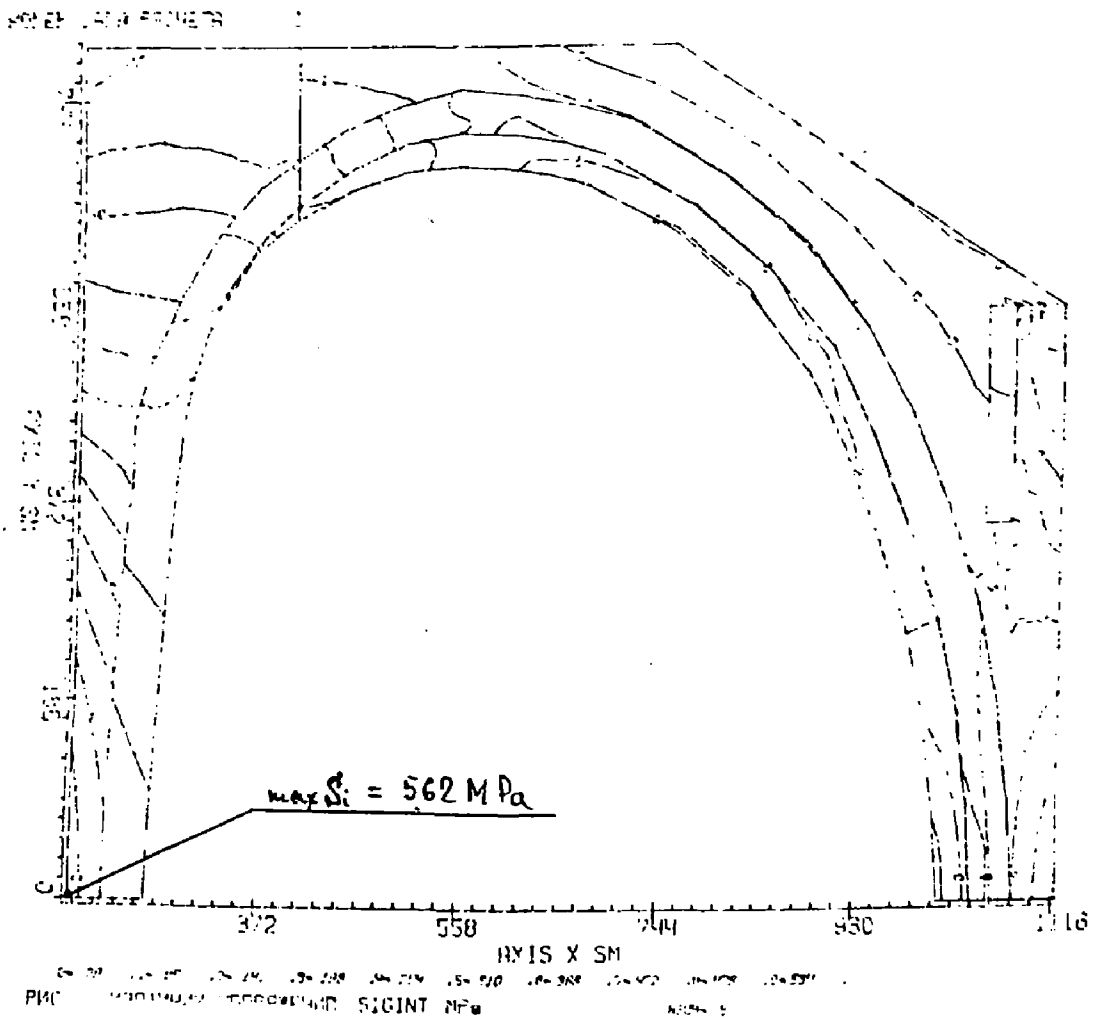

Figure 6.10: ITER TFC Case: Si, MPa.

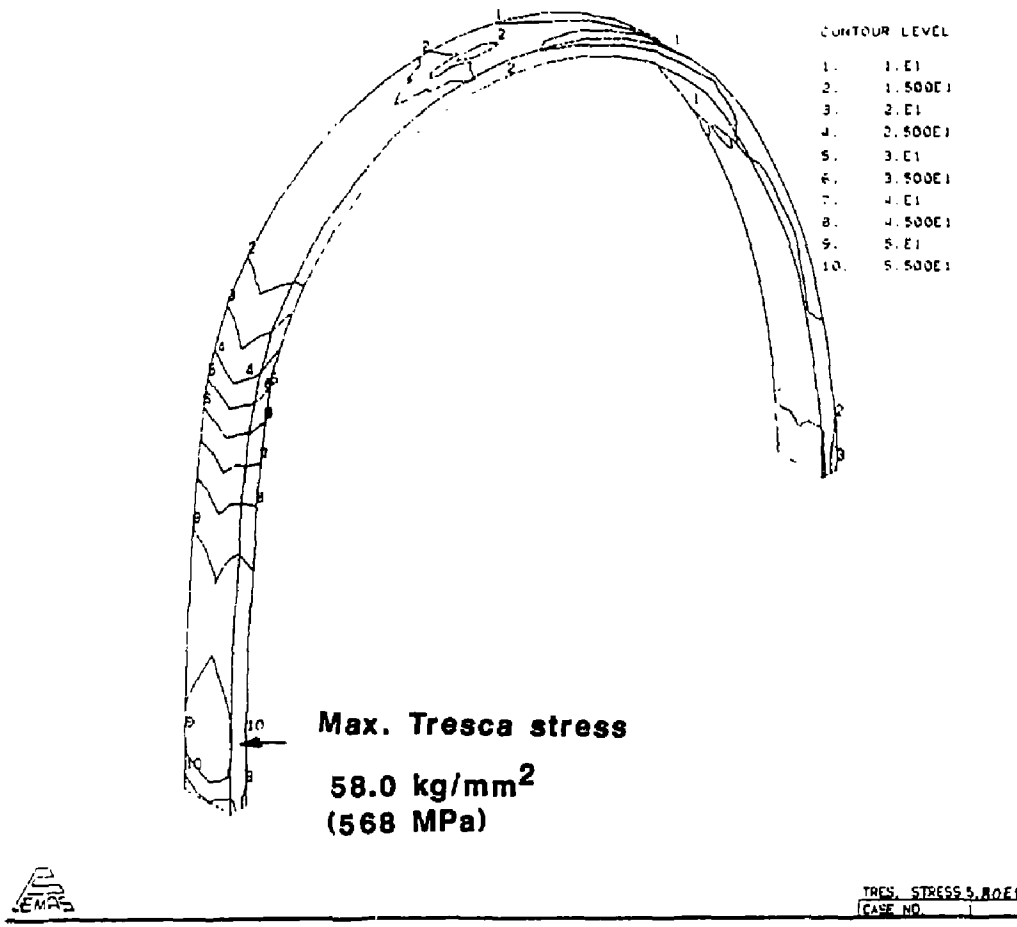

Figure 6.11: Contours of constant Tresca stress in the outer ring of ITER TF coil due to *hoop force*: Model 3D-2.

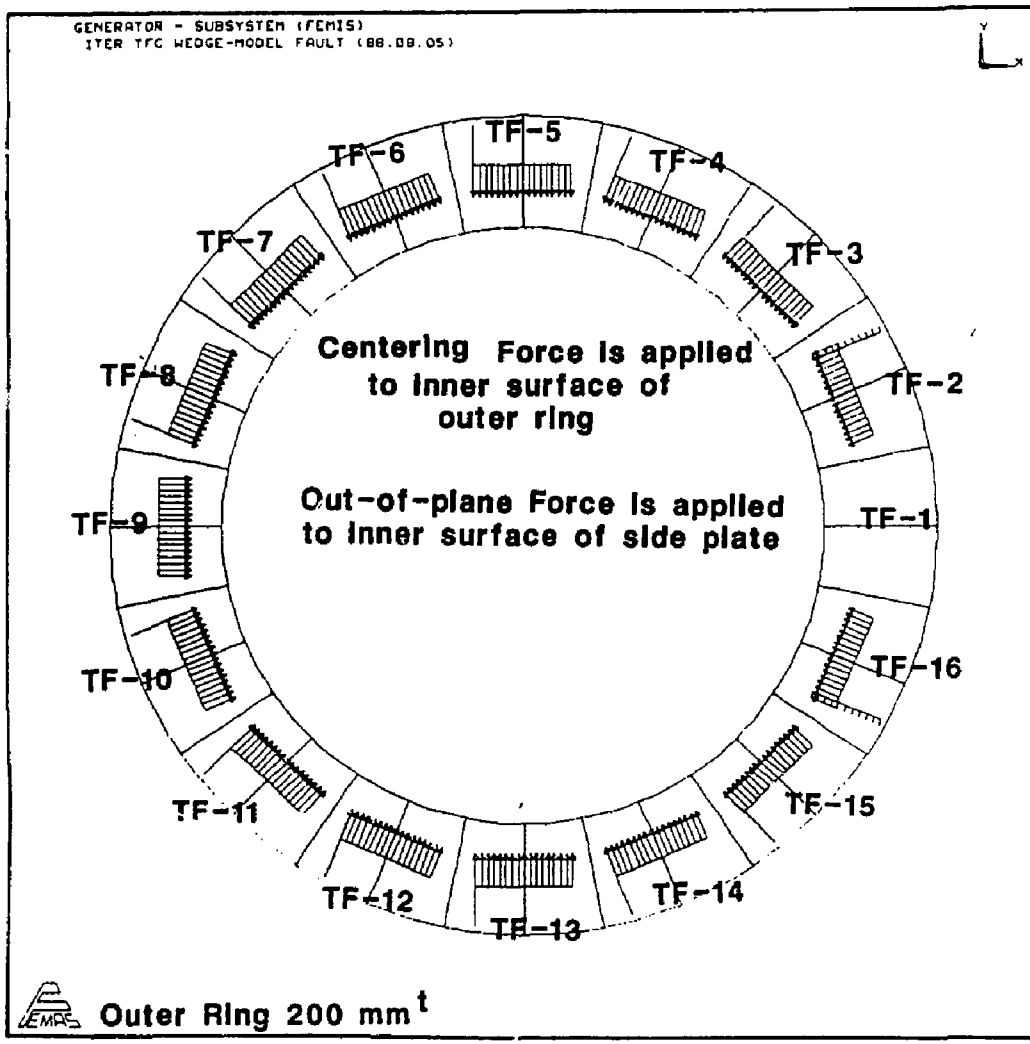

Figure 6.12: Loading condition of centering force and out-of-plane force.

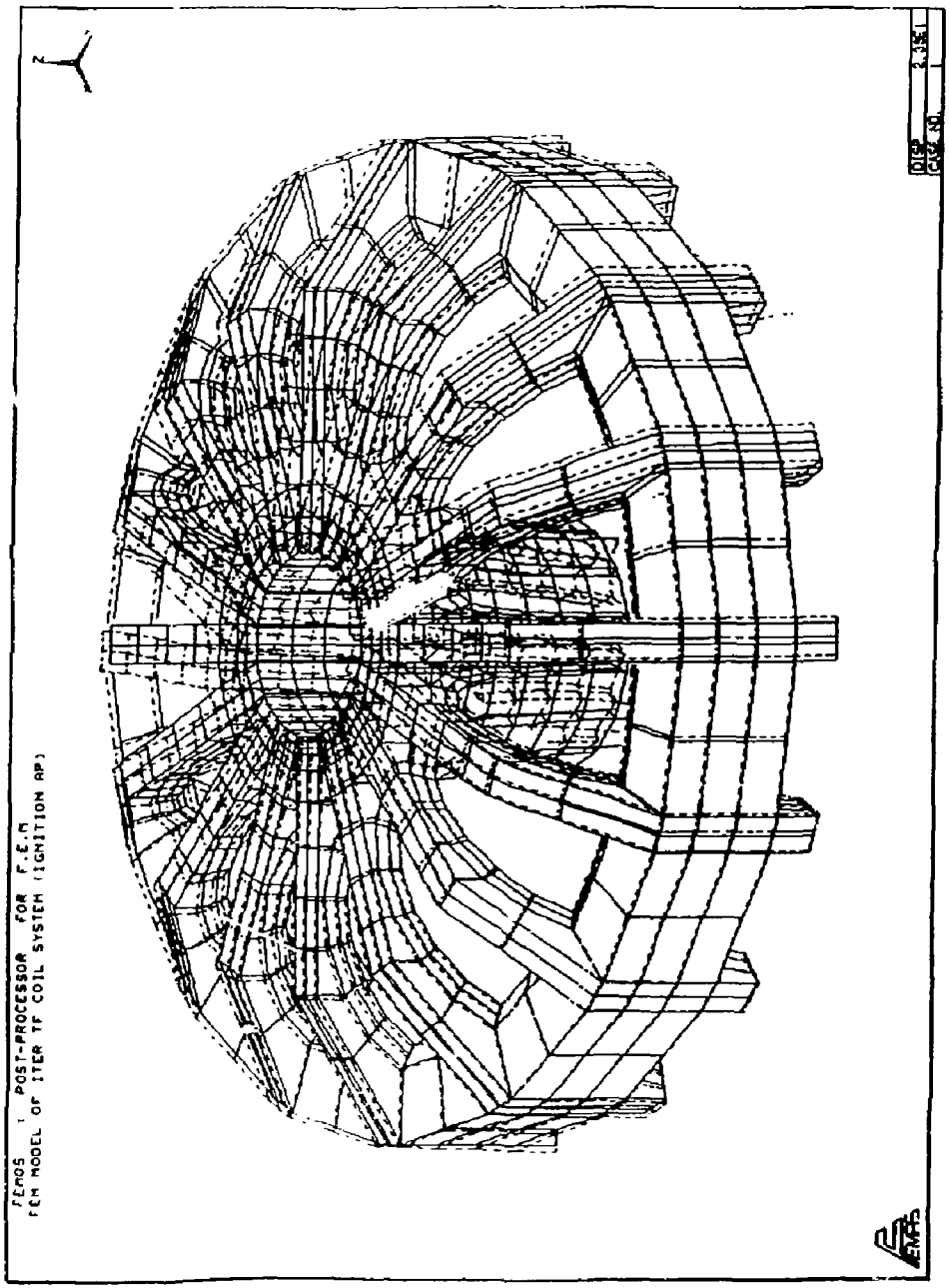

Figure 6.13: Deformation of ITER TF coil due to over-turning load (ignition approach). Upper half of TF coil system: Model 3D 7.

distributions in the complete assembly are very complex with shear transmission due to TF coil hoop and out of plane forces at the various interfaces rather difficult.

The analyses indicate that in order for the alternative to be structurally viable, a torsion cylinder between TF coils and solenoid is necessary (this can also take the form of a solenoid outer case). The TF coils can slip vertically against this cylinder but are supported radially and toroidally. The cylinder supports the out of plane torsion of the TF coils. It appears from these preliminary analyses that shear transmission and shear levels in insulation breaks are the dominant problems, and that when proper design solutions are derived, the radial build for the alternative solution and for wedging are similar. The difficulties for the interfaces are compounded by the range of out of plane load distributions that the TF coils must support. This makes it necessary to design an inner leg region that can support shear, even if in some operating conditions this may not be necessary.

A more detailed analysis of the shear/interface problems is underway [5] (Fig. 6.14).

6.6 Conclusions

The reference TF coil geometry and concept produces broadly acceptable stress levels. Critical regions are shear levels in the winding pack and compression in the central vault. However, the stresses in these regions can be kept to acceptable values using the space allocated.

Both inner and outer intercoil structure are important in reducing coil stress levels. The inner structure should extend radially outward around the coil requirements for maintenance gaps allow. The outer intercoil structure should support hoop tension due to the in plane forces and shear due to the overrturning moments.

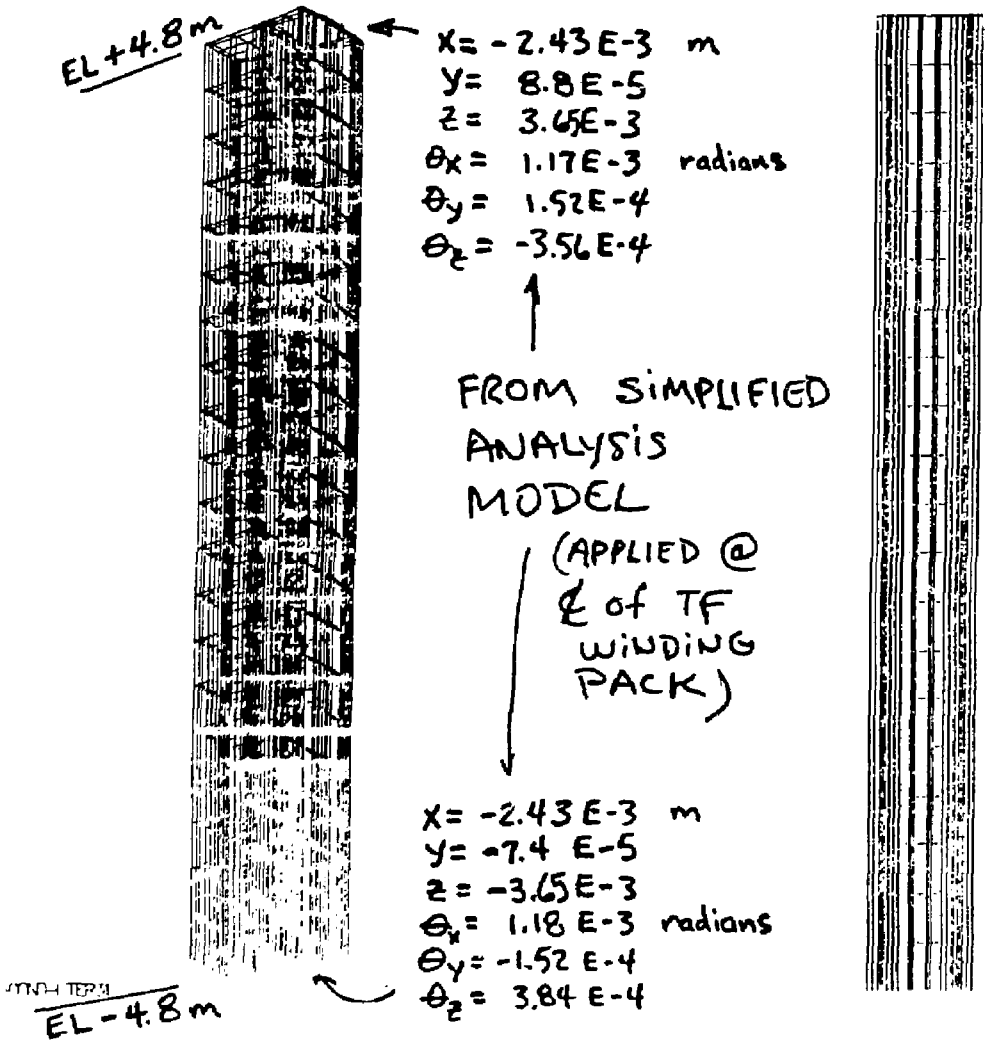

Figure 6.14: Detailed model of the inner leg with bucking onto the central solenoid.

Bibliography

[1] Preliminary Stress Analysis of the ITER TF Coils N. Mitchell, R. Annandale, D. Collier, B. Esser, F. Fischer NET/IN88-34

[2] Stress Analysis of the Wedging for the ITER TF Coil, K. Koizumi, K. Yoshida, JAERI doc JA88-JA249

[3] Preliminary Results of TFC Stress Analysis (In-plane forces), A. Malkov.

[4] Stress Analysis of ITER TF Coil, K. Koizumi, K. Yoshida, JAERI doc JA88-JA248

[5] Structural Evaluation of ITER Bucked Toridal Field Coil System, V. Dennis Lee

Chapter 7

Stress Analysis for the ITER Central Solenoid—N. Mitchell

7.1 Introduction

The ITER central solenoid occupies a critical position in the centre of the machine. It is desirable from the point of view of making the machine as compact as possible that the solenoid be designed to operate at its design limits. These limits are generally determined by the stresses in the jacket of the superconductor. To determine how the actual jacket stresses relate to the average force/unit area on the winding, two stress analyses have been performed. These relate to the solenoid shown in Fig. 7.1.

This first is shown in Figs. 7.2 and 7.7. The critical centre region of the solenoid stack is considered, initially as a symmetric hollow cylinder with averaged elastic properties. The inner central region of this is then defined in Fig. 7.1 to allow the actual jacket stresses to be found. This analysis assumes that the conductors are vertically aligned all round the circumference.

In the second analysis, Fig. 7.17, a 2-D mesh is used to look at a coil section when the conductors are not vertically aligned. Such a region can occur on the top of a layer round coil or distributed throughout a pancake wound coil.

Because of the uncertainty of the ITER parameters at the time this analysis was started, the coil geometry and conductor types are inconsistent between the different model results.

7.2 Results

The materials properties and geometric dimensions are given in Table 7.1. Figures 7.3–7.6 show the overall winding stresses, with the usual peak hoop stress on the inside. Figures 7.8–7.11 show the jacket stress for the refined model, and Figs. 7.12–7.16 show the stresses in the insulation surrounding the jacket. The radius on the inside of the jacket is sufficient to prevent major stress concentrations in the vertical stress distribution. The peaking in the hoop stresses is rather less. The short (horizontal) ends of the jacket carry more of the hoop

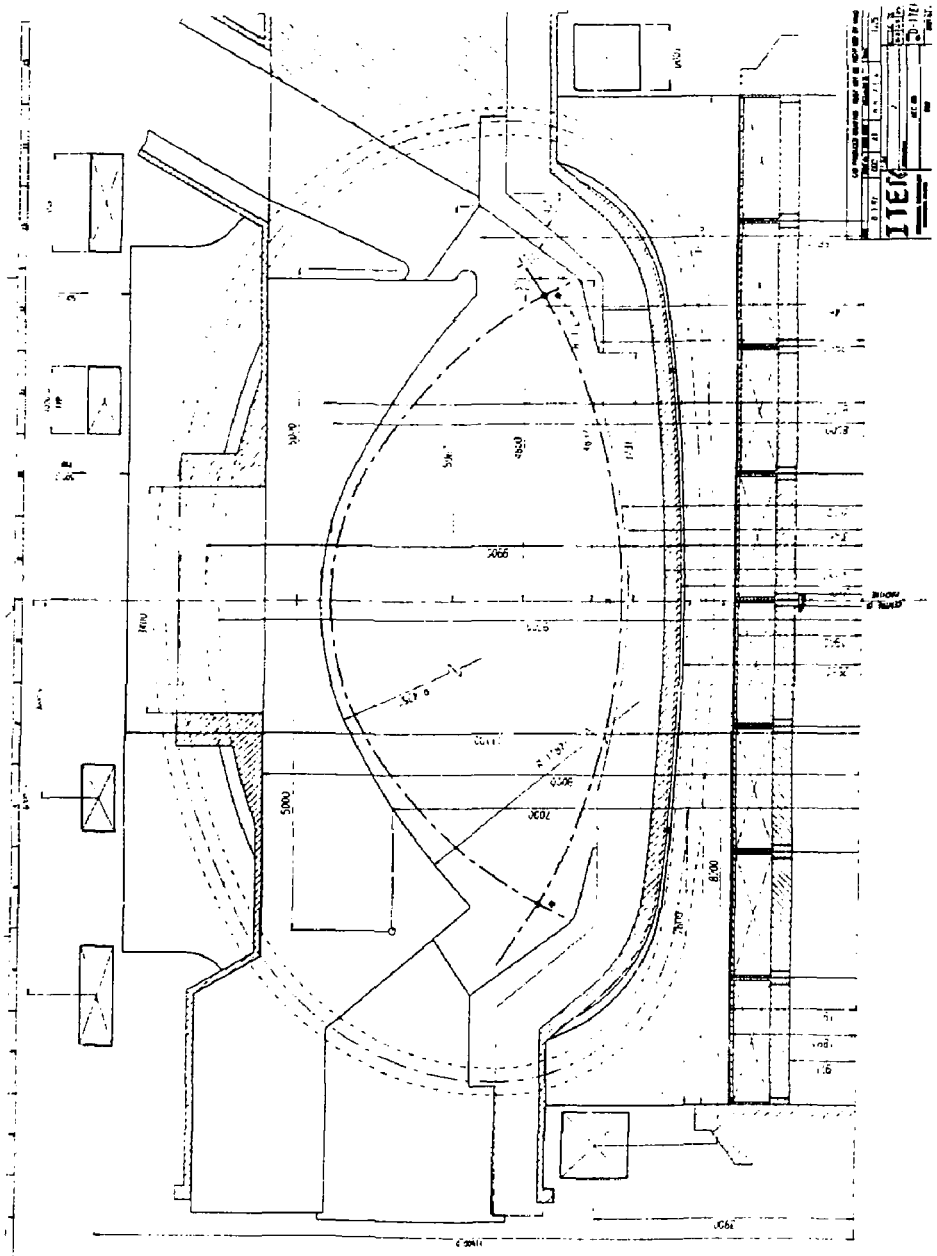

Figure 7.1: ITER magnet system.

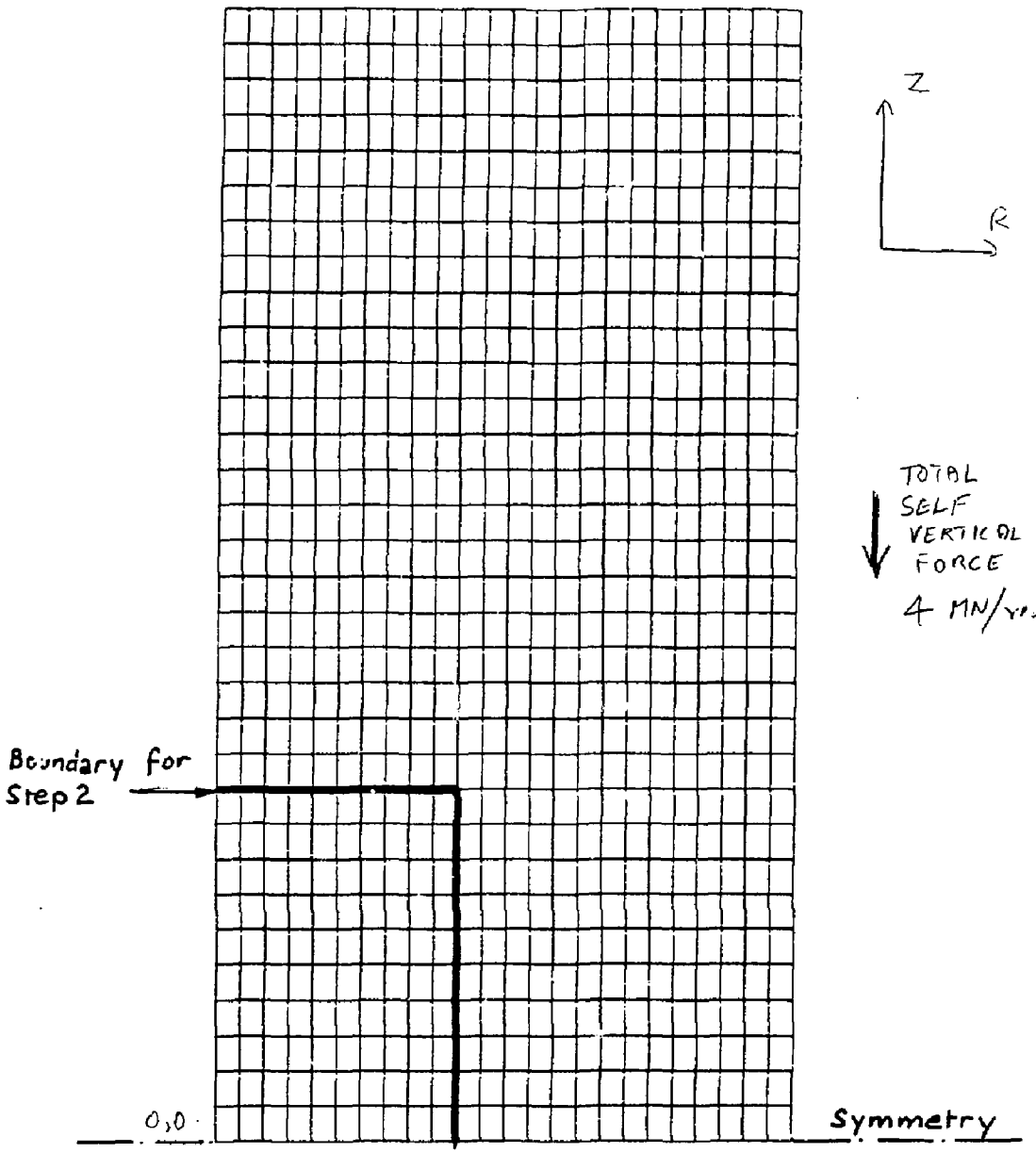

Figure 7.2: Mesh of central coil.

Table 7.1: Material properties.

Average winding peak (axisymmetric)		
E_{long}	104	GPa
E	47	GPa
E_z	65	GPa
E	22	GPa
E_z long	34	GPa
G long	31	GPa
Detailed crossection		
E_{ins}	26	GPa
E_{steel}	210	GPa
$E_{superconductor}$	10	GPa (long)
	1	GPa (transverse)
Average winding peak (2-D)		
E	50	GPa
Jacket thickness:		
Axisymmetric model:	5 mm	
2 - D model	4 mm	
Average current density:		24 MA/m^2
Conductor dimensions 48 × 31 mm (without insulation)		

loading than the side pieces. The insulation stresses show sharp (unrealistic) peaks due to stress concentrations at the jacket corners.

For the crossover region model, Fig. 7.18 shows the distorted jacket shape. As would be expected, the misalignment causes bending of the end region. The stress plots are shown in Figs. 7.19, 7.20, 7.21. This end bending accentuates the stress concentration at the corner radii with the vertical stress, since the bending stress in this region is also compressive. There is a considerable tensile bending stress on the end of the conductor. The shear stress in the insulation (Fig. 7.17) peaks, as may be expected, roughly 25% of the way along the conductor edge, halfway between the centre and end symmetry points.

7.3 Generalisation of Results

By using the stress analysis results for this specific geometric to derive stress concentration factors, they can be applied to a range of solenoids and loading conditions.

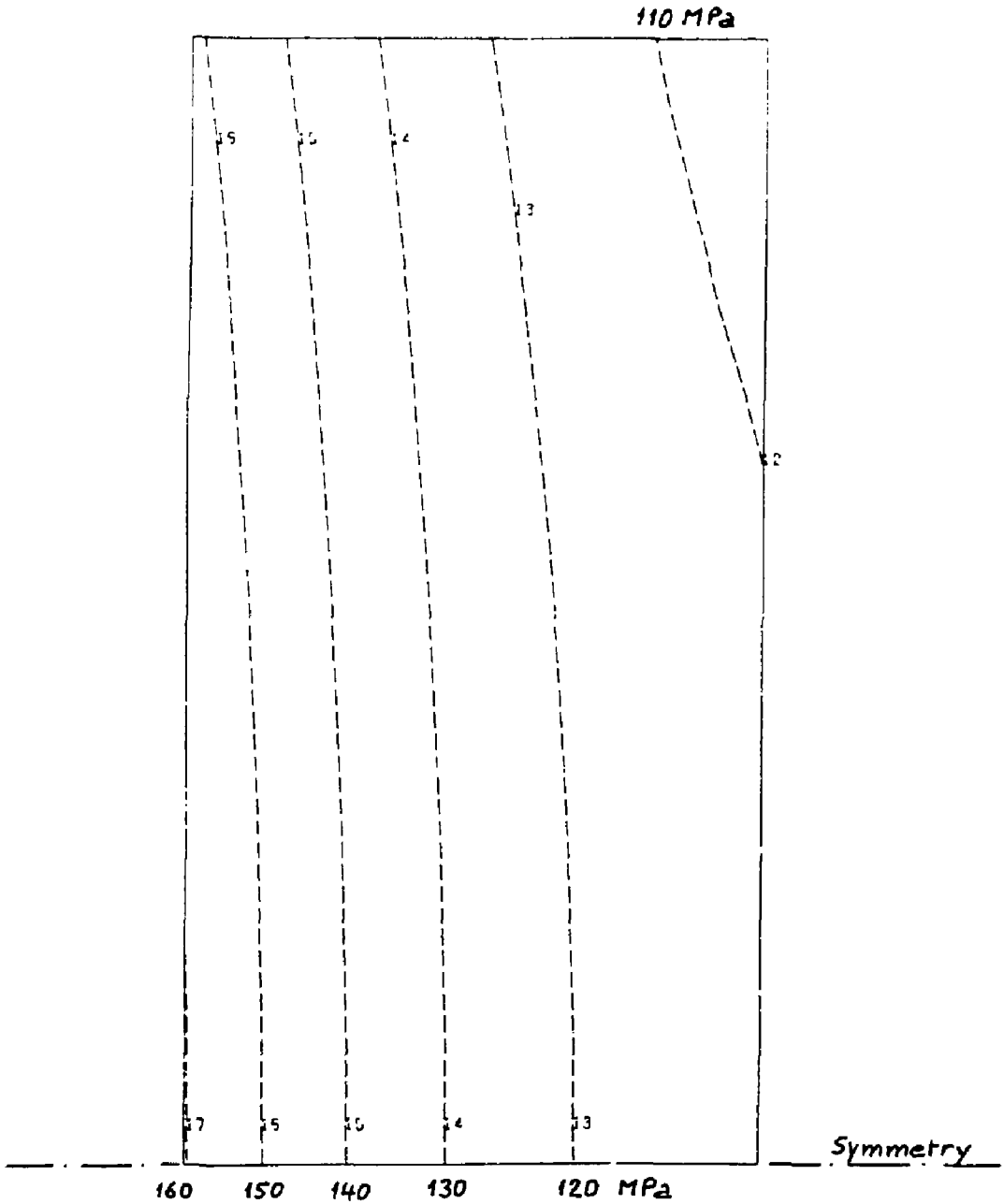

Figure 7.3: Hoop stresses.

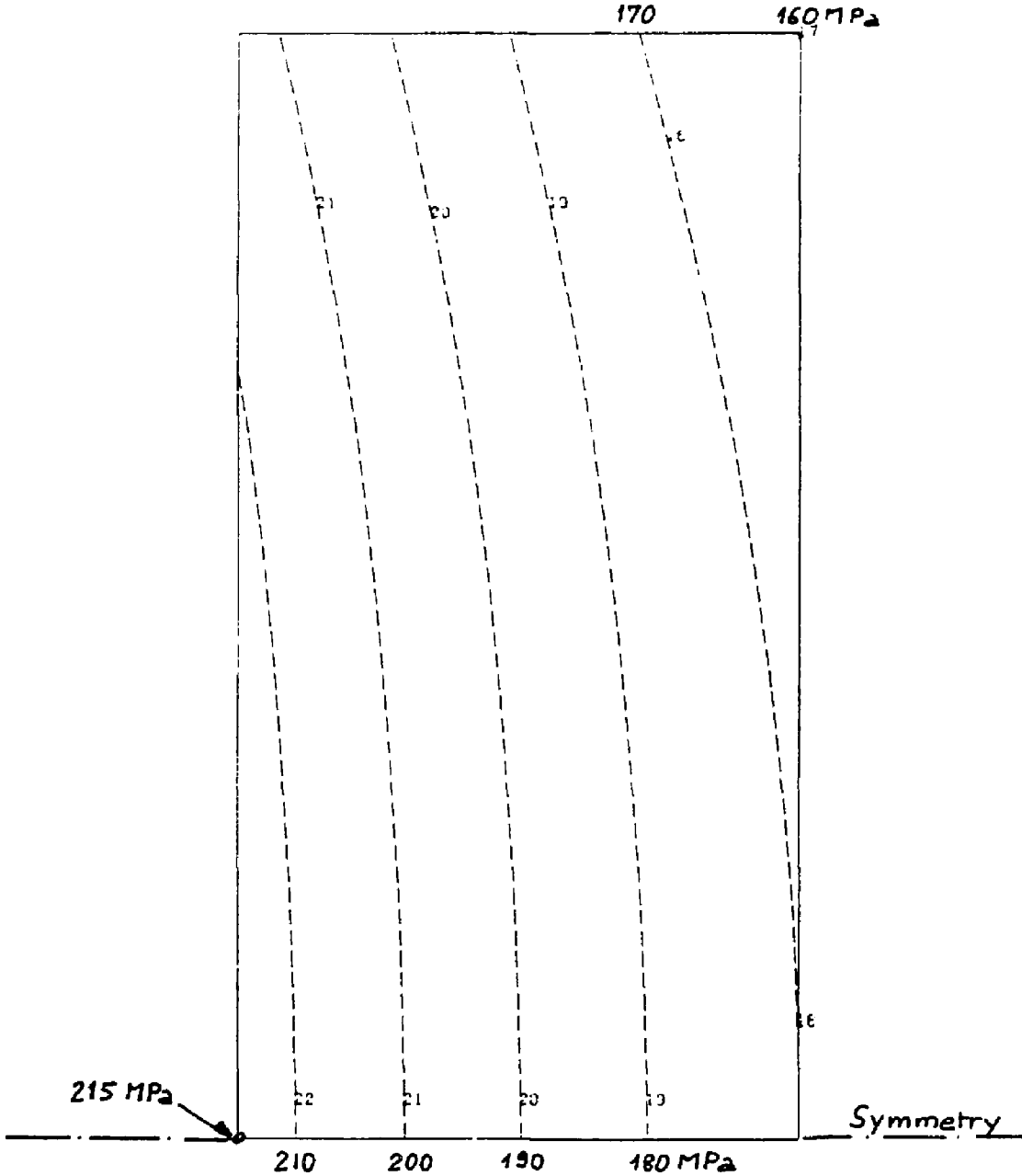

Figure 7.4: Von mises stresses.

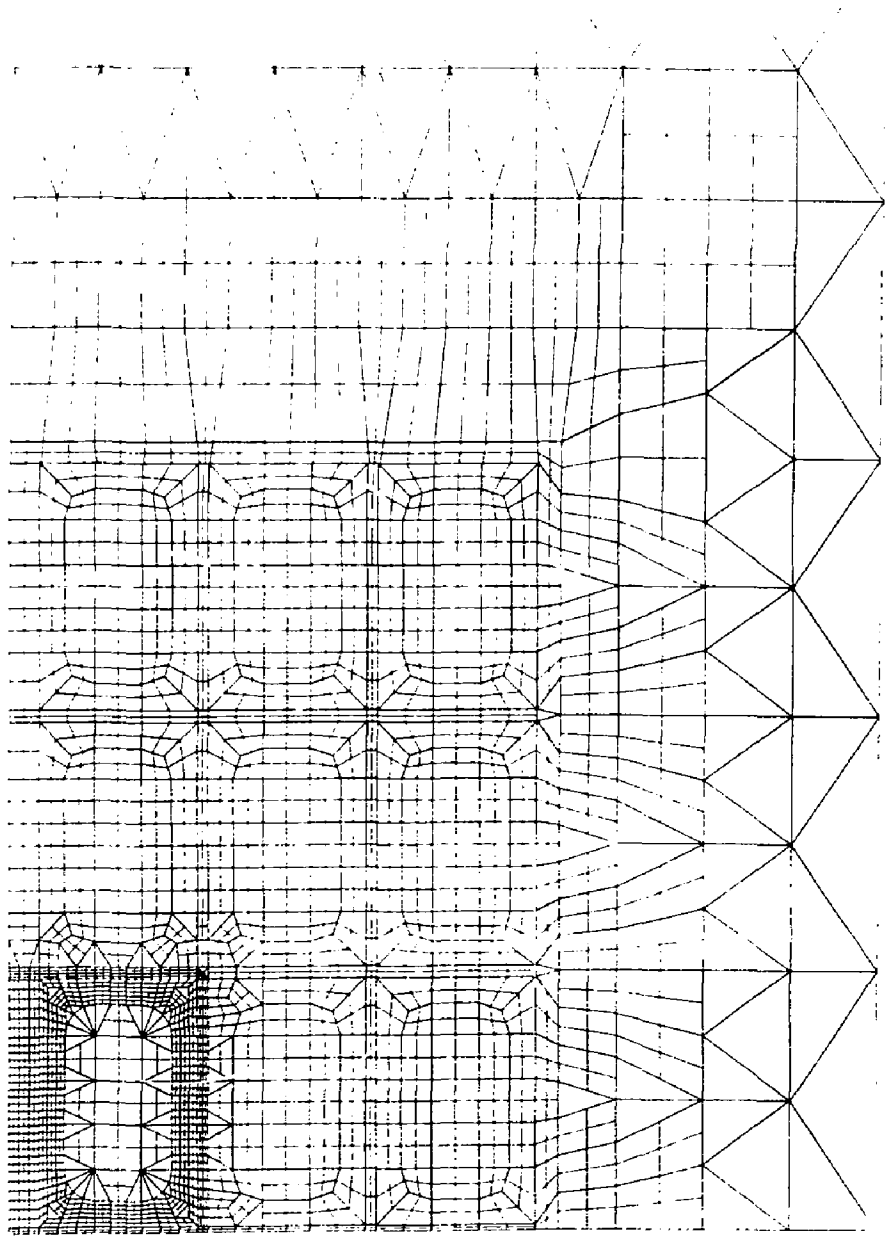

Figure 7.5: Detailed stress contours.

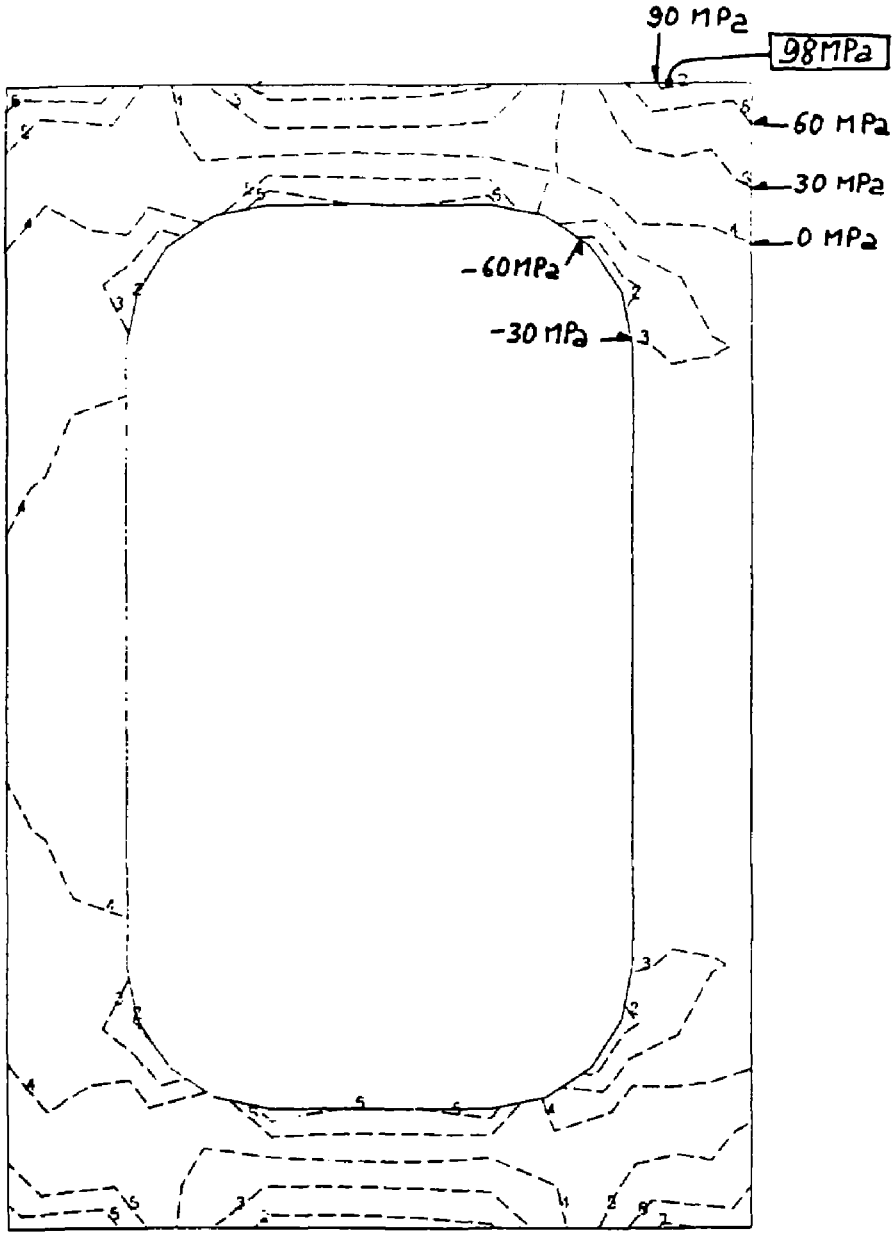

Figure 7.6: Jacket radial stress.

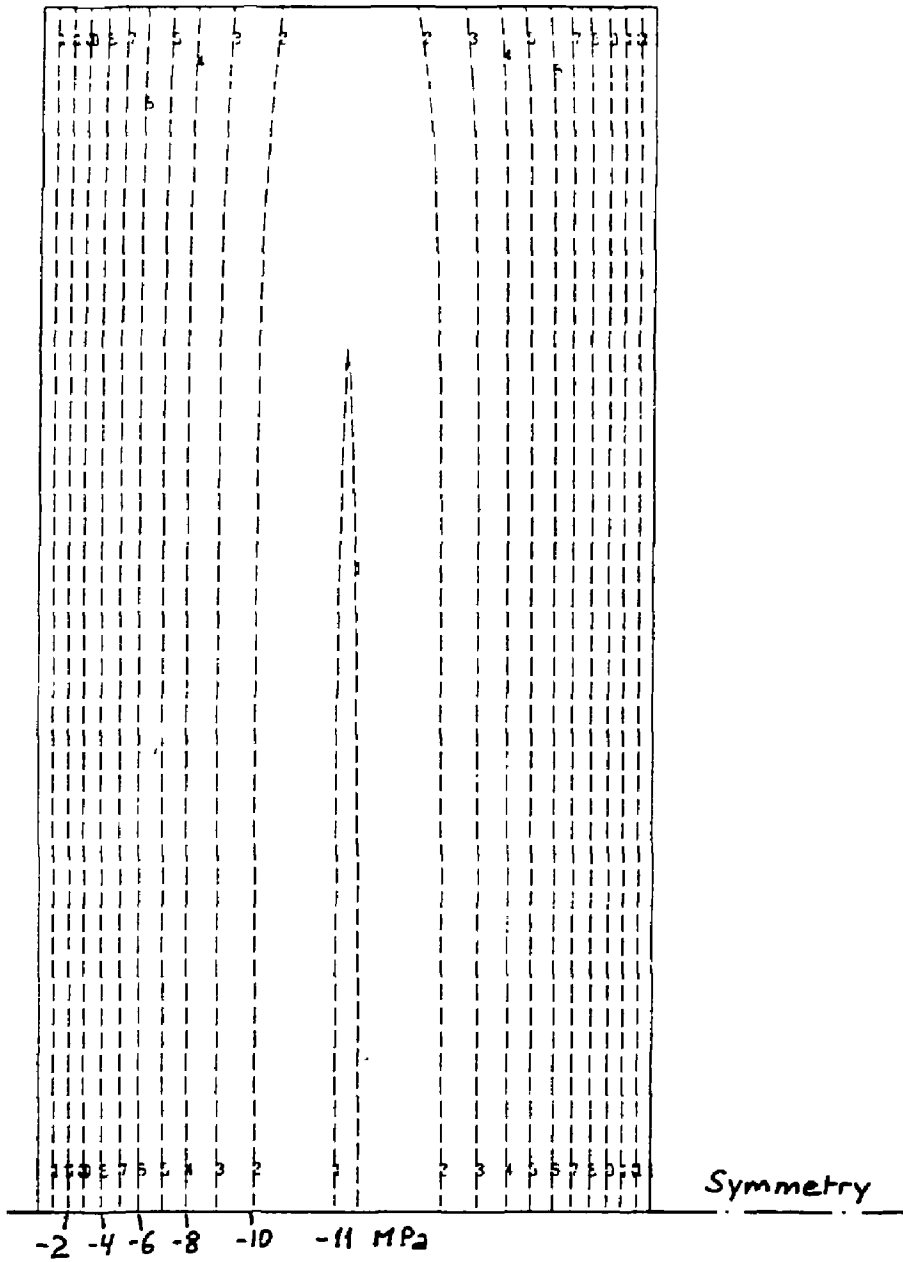

Figure 7.7: Radial stresses in solenoid.

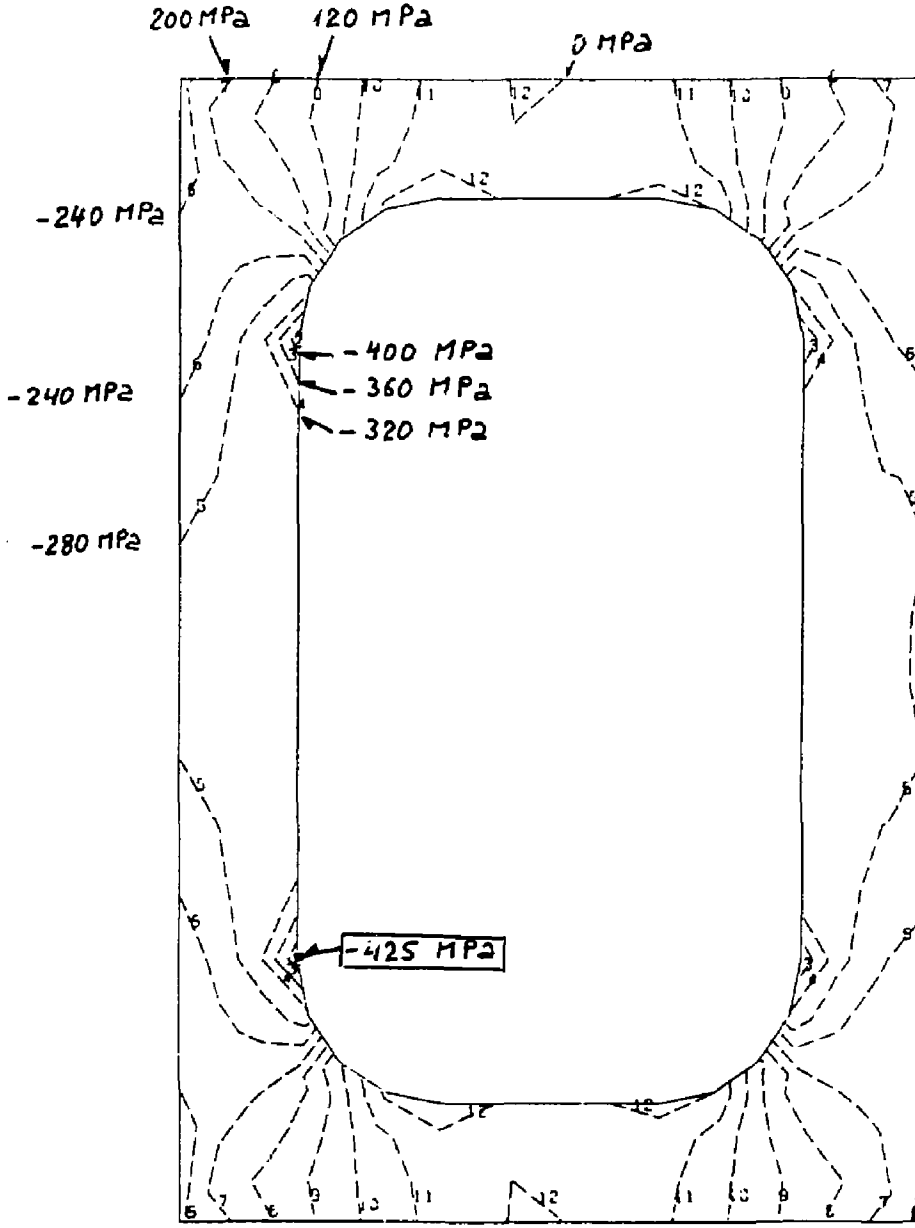

Figure 7.8: Vertical stress.

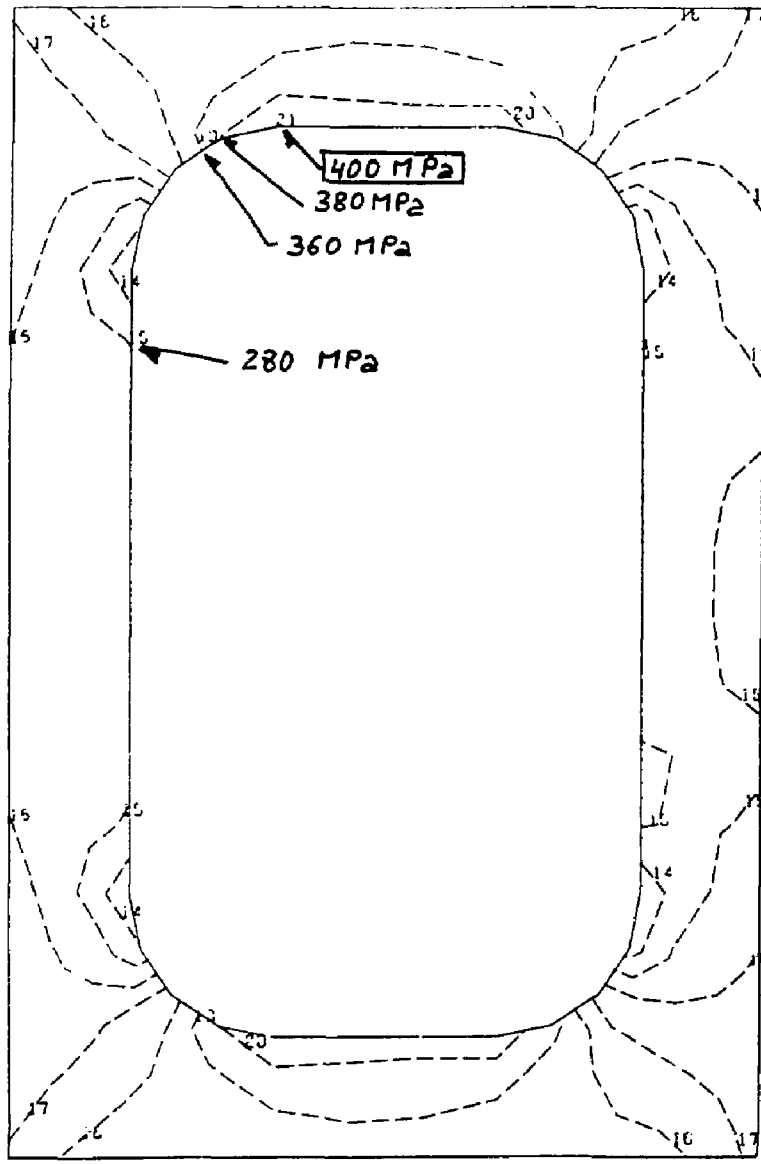

Figure 7.9: Jacket hoop stress.

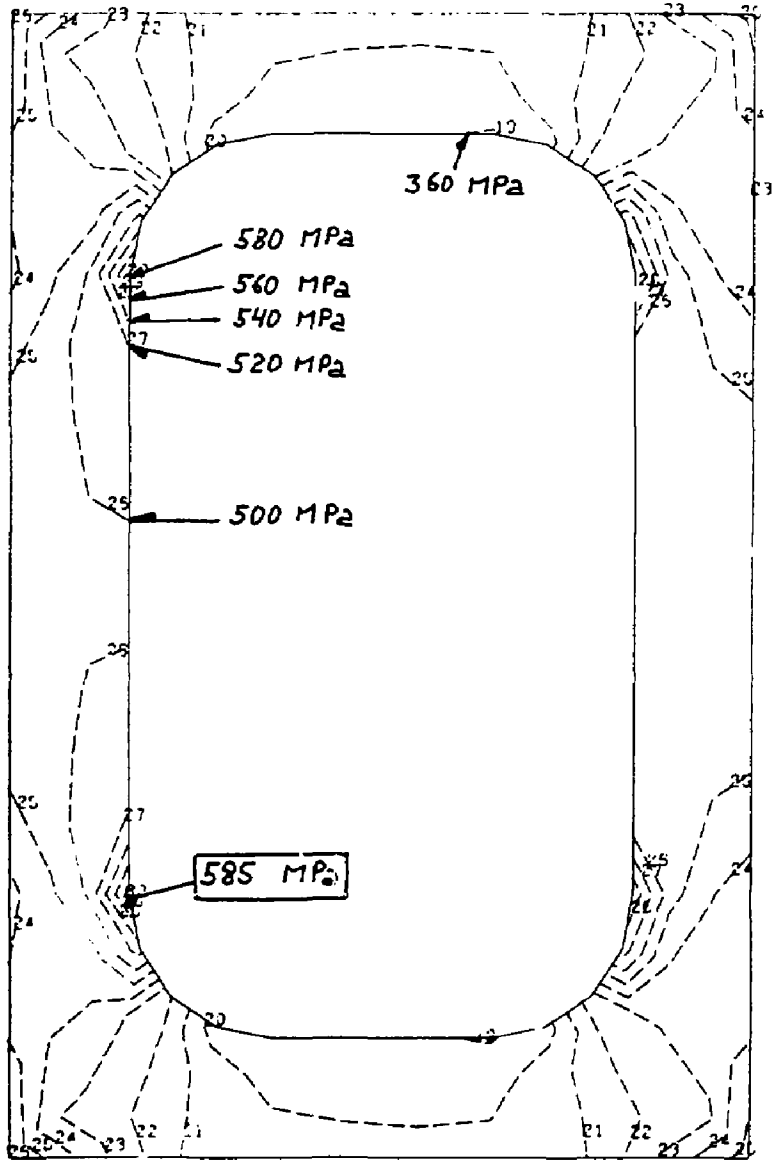

Figure 7.10: Jacket Von mises stress.

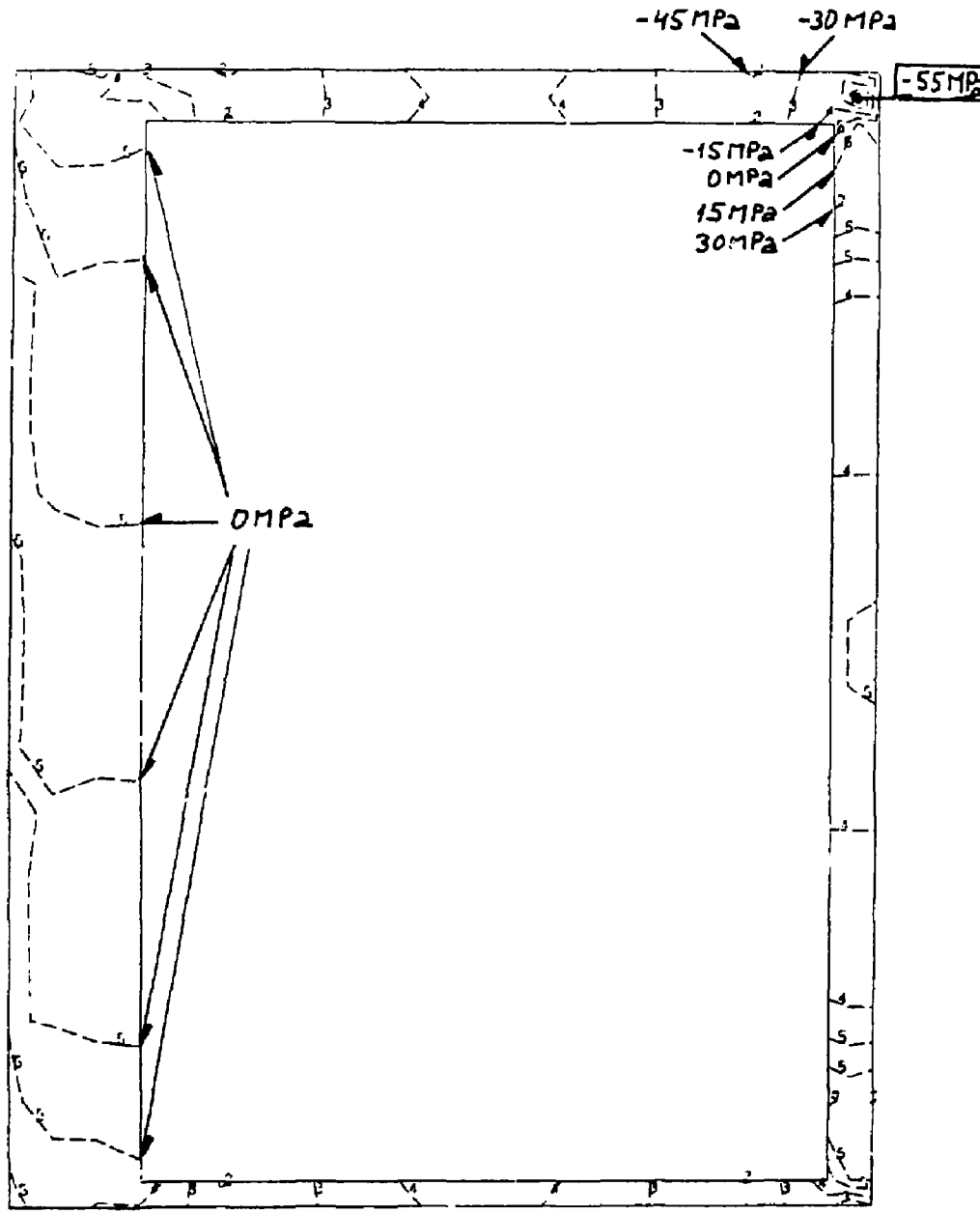

Figure 7.11: Insulation radial stress.

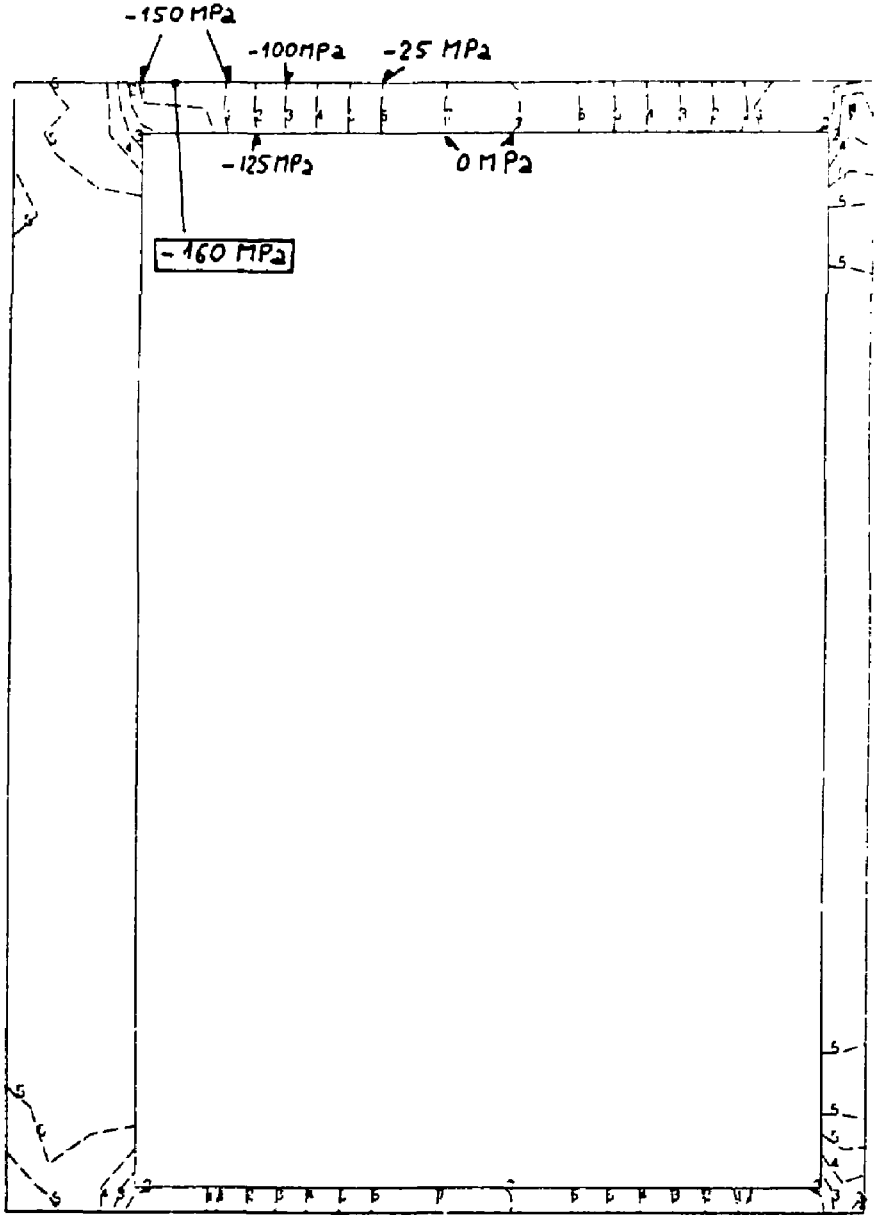

Figure 7.12: Insulation vertical stress.

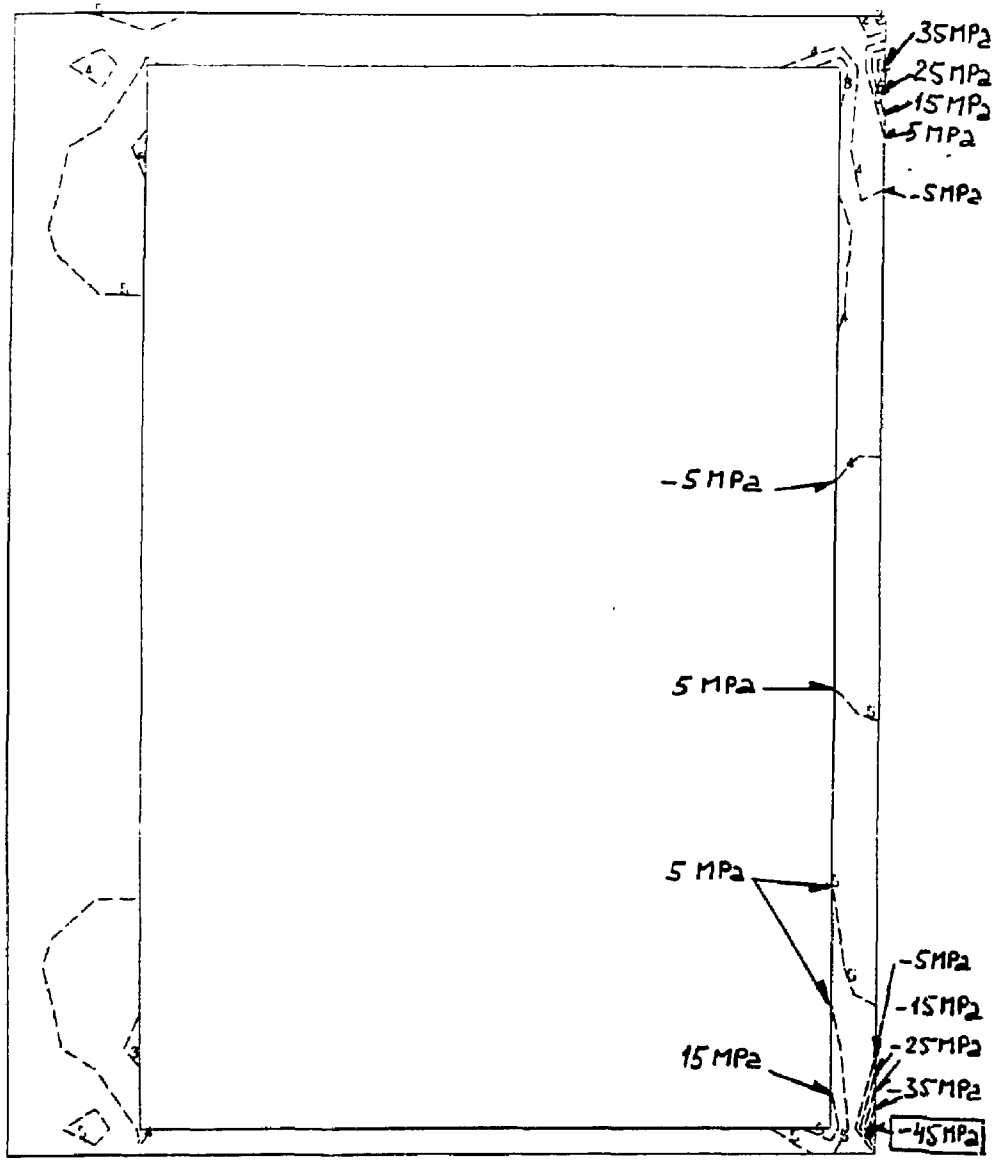

Figure 7.13: Insulation shear stress.

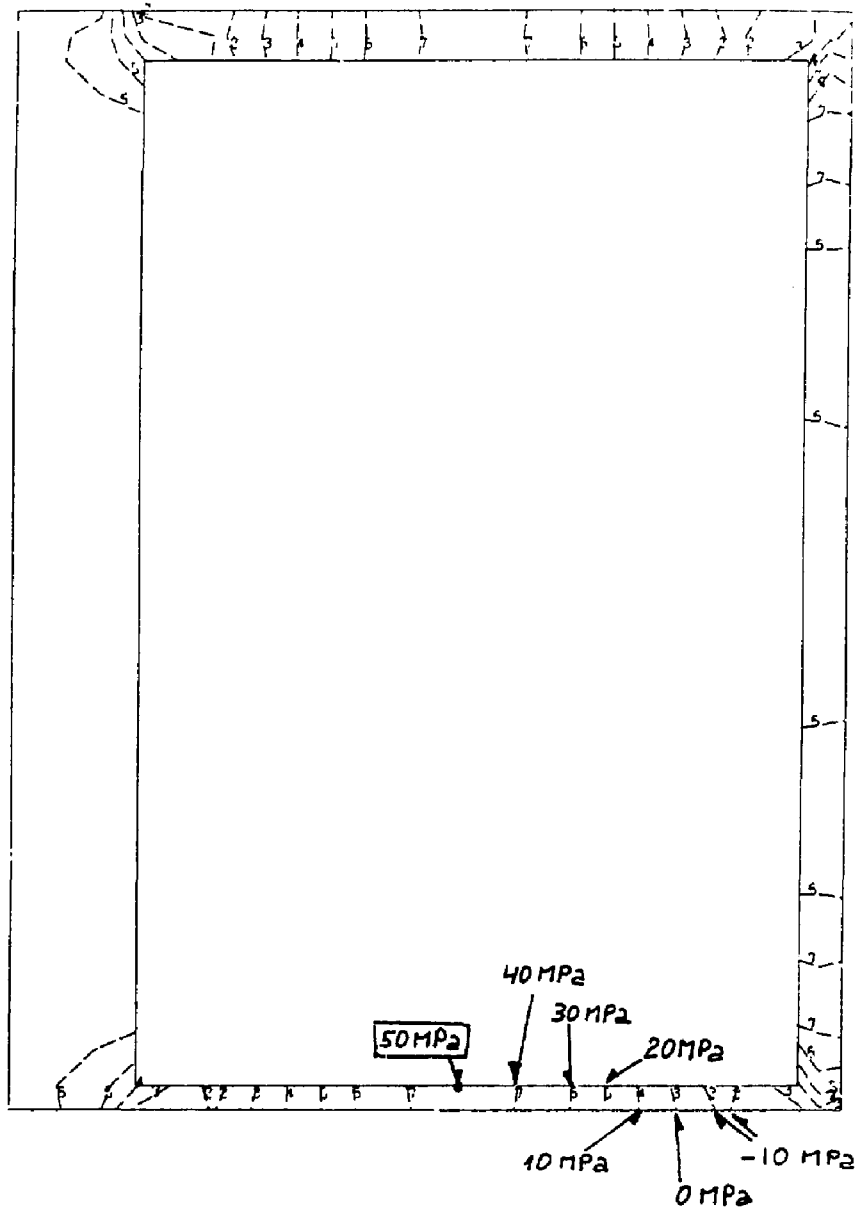

Figure 7.14: Insulation hoop stress.

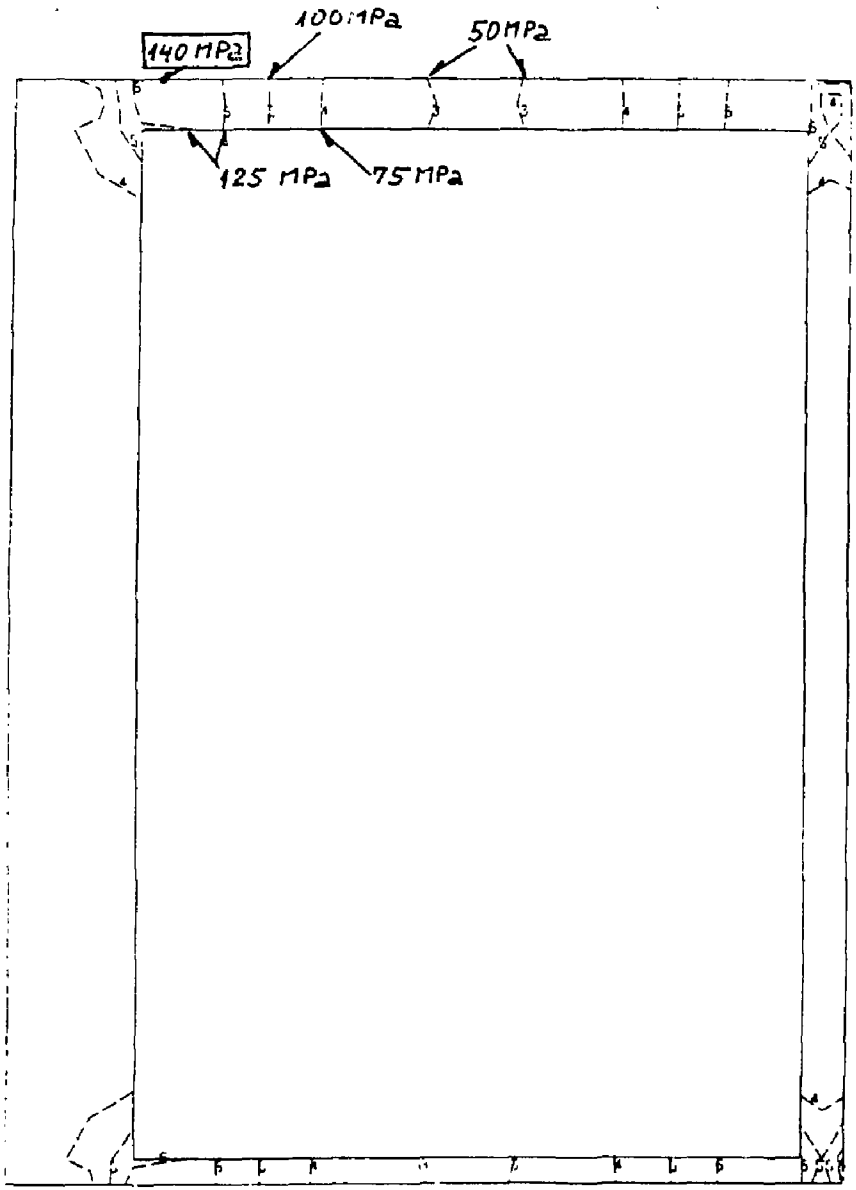

Figure 7.15: Insulation Von mises stress.

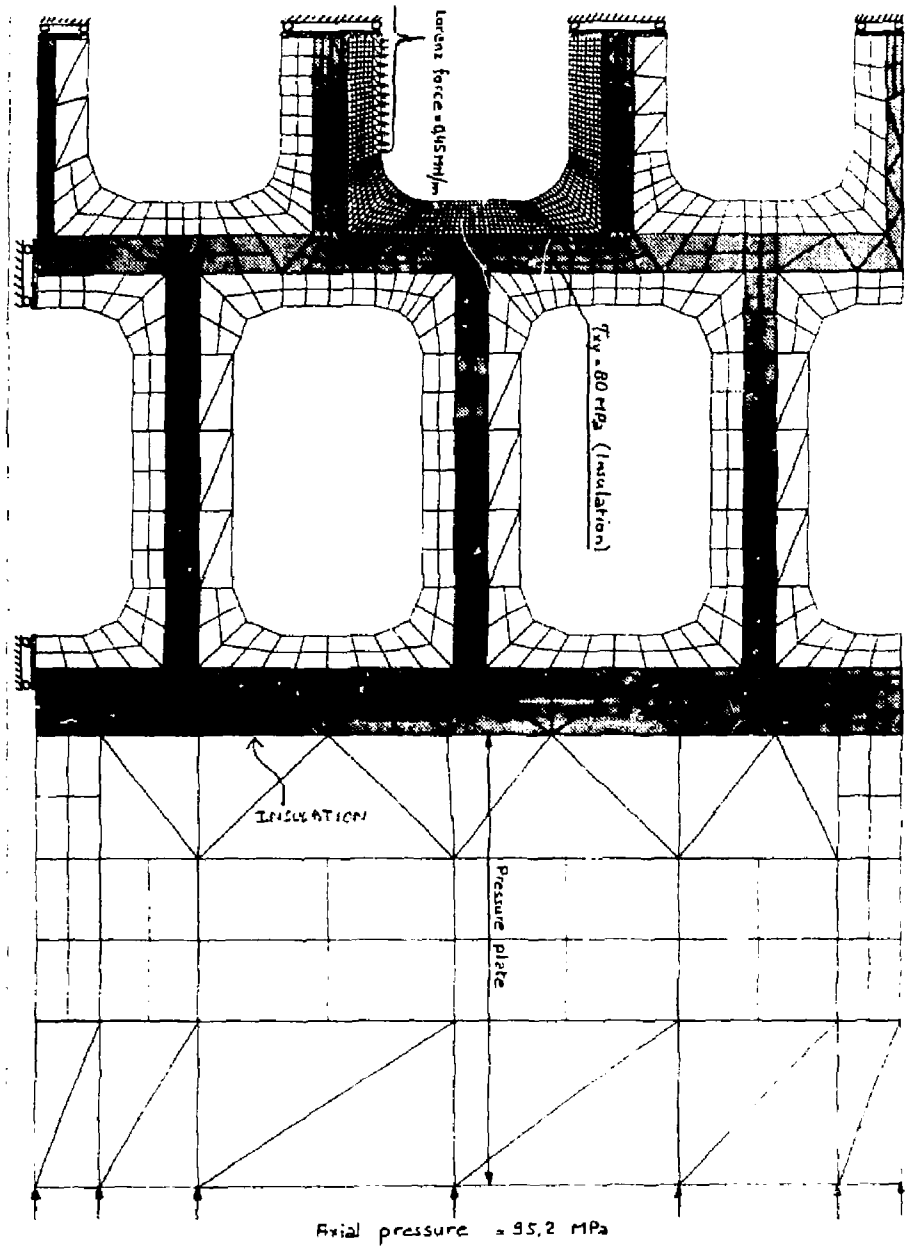

Figure 7.16: Mesh of vault region.

7.3.1 Axisymmetric Coil Analysis (Figs. 7.2-7.6)

The minimum vertical fraction of steel that can support the vertical force is 0.3 (based on a horizontal cut in the R-R plane through the winding). The average steel fraction in the winding is 0.46 based on area. It is assumed that only the steel is effective in supporting the applied loads.

The average vertical stress in the winding is 89 MPa, which agrees well with the stresses shown in Fig. 7.5. The peaking factor is negligable. The average hoop stress is 139 MPa (Fig. 7.3) and the peaking factor to the maximum (163 MPa) is 1.18. The radial stresses (Fig. 7.3) are negligable.

7.4 Detailed Axisymmetric Analysis (Figs. 7.1-7.16)

Based on the vertical and overall steel fractions, the average jacket stresses based on a peak winding stress of 164 MPa are:

- Hoop 356 MPa
- Vertical 297 MPa.

From Fig. 7.9, the peak jacket vertical stress is 425 MPa. Thus the concentration factor from the average jacket stress is 1.43.

From Fig. 7.10, the peak jacket hoop stress is 400 MPa. Thus the concentration factor is 1.12. The peaks in Figs. 7.9 and 7.10 are not coincident. The radial stress (Fig. 8) ranges from -60 to 98 MPa but these peaks are not coincident with the hoop or vertical stress peaks.

It is difficult to generalize the results for the insulation stresses, Figs. 7.12–7.16.

From Fig. 7.13, the peak vertical pressure in the insulation is 160 MPa. The concentration factor form the average winding peak stress is 1.8.

From Fig. 7.15, the peak hoop insulation tension is 50 MPa, a concentration factor of 0.3 from the peak winding peak stress.

The shear values shown in Fig. 7.14 are rather high, but are certainly due to the stress concentrations at the sharp jacket corners, and are not realistic. Away from these regions the shear stresses are less than 5 MPa.

7.4.1 2-D Crossover Region Analysis

This analysis does not consider the effect of the hoop tension. The vertical steel fraction in this model is 0.23. Based on the winding peak pressure of 95.2 MPa, the average vertical (z) stress in the jacket is thus 77MPa

From Fig. 7.19, the vertical stress is 77 MPa, a concentration factor of 1,87 over the average jacket stress.

From Fig. 7.20, the vertical pressure creates radial stresses due to bending. These peak at 421 MPa (tensile), a concentration factor of 1,02 over the average jacket peak hoop stress region shown in Fig. 7.10.

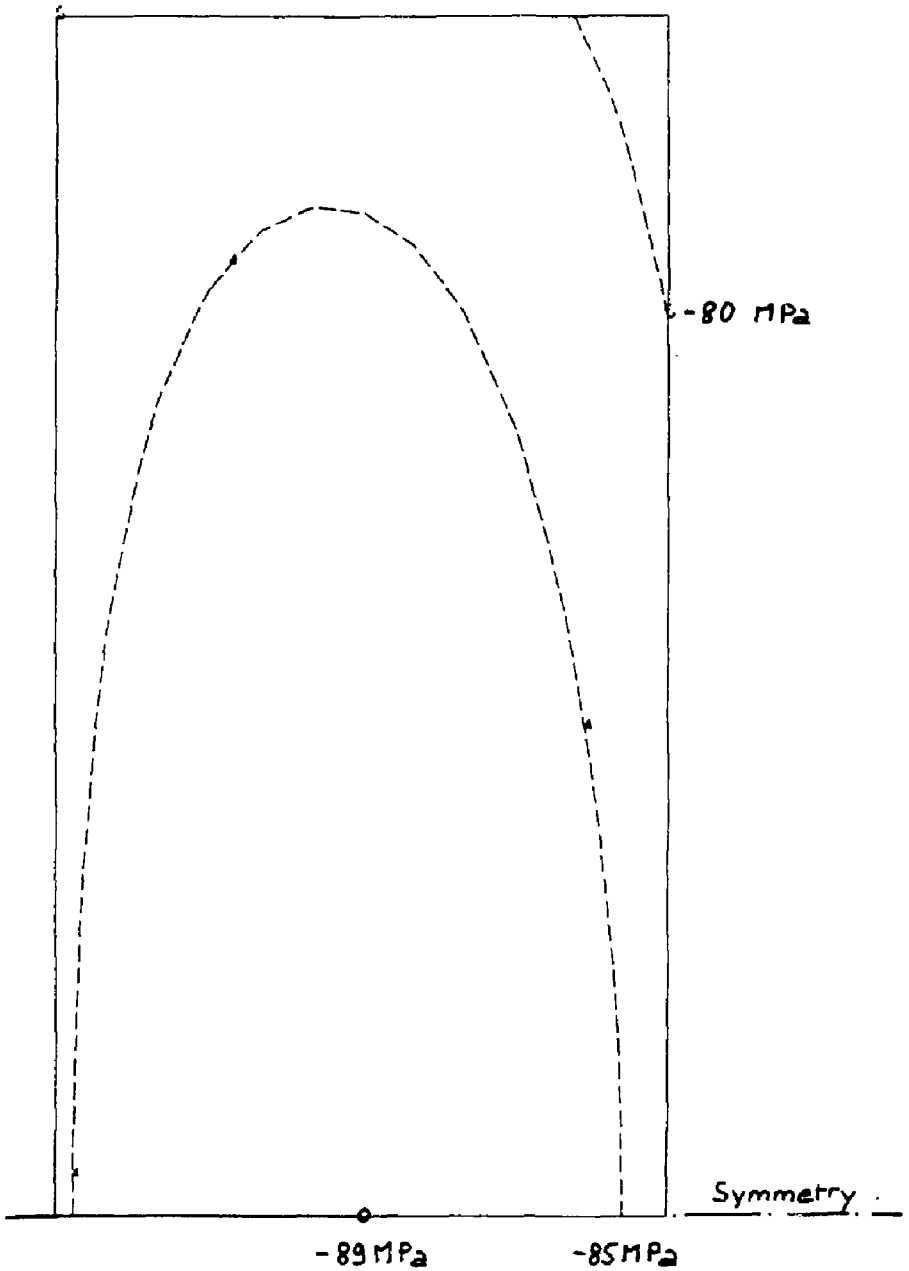

Figure 7.17. Vertical stresses.

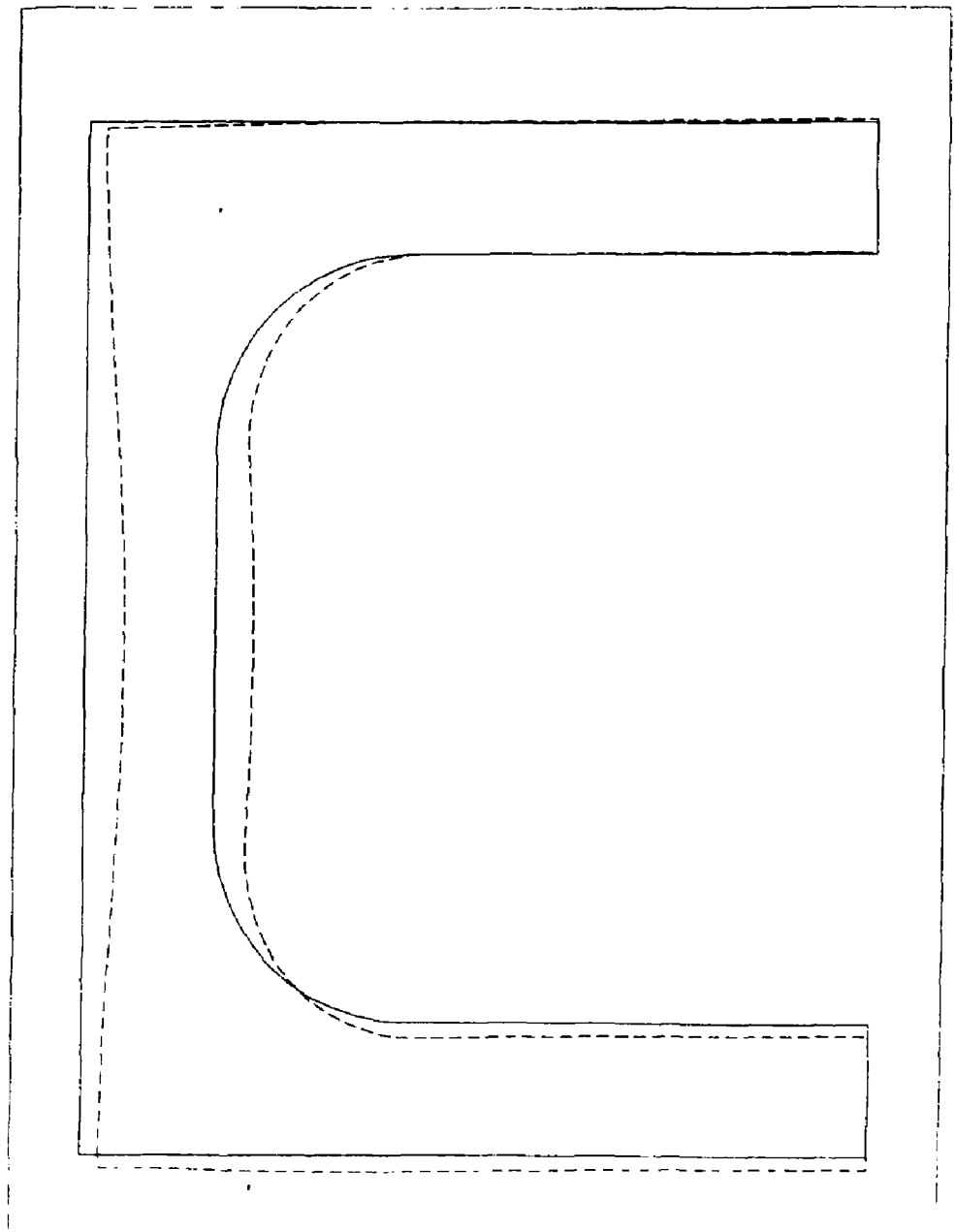

Figure 7.18: Jacket distortion.

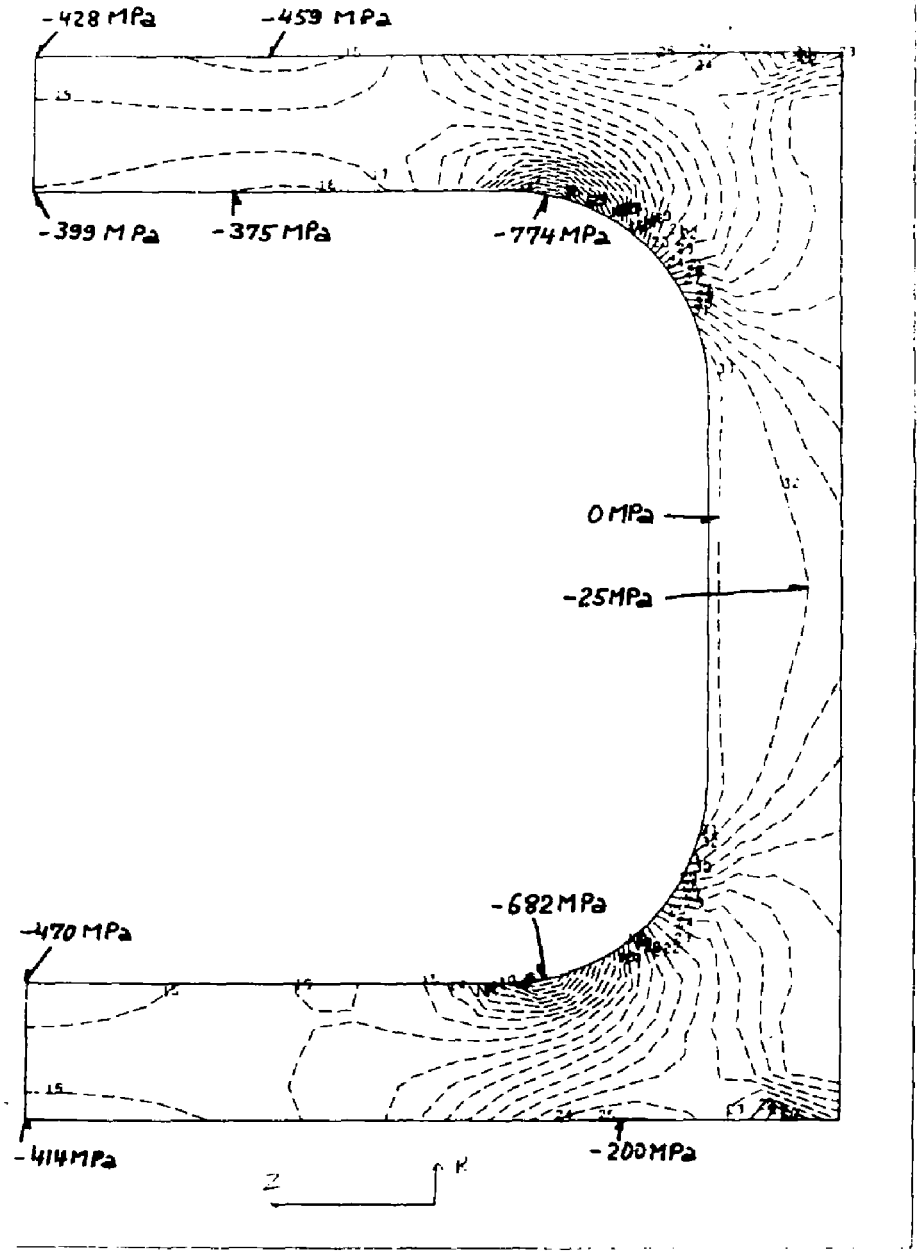

Figure 7.19: Jacket streses.

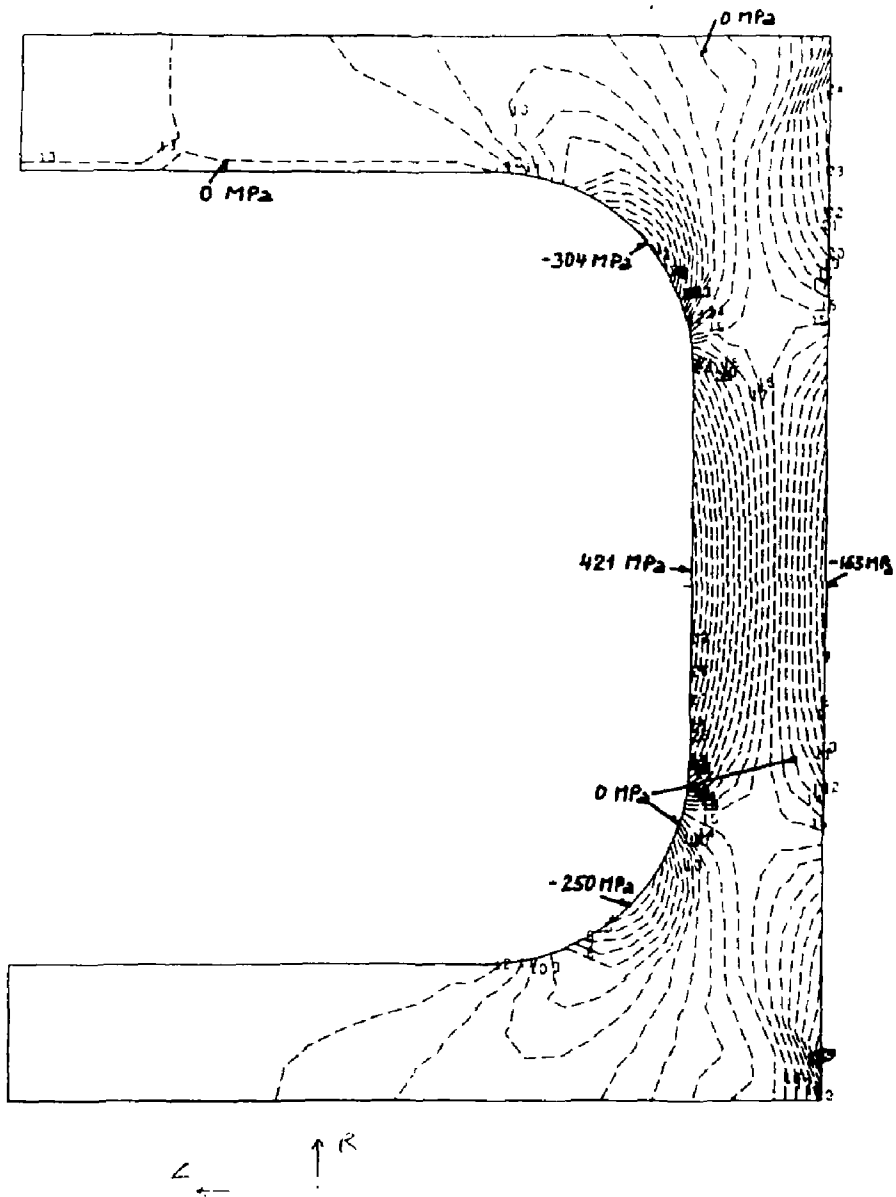

Figure 7.20: Vertical pressure creates radial stresses due to bending.

The peak shear stress in the insulation is shown in Fig. 7.17 as 80 MPa. This value is away from the corner regions and will be real. It is realistic to relate this to the radial bending stresses since it is caused by the bending of the jacket end. We can therefore consider that the maximum shear is a factor of 0.19 of the average jacket vertical compressive stress.

These last two stress concentration factors may be reduced by two factors. Firstly, the crossover region is three dimensional in nature, so that the geometric arrangement of Fig. 7.7 is transitory around the circumference. Secondly, the jacket thickness of 5 mm will reduce the bending stress shown in Fig. 7.19, 20 substantially.

7.4.2 Allowable Stress Value

The present design of ITER envisages a solenoid with an overall steel fraction of 0.5 and a vertical steel fraction of 0.4. The maximum allowable tensile stress is taken as 500 MPa and the maximum Tresca stress as 800 MPa.

For the uniform coil away from the crossover region, this implies an average hoop tension over the winding of 189 MPa. Simultaneously an average compression of the winding of 84 MPa is allowed.

In the crossover region, if we assume that the winding has this average hoop tension of 189 MPa, the allowable vertical compression is 64 MPa. The radial bending stress (tensile) of 163 MPa in the jacket does not contribute to increasing the value of the total Tresca stress. The insulation shear for this case is 30 MPa, which is at the allowable limit. In view of the pessimism of the crossover analysis a vertical stress limit of about 70 MPa, averaged over the winding, seems reasonable.

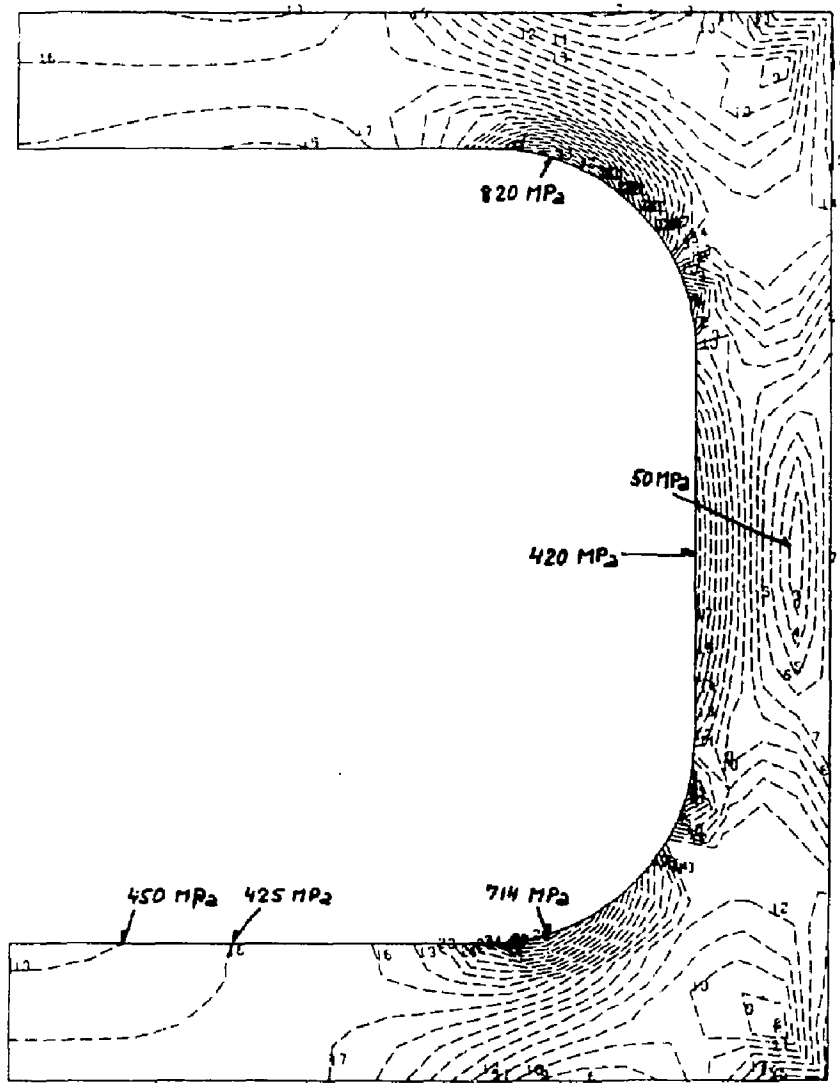

Figure 7.21: Conductor jacket stresses.

Chapter 8

Volt-Second Capabilities and PF Magnet Configurations

8.1 Introduction

The poloidal field coils in ITER have two functions. Firstly, they generate the magnetic fields to hold the plasma in equilibrium and secondly they act as a transformer to drive the plasma current. As a rough generalization, the outer coils have mainly an equilibrium function and the central solenoid mainly a transformer function. The outer coils lie outside the toroidal field coils and do not occupy a region where space is at a premium. Thus space is available for adequate mechanical support and at the same time the field levels in the coils can be kept low (7-9T) with a low current density. The inner central solenoid occupies a region where space is critical and exerts a significant necessary that it operates at high field levels (12-13T) and with the minimum necessary structural support.

The configuration of the outer coils is achieved by an iterative procedure between the need to place coils in near optimum positions to reduce their currents, the overall energy of the p.f. system and the out of plane forces on the t.f. coils and the need to satisfy machine maintenance requirements since the outer coils block access to the internal components. Once the outer coils are positioned the plasma performance is determined by the design of the central solenoid.

8.2 Poloidal Field Coil Configuration

During the predesign phase of ITER a number of configurations and basic machine parameters have been considered. The parameters used for the calculations presented here are therefore defined in Tables 8.1, 8.2, and 8.3. Table 8.1 shows the coil positions and the inductance matrix. The mutual inductances with the plasma refer to an elongated plasma with a current distribution proportional to the major radius and R = 5.8 m, a = 2.0 m. Table 8.2 gives the coil configuration required to give a maximum prebias on the coils with minimum stray field in the plasma region. There are many configurations which give a satisfactory stray field level in the plasma region (<50 gauss) and the one shown here uses a uniform

Table 8.1: Poloidal field description.

Coil Positions

	R	z	Δr	Δz
P1	1.6	1.5	0.6	3.0
P2	1.6	4.0	0.6	2.0
P3	1.6	6.5	0.6	3.0
P4	4.0	8.2	1.0	1.0
P5	11.5	6.0	0.5	1.0
P6	11.5	3.0	0.5	1.0

Inductance Matrix μH

	1	2	3	4	5	6	P1
1	4.672						
2	1.286	4.853					
3	0.2599	1.161	3.816				
4	0.487	0.893	2.036	23.15			
5	1.237	1.230	1.159	6.748	115.2		
6	1.580	1.432	1.182	6.145	58.07	129.1	
P1	1.398	1.023	0.595	2.129	8.659	11.87	9.5

Each coil has 2 turns, one above and one below the equator.

current density in the solenoid. Table 8.3 gives an outline of the equilibrium currents at end of burn (20, 30 MA plasmas) and start of flat top (before heating the plasma) taken from ITER-IL-PF-1-8-52. Tables 8.2 and 8.3 define the coil currents that should mark the limits of plasma performance. They are an initial estimate of the expected mechanical limits that will require adjustment on the basis of a proper analysis of the central solenoid. The performance in terms of inductive drive is given by ψ eq, the flux linking the plasma from the equilibrium coils.

8.3 Central Solenoid Concepts

Before proceding with a structural assessment of the central solenoid, it is necessary to establish design concepts. Two basic concepts can be used to include most of the variations, although elements of these concepts can be incorporated in different ways. The two are illustrated in Figs. 8.1 and 8.2. Both utilize cable in conduit type superconductor with and overall cable space current density of about 50 MA/m^2 and a steel fraction of about 0.5 in the winding. Optimization calculations show that this gives a maximum flux capability with fields of about 12.5 T.

The solenoid fits inside the toroidal field coils with an inner bore of 2.0 m. A 10 cm clearance is allowed between the T.F. coils and the main solenoid winding to operation, assembly of the solenoid into the bore, cooling pipes and current leads and pancake crossovers

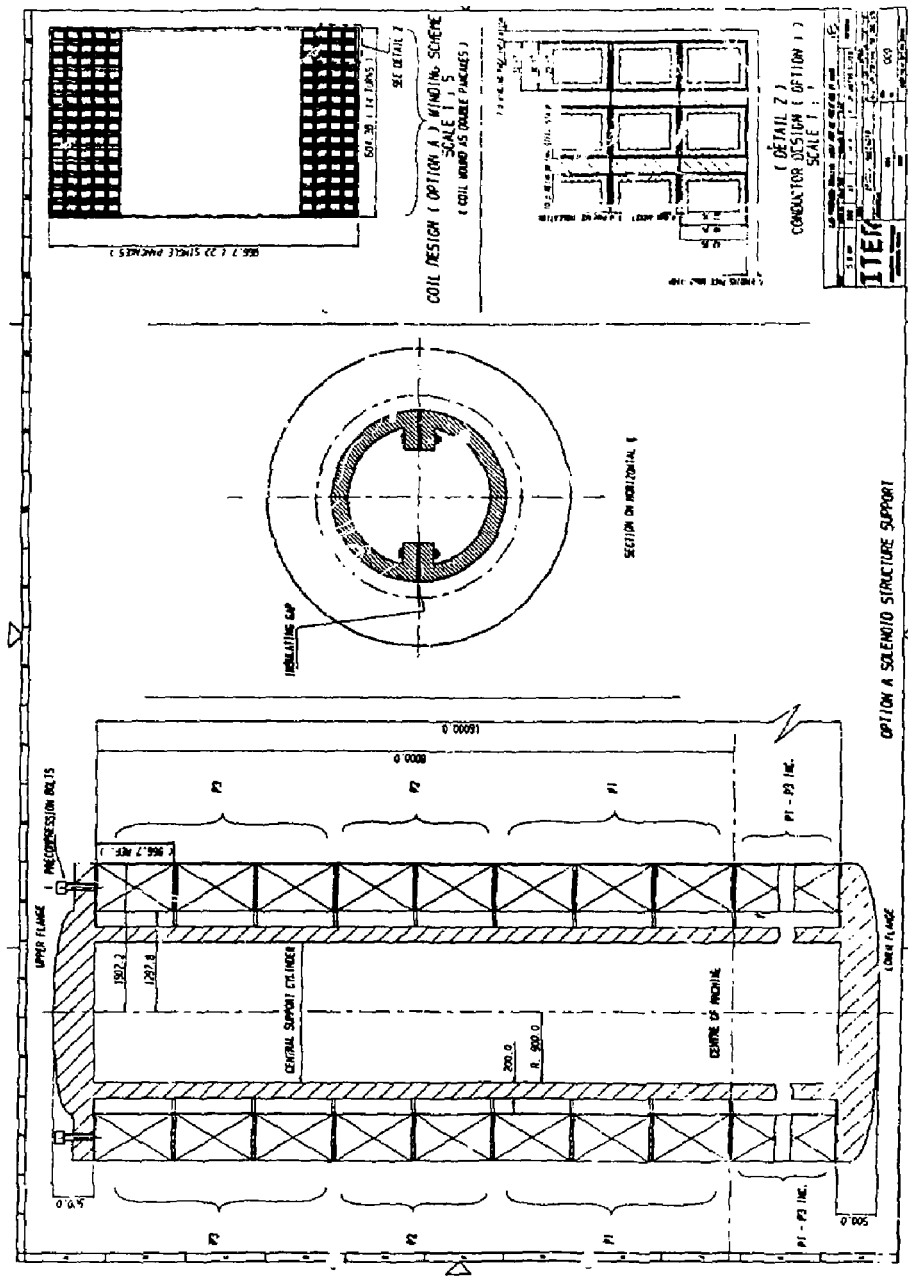

Figure 8.1: Option A central solenoid structure.

Table 8.2: Transformer currents.

The following coil currents			
P	1	29.448	MA
	2	19.632	
	3	29.448	
	4	6.514	
	5	0.675	
	6	0.13	

give a maximum stray field in the region defined by
R_o = 5.8 m, a = 2.0 of 7.18 gauss.

The solenoid forces are:

Coil	F_R (MN/m)	F_z (MN)
1	181.4	-1.1
2	120.4	-8.7
3	166.6	-331.8

The peak field occurs at R = 1.3, z = 0. and is 12.3 T.
There are 100 Vs linking the plasma region.

(where these are present). The coils are precompressed and supported against internal forces by a structure inside the solenoid.

In Fig. 8.1 the stack is built up of 1 m coil blocks, connected in twos or threes to make up the P1-P3 coil units. The coils are formed by a react-and-wind technique with a 4 mm thick steel jacket on the cable. Extra steel reinforcing is wound together with the conductor. The winding process forms double pancakes with helium inlets on the inside high field region and current leads and helium outlets on the outside. The coil blocks rest on each other with load transmission to the central support by a massive end flange.

Figure 8.2 shows a structure with intermediate vertical support flanges and using the preformed armour technique to form the coil. The coil is connected as double pancakes. The performed armour method allows a thick (7.2mm) jacket wall to be used without the risk of section deformation.

8.4 Structural Assessment

The original equilibrium current distributions for start and end of burn were calculated so that at the end of burn the solenoid (and in particular the P1 coil) is at its mechanical limit. These final configurations are given in Table 8.4 together with the peak fields and forces on the coils.

The stress limits in the central solenoid are dominated by the allowable stresses in the

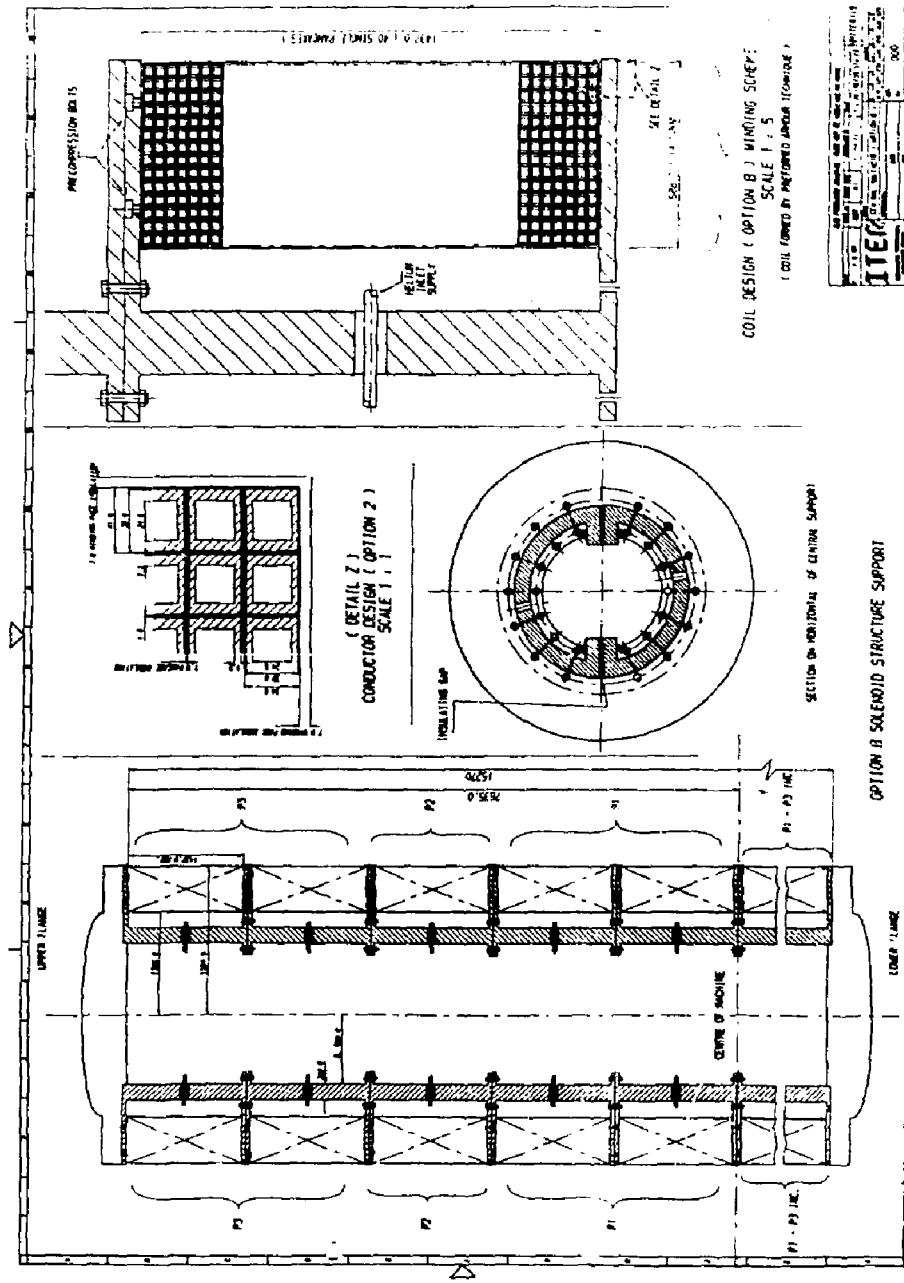

Figure 8.2: Option B Central solenoid structure.

Table 8.3: Equilibrium coil currents MA.

Coil	End of burn	Before heating	End of burn 30 MA
P1	26.5	-18.4	-20.0
P2	-10.5	- 2.1	-21.0
P3	1.0	4.55	-6.8
P4	12.0	18.0	15.0
P5	-8.0	13.7	-4.2
P6	-5.1	0.26	-10.0
I_p	20	20	30
ϕ_{eq}.eq.Vs	-151.	-102	-177

Forces

	F_R (MN/m)	F_Z MN	F_R MN/m	F_Z MN	F_R MN/m	F_Z MN
P1	88.7	-106	25.1	-98	42.5	101
P2	22.0	-165	-0.14	-28.4	63.7	-152
P3	0.5	10	9.8	26.8	1.4	-104

The fields are under 12 T.

conductor jacket. These, from the design criteria established for MPa (Tresca, steady and/or compressive). The stress concentration factors are as follows:

Peak winding pack tensile stress/average 1.35
(based on finite element calculations)

Peak packet tensile or compressive stress/average 1.2

The average winding pack stress is derived from the bursting force/unit circumference (F_R) as

$\sigma_{wt} = \frac{FR}{zt}$ R is mean radius
z is height
t is thickness

The average tensile stress is a single jacket cross-section is derived from the peak winding pack stress by

$\sigma_t = \frac{\sigma_{wt}}{f}$ where f is the fraction of steel in the winding, assuming no other structured components

Table 8.4: End of burn plasmas.

Coil (MA)		20 MA	30 MA
P1		-35	-30
P2		-17.2	-26
P3		- 0.6	-9.4
P4		8.7	13.5
P5		- 7.4	-4.2
P6		- 5.6	-10.0
ϕ_{eq} (VS)	-180	-200	
Forces			
	F_R MN/m	180	120
P1			
	F_Z MN	-132	114
	F_R MN/m	65	116
P2			
	F_Z MN	-334	-298
	F_R MN/m	0.4	10
P3			
	F_Z MN	-8	-173
B_{max}T		12.5	12.5

The average compressive transverse stress in a single jacket crossection is derived from the average winding pack compression (σ_{wc}) by

$\sigma_{wc} \approx \frac{\sigma_{wc}}{f_s}$ where f_s is the minimum fraction of steel in any crossection

For these solenoids, f *approx* 0.5
f_s *approx* 0.4

For the transformer configuration of Table 2, the peak jacket tensile stress is 502 MPa, the peak jacket compressive stress is 158 MPa and the Tresca stress 660 MPa. The end of burn configurations in Table 4 have stress levels as follows:

	20 MA	30 MA
Peak jacket tensile	518	501
Peak jacket compressive	232	234
Tresca	750	735

These values are at the acceptable operating limits.

8.5 Volt second capability

The volt-second capabilities of the machine are therefore defined by Tables 2 and 4 as follows

20 MA 4 280 Vs
30 MA 4 300 Vs

Chapter 9

RESEARCH AND DEVELOPMENT–C. Henning

9.1 Introduction

The design effort for ITER is accompanied by a significant magnet R&D effort as summarized in Table 9.1. This is needed, because a large ignited/burning plasma as in ITER will require higher steady-state magnetic fields than previously achieved. TF coils of 12 T and large size require high-current, niobium-tin superconductors to operate under conditions of high stress, cyclic loading, and nuclear heating. Ignition places large demands on the poloidal coil system, because a large amount of energy is required to start up and burn the plasma. Accordingly, the conductors must operate near 40 kA and about 12 T or greater in the central solenoid.

If the TF magnets can be made more radiation-tolerant, the neutron shielding may be reduced to permit a smaller tokamak, or conversely a larger, higher-current plasma to achieve ignition. Insulators such as polyimides, or advanced epoxy-glass with forced-flow conductors, capable of high-neutron heat removal and good stability, even with radiation-damaged copper stabilizers, are being studied to see if this goal can be achieved. Of course, large cryogenic components will be needed to remove the nuclear heat loads and pulsed field losses.

Table 9.1: Participants in ITER magnet R&D.

	Task	EC	US	Japan	USSR
MT	Toroidal coil	X		X	X
MP	Poloidal coil	X		X	
MI	Insulation material	X	X		X
MS	Magnet structure material	X		X	
MA	Radiation-tolerant magnets		X		
MC	Cryogenics		X	X	

9.2 Task Description

Task MT–Toroidal Coil. Three participants (EC, Japan, and USSR) offered to contribute TF conductor development, and the US plans to develop TF conductor concepts through an integrated program emphasizing radiation-tolerant magnets. Three concepts have been proposed: React-and-wind by the EC, USSR, and Japan; wind-and-react by the US; and the preformed armor technique, discussed by Japan, an intermediate variant that allows special high-strength steels to be added as distributed structure to the conductor after reaction. Development of these different concepts provides options that would be lost if only one course were pursued. The cost of development of such pre-prototypical conductor models is small, compared to the quantity and quality of information that can be obtained by fabricating and testing them.

Although all the teams have proposed developing and testing full-scale TF conductors, no participant possesses a test facility of sufficient size and field strength. The requirements for such test facilities (useful also for testing developmental PF conductors) can be roughly described as follows: High, transverse-field exposure of at least 0.3 to 0.4 m of conductor (the conductor must be meters in length to allow joints outside the high-field region) to magnetic fields from 12–14 T; access for a conductor of about 50-mm lateral dimension; and application of current of about 40 kA. Critical-current at the designed operating field and current can be determined by raising the temperature. Suggestions for such a test facility are being examined.

Task MP–Poloidal Coil. Development of conductors appropriate for the PF central solenoid has been proposed directly by the EC, in generic fashion by the US, and as part of a PF coil development by Japan. Both the US and the EC (with vocal support from the USSR) favor wind-and-react, cable-in-conduit approaches to PF central solenoid fabrication and have chosen their conductor development paths accordingly. The approaches of these teams differ, however, in the fabrication techniques being investigated.

The Japanese preformed armor conductor, sometimes proposed by them as an PF central solenoid conductor candidate, offers alternatives for fabrication techniques and materials. Japan has been fabricating a coil (DPC–TJ) using this preformed armor cable-in-conduit conductor. The DPC–TJ is not a pulsed coil; however, it will verify the production feasibility of this new concept and mechanical advantages.

The PF central solenoid will be an extension of the state of the art: Therefore, participants were encouraged to modify their development of plans to include the ITER PF central solenoid requirements (magnetic fields of 12 T and higher, currents near 40 kA, and ramp rates of about 1 T/s).

Task MI—Insulation Material. All participants have proposed work on irradiating and testing the magnet insulations. The US plans to extend the testing to higher exposures (10^{10} rad) and to systems that do not rely on shear bonding. Some studies indicate that the insulation systems proposed by the EC will tolerate higher exposures than the 5×10^8 rads planned for their tests.

Task MS—Magnet Structure Material. For magnet cases, the Japanese and the USSR teams have emphasized developing cryogenic steels with dramatically improved

properties. Particularly in Japan, reliable cryogenic steels (JCS) have been developed and are commercially available.

Task MA—Radiation-Tolerant Magnets. The US has proposed an overall reduction in machine size and costs by simultaneously elevating the reliable performance levels of the superconducting magnet systems and designing them to accept higher radiation exposure. This integrated approach is one that both feeds and is fed by the developments of individual magnet system components, such as conductors, cryogenic components, insulation systems, and structural materials. The US team believes this development approach is essential to significantly improve performance in these areas.

Task MC—Cryogenics. The cryogenic system of ITER must absorb approximately 100 kW at 4.5 K, corresponding to power consumption from the grid of several tens of MW. Japan and the USSR propose complementary approaches—the USSR emphasizing development of the largest components such as compressors, and Japan choosing to develop more sophisticated components such as turbo-expanders and helium pumps.

Chapter 10

CONCLUSIONS—C. Henning

The magnet systems required by the ITER Baseline Design are challenging. As a whole, they represent a significant advance in the state-of-the-art in superconducting magnet technology, but no particular component technology is pushed to unreasonable limits. Therefore, the ITER requirements can be satisfied by the application of detailed analyses, careful design, and a well-coordinated research and development program.

The PF scenarios that have been generated thus far will result in peak combined stresses in the winding pack of the present CS design around 690 MPa at the end of burn. Since the operation is cyclic, this value causes concern of fatigue. Axial loads are also high with both compressive and tensile loads experienced by parts of the CS stack at specific periods of the PF scenario. These strong axial loads of alternating sign will require a stiff axial support member designed to provide initial precompression of the CS stack to prevent axial gaps from opening during operation.

Preliminary analyses have been made of the ac losses resulting from normal operation of the PF system to assess the impact on the cryogenic system. Losses in the TF system have been estimated in the 2- to 3-kW range, and losses in the PF system will likely be appreciably larger, on the order of 10 kW. Eddy currents in these cases are the largest contributors to the TF losses, while superconductor hysteresis dominates the PF system losses. The levels of the PF system losses are significantly affected by whether NbTi conductors are chosen for the outer coils, where fields are low enough to permit their use. The losses quoted are the averages over the nominally 500-s pulse. The peaks are significantly higher in the PF system during the plasma breakdown, but these are brief and can be safely absorbed by the enthalpy of the conductor coolant. Cyclic operation of certain Pf coils to provide the plasma divertor swing indicates a drastic increase in these loss levels.